

DIPLOMARBEIT

Measurement Based Evaluation of Interference Alignment on the Vienna MIMO Testbed

Ausgeführt zum Zwecke der Erlangung des akademischen Grades eines Diplom-Ingenieurs
unter der Leitung von

Univ.Prof. Dipl.-Ing. Dr.techn. Markus Rupp

und

Dipl.-Ing. Martin Lerch

am

Institute of Telecommunications

eingereicht an der Technischen Universität Wien
Fakultät für Elektrotechnik und Informationstechnik

von

Martin Mayer

0725729

Blödlweg 5

6820 Frastanz

Wien, Oktober 2013

I hereby declare that this thesis is my original work and it has been written by me in its entirety.
I have acknowledged all the sources of information which have been used in the thesis.

Martin Mayer
Vienna, October 2013

Abstract

Most modern wireless multi-user networks suffer from undesired interference that impairs the data transmission over the individual radio links. In order to maximize the data throughput in such systems, several interference mitigation schemes have been investigated recently. Interference alignment stands out as one of the most promising ones, able to attain the maximum data throughput over interference disturbed links in theory, given the right conditions. As the theoretical research progresses, practical implementations have to be considered in order to confirm the theory and discover limitations introduced by hardware.

Interference alignment utilizes linear filtering at each transmitter and receiver of the network. The transmit filters thereby partition the signal space at the receiver into two subspaces, a desired signal subspace containing the signal from the desired transmitter and an interference subspace accumulating all the interfering signals. The aligned interference is then forced to zero by the receive filter and only the desired signal is retained. For this to be accomplished, cooperation of all users in the network is required.

This work first deals with the theoretical foundations of interference alignment by introducing the relevant system model and discussing feasibility and filter computation. It then advances to the characterization of the Vienna MIMO testbed on which interference alignment was implemented throughout this work. The testbed employs two outdoor transmitters on rooftops, one indoor transmitter and one indoor receiver. The radio channels in the considered setup are quasi-static. Hardware, software and the used signals are described. Performance measures for evaluation are introduced. Finally, measurement results are presented. The feasibility of interference alignment is shown, and the performance measures are evaluated over variable signal to noise ratio and variable signal to interference ratio. The results are discussed, and impairments introduced by hardware are highlighted.

Kurzfassung

Moderne drahtlose Multiuser-Netzwerke werden oft durch unerwünschte Interferenz gestört, welche die Datenübertragung über die jeweiligen Funkverbindungen verschlechtert. Einige Methoden zur Steigerung der Datenrate in solchen Systemen wurden kürzlich untersucht. “Interference Alignment” sticht dabei als eines der vielversprechendsten Verfahren hervor, da es in der Theorie die maximale Datenrate erreicht, wenn die richtigen Umstände gegeben sind. Mit dem Fortschritt der theoretischen Forschung werden praktische Implementierungen relevant, damit die Theorie bestätigt und mögliche hardwarebedingte Limitationen entdeckt werden.

“Interference Alignment” verwendet lineare Sende- und Empfangsfilter. Der Signalraum am jeweiligen Empfänger wird dabei durch die Sendefilter in zwei Unterräume unterteilt, einen Unterraum für das erwünschte Signal und einen Unterraum, in dem alle Interferenz-Signale überlappen. Die gesammelte Interferenz wird dann mittels Empfangsfilter eliminiert und nur das erwünschte Signal bleibt bestehen. Das Verfahren ist nur möglich, wenn alle Benutzer des Netzwerks kooperieren.

Diese Arbeit beginnt mit einer theoretischen Abhandlung von “Interference Alignment”. Dabei wird zuerst das relevante System-Modell eingeführt, anschließend werden Voraussetzungen und Filterberechnung besprochen. Als nächstes wird das “Vienna MIMO testbed” charakterisiert, auf welchem “Interference Alignment” im Zuge dieser Arbeit implementiert wurde. Es besteht aus zwei Outdoor-Sendeanlagen auf Häuserdächern, einer Indoor-Sendeanlage und einer Indoor-Empfangsanlage. Die Funkkanäle sind dabei quasi-statisch. Hardware, Software und die benutzten Signale werden beschrieben. Performance-Maße werden eingeführt, die zur Bewertung der “Interference Alignment” Qualität dienen. Anschließend werden Messergebnisse präsentiert. Die Machbarkeit von “Interference Alignment” wird gezeigt, und das Verhalten der Performance-Maße wird untersucht, einmal für variables Signal-Rausch-Verhältnis und einmal für variables Signal-Interferenz-Verhältnis. Beeinträchtigungen durch die verwendete Hardware werden aufgezeigt.

Contents

| | | |
|----------|---|-----------|
| 1 | Introduction | 1 |
| 1.1 | The Virtues of Interference Alignment | 2 |
| 1.2 | Testbed Aided Evaluation | 4 |
| 1.3 | Outline | 5 |
| 2 | System Model and Interference Alignment | 6 |
| 2.1 | K -User MIMO Interference Channel | 6 |
| 2.2 | Mutual Information and Degrees of Freedom | 7 |
| 2.3 | Interference Alignment | 10 |
| 2.3.1 | Feasibility | 11 |
| 2.3.2 | Closed Form Solution | 12 |
| 3 | Vienna MIMO Testbed | 13 |
| 3.1 | Hardware and Deployment | 13 |
| 3.1.1 | Transmitter | 15 |
| 3.1.2 | Receiver | 16 |
| 3.2 | Measurement Methodology | 18 |
| 3.3 | Signals and Channel Estimation | 18 |
| 3.3.1 | Transmit Signals | 19 |
| 3.3.2 | Receive Signals | 21 |
| 3.3.3 | Channel Estimation | 23 |
| 3.4 | Software and Control | 24 |
| 3.4.1 | Measurement | 24 |
| 3.4.2 | Transmit Routine | 29 |
| 4 | Evaluation and Quantities of Interest | 31 |
| 4.1 | Assumptions and Detailed Frame Structure | 31 |
| 4.2 | Measured Mutual Information | 33 |
| 4.2.1 | Mutual Information from Channel Estimates | 33 |
| 4.2.2 | Mutual Information from Receive Data Covariance | 35 |
| 4.3 | Interference Suppression | 36 |
| 4.4 | Power, SNR and SIR | 38 |
| 5 | Measurements | 40 |
| 5.1 | Validation of Interference Alignment | 40 |
| 5.2 | Variable SNR at Fixed SIR | 47 |
| 5.2.1 | Measured Powers, SNR and SIR | 48 |
| 5.2.2 | Interference Suppression | 51 |
| 5.2.3 | Mutual Information | 53 |
| 5.3 | Variable SIR at Fixed SNR | 55 |
| 5.3.1 | Measured Powers, SNR and SIR | 55 |
| 5.3.2 | Interference Suppression | 59 |

| | |
|------------------------------------|-----------|
| 5.3.3 Mutual Information | 62 |
| 6 Conclusion and Outlook | 64 |
| List of Figures | 66 |
| Bibliography | 68 |

Chapter 1

Introduction

Interference lowers the achievable data rates in wireless multi-user networks. Transmissions that naturally occupy a certain bandwidth are thereby disturbed by interferers that transmit in the same frequency band. As a result, the superposition of the signals at the receiver impairs the desired signal, since its waveform and amplitude are altered by the interference.

Where in former times, we were able to divide applications into individual frequency bands and thereby avoid interference, we soon reached a point where these bands were highly occupied and the resource of frequency became scarce. The bandwidth and operational frequency of an application are also constrained by physical properties like antenna size. We had to come up with new ideas to maximize the (spectral) efficiency of our wireless transmission schemes in order to accommodate more channels in the same frequency band. Schemes that successfully manage interference yield tremendous potential in that area.

With a steadily increasing number of users in wireless networks such as the cellular system in mobile communications, the need of multiple access schemes emerged. Users can be distinguished in frequency domain (designated frequency/channel), in time domain (designated time slot), in code domain (designated signature) or in space domain (designated direction of radio beam). The realizations of these ideas are called Frequency Division Multiple Access (FDMA), Time Division Multiple Access (TDMA), Code Division Multiple Access (CDMA) and Space Division Multiple Access (SDMA), respectively. What all these multiple access schemes have in common is the effect of decreasing maximum data rate per user with increasing number of users. This is due to the fact that the frequency/time/code/spatial domain can not be fully exploited for data transmission as in the single user case. The channel can be seen as a cake, and every user gets only a slice of it. A simple example illustrating this behaviour is the one of K users that want to transmit data within one second - each user gets only the fraction $\frac{1}{K}$ of a second to transmit its data or put differently, it takes each user K seconds to transmit the same amount of data as in the single user case.

In cellular networks, interference will always be an issue. Despite frequency planning¹, frequencies have to be reused, either in adjacent cells as in UMTS² or in further separated cells as in GSM³. The difference manifests itself in the strength of the interference and how it is handled. With increasing number of users, these networks ultimately become interference limited, meaning that an increase of transmit power does not result in better signal quality and higher data throughput as in noise limited networks. This behaviour also applies to other multi-user networks such as WLAN⁴.

¹Frequency planning here refers to the downlink in a cellular system, namely the channel from serving base station to user equipment. The so called inter-cell interference comes from neighbouring cells that operate on the same frequency as the serving cell.

²Universal System of Mobile Communications (in 3rd generation mobile networks)

³Global System for Mobile Communications (in 2nd generation mobile networks)

⁴Wireless Local Area Network, IEEE 802.11

Conversely to the somewhat old fashioned cake cutting analogon where every user gets only a “slice” of the channel, it has recently been shown in [1] that the maximum data rate per user is not necessarily decreasing with increasing number of users. The refined statement claims that “every user is able to get half the cake”, the rate-penalty of having K users communicating on the same resource would only be $\frac{1}{2}$ instead of $\frac{1}{K}$. Several interference management approaches have been researched, but Interference Alignment (IA) stands out as one of the most promising ones. As a future technology, it might be employed as an interference mitigation technique in the further progression of LTE⁵.

In Section 1.1, the advances in interference management are sketched, the basic idea behind IA is explained and finally, its requirements are listed. Section 1.2 then illuminates the benefits of testbed driven evaluation in the context of IA and compares the approaches that have been taken up to the point where this work was written. An outline of this work is subsumed in Section 1.3.

1.1 The Virtues of Interference Alignment

The choice of the proper interference management approach heavily depends on the aspects of the considered system, such as the Signal to Noise Ratio (SNR) and the interference strength which is usually expressed by the Signal to Interference Ratio (SIR). Three classic approaches are now listed, loosely following the introduction in [1]:

- **Treat as noise:** In case of weak interference, the interfering signals can be treated as noise. Single user encoding and decoding is performed. However, this approach is sub-optimal from an information theoretic point of view since the structure in the interfering signals is not exploited.
- **Orthogonalized access:** In case of interference being about as strong as the desired signal, it can be avoided by orthogonalizing the channel access with multiple access schemes. This is the “cake cutting” approach where every user accessing the medium gets only a “slice”.
- **Decode:** In case of strong interference, the interfering signals might be decoded along with the desired signal. While improving the data rate of the desired user, the interfering users experience lowered rates due to the necessary overhead for multi-user detection.

Interference Alignment (IA) addresses the case where interference and desired signal are about equally strong. It redeems the “cake cutting” approach and - given the right conditions - is able to serve every user “half the cake”. This results in heavily increased data rates in multi-user systems.

Consider such a multi-user system with three transmitter-receiver pairs (users) where each transmitter wants to communicate only with its corresponding (desired) receiver. Each user receives two interfering signals on top of the desired signal. The approach using TDMA is depicted in Figure 1.1. Each user is assigned to a designated time slot. In the example, all propagation delays are equal and no inter-symbol interference occurs. At the receive side, the signals can be separated perfectly. However, the time until every user is served linearly increases with the number of users. Equivalently, the users could be separated on different

⁵3GPP Long Term Evolution (in 4th generation mobile networks)

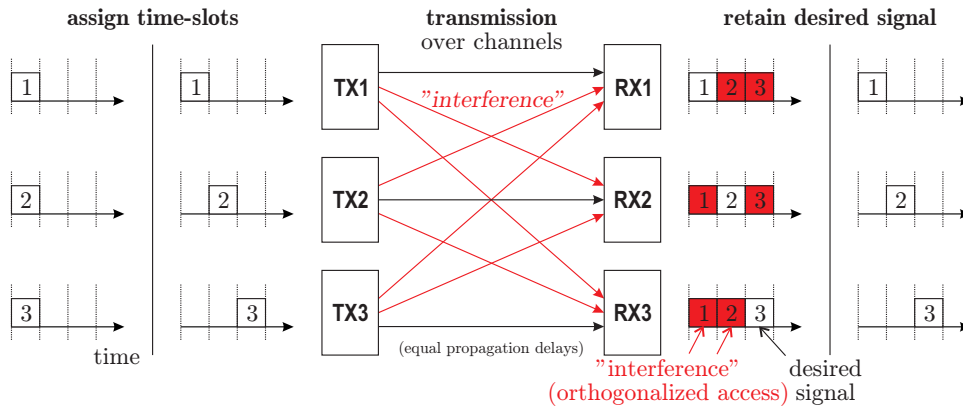


Figure 1.1: Basic principle of TDMA in the three user case

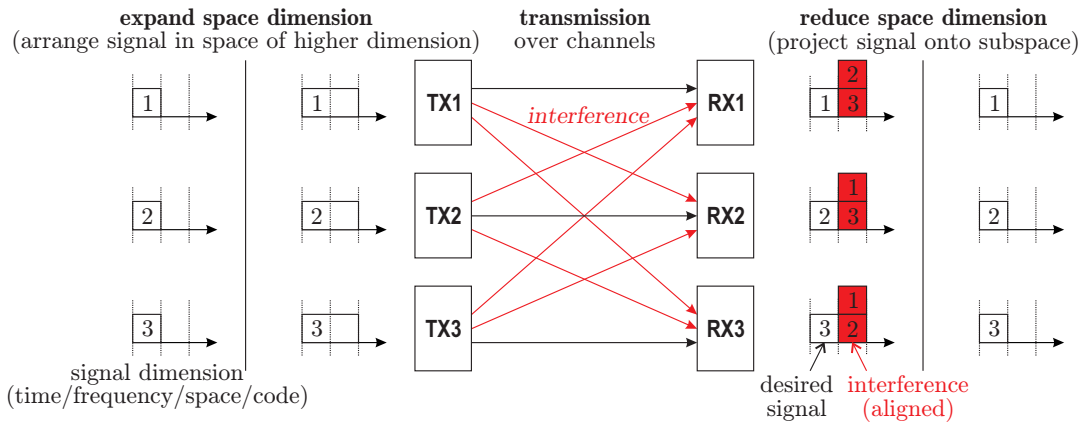


Figure 1.2: Basic principle of IA in the three user case

carrier frequencies in FDMA and different code signatures in CDMA. The idea of IA illustrated in Figure 1.2 is more complicated, yet rewarding. At the transmit side, the signals are mapped onto a higher dimensional space in such a way that the interference overlaps in a subspace at the receive side. In the simple example, a one dimensional transmit signal is arranged in a two dimensional space at each transmitter. After transmission over the channels, desired and interfering signals add up at each receiver. The received signals are partitioned into one dimension containing the desired signal and one dimension accumulating interference. The receiver then retains only the desired signal by projecting the receive signal onto the desired signal dimension, thereby eliminating the accumulated interference. This step is called *interference suppression*.

The nature of the exploited signal space dimension - time, frequency, space or code - is dictated by the system and its channel characteristics. For instance, IA on Multiple-Input Multiple-Output (MIMO) systems incorporating multiple antennas at each user node is able to exploit the spatial dimension. In that context, the operation of expanding the signal space at the transmit side is called *beamforming* and is performed with *precoding* matrices. This work deals with that particular case. Not relying on multiple antennas, the time dimension can be exploited by coding across time-varying channels [1], the frequency dimension by coding across multiple carriers with frequency selective coefficients. This already implies that the channels

have to be uncorrelated (i.e. full rank channel matrices in MIMO transmissions) for optimal results. To realize the separation of desired signal and interference at the receiver, overall channel knowledge is required. Only then, the signals can be precoded at the transmit side so that interference aligns at the receive side. The users therefore need the ability to communicate with each other (i.e. *feedback*). By cooperation of all user nodes, a jointly optimal beamforming scheme called IA is possible. Furthermore, the $\frac{1}{2}$ rate penalty (“every user gets half the cake”) is only attained in the high SNR regime.

1.2 Testbed Aided Evaluation

The foundation of scientific innovation is based on ideas that develop into theories followed by mathematical descriptions and models. As soon as we are able to imagine how something could work, we start to abstract the problem. Especially at the beginning, this might lead to very conceptual drafts that are far from reality and can not directly be applied in the real world. Section 1.1 dealt with a similar case and explained the principles of IA in a very abstract way.

The next step is to build upon the theoretical foundation and dare the step into the real world. The best idea is not worth the effort if it is not feasible. Where Section 2.3.1 deals with the aspects of feasibility in detail, the remainder of this section lists the achievements in the implementation of real world IA utilizing measurements and testbeds. These results act as a first benchmark of how IA performs in the field. Substantiating the IA theory by realizing the IA precoder computation algorithms on a live testbed and demonstrate their capabilities in a real world environment is an important step that brings IA one step closer to its possible future implementation in wireless networks.

IA has been emulated in [2] using measured indoor channels. They used software defined radio at carrier frequency 2.4 GHz and built a⁶ $(2 \times 2, 1)^3$ MIMO Orthogonal Frequency Division Multiplexing (OFDM) testbed with accurate node-synchronization. They experimented with node-positioning and realized Line of Sight (LOS) and Non Line of Sight (NLOS) channels that were relatively static (i.e. highly correlated channel coefficients over time). The results in static environments such as a laboratory room suggest that the calculated IA precoders can be used for many successive frame transmissions, which in turn reduces the computational complexity of the implementation. They used iterative algorithms defined in [3, 4] for their IA precoder calculations. They compared the average sum rate vs. SNR and concluded that IA outperforms TDMA in the high SNR regime. The same testbed was further exploited in [5] where they added outdoor channel measurements to the evaluation. Again, IA outperformed TDMA in the high SNR regime.

A different testbed was used in [6]. They performed IA in a $(2 \times 2, 1)^3$ MIMO OFDM system in the 5 GHz band. Indoor channels were considered static with no moving objects in the room. Conversely to the testbed in [2, 5], channel estimation, precoder calculation and signal generation were executed online⁷ within five seconds. Furthermore, they studied the impact of channel estimation errors and found it to be a key limiting factor on IA performance. This fact was also highlighted by simulations in [7]. Once again, it was shown that IA outperforms TDMA in the high SNR regime. The testbed has been used again in [8] to take a closer look at the sum rate optimizing IA solution, and the sum rate degradation due to channel estimation

⁶A system denoted $(M_T \times N_R, d)^K$ consists of K transmitter-receiver pairs, each transmitter transmitting d data streams over M_T antennas and each receiver receiving d data streams over N_R antennas.

⁷Online means that the mentioned processes take place during the measurement rather than afterwards.

error was demonstrated.

Where it took the testbeds in [6, 8] roughly five seconds for computations between frame transmissions, the testbed in [9] reduces this time to the tenth of a second. They built a movable testbed operating at 2.49 GHz that constitutes a $(2 \times 2, 1)^3$ MIMO OFDM system. Various indoor positions for the mobile stations were considered. IA was compared to coordinated multipoint with ideal and measured results. The gains over the reference schemes of the single user MIMO case achieved by measurements were much smaller than stated by theory, which was presumably caused by spurious Radio Frequency (RF) effects. Nevertheless, IA and coordinated multipoint outperformed the reference schemes of the single user MIMO case, such as TDMA.

1.3 Outline

In this work, the Vienna MIMO Testbed (VMTB) is used to demonstrate the feasibility of Interference Alignment (IA) in a $(4 \times 4, 2)^3$ MIMO OFDM system at carrier frequency 2.5 GHz. A heterogeneous urban scenario consisting of two outdoor transmitters, one indoor transmitter and one indoor receiver is investigated. The channels are considered static, the receive antennas are mounted on a x - y - ϕ table to create different channel realizations. Precoder computation and signal generation are performed online within approximately 70ms. Aside from the feasibility demonstration, the impact of variable SNR and SIR on the data rate is observed. The first IA results utilizing this testbed setup were published in [10].

This work is structured as follows. Chapter 2 introduces the underlying system model and explains how the mutual information (representing the possible data rate) is obtained, with and without IA. It then discusses the role of the Degrees of Freedom (DoF) and advances to the principles of IA. Chapter 3 deals with the VMTB in detail. Hardware, software, the principles of measurement and the used signals are explained. Chapter 4 introduces measures for the evaluation of measurements. Chapter 5 shows the measurement results and discusses their implications. Chapter 6 subsumes the work and gives an outlook.

Chapter 2

System Model and Interference Alignment

The system model representing the basis of further characterizations is introduced in Section 2.1. Section 2.2 then compares how mutual information and the Degrees of Freedom (DoF) behave with and without Interference Alignment (IA). Based upon these fundamentals, Section 2.3 deals with the theory behind IA and how it is applied. Note that if not stated otherwise, the considered models are the ones used for IA.

2.1 K -User MIMO Interference Channel

The K -user MIMO interference channel comprises K transmitter-receiver pairs (also called links), where each receiver suffers from $K - 1$ interferers. This work restricts itself to the *symmetric* case, where every transmitter has M_T antennas and every receiver has N_R antennas. Furthermore, each link communicates on d data streams. Such a system is denoted as $(M_T \times N_R, d)^K$. An exemplary $(4 \times 4, 2)^3$ system is depicted in Figure 2.1.

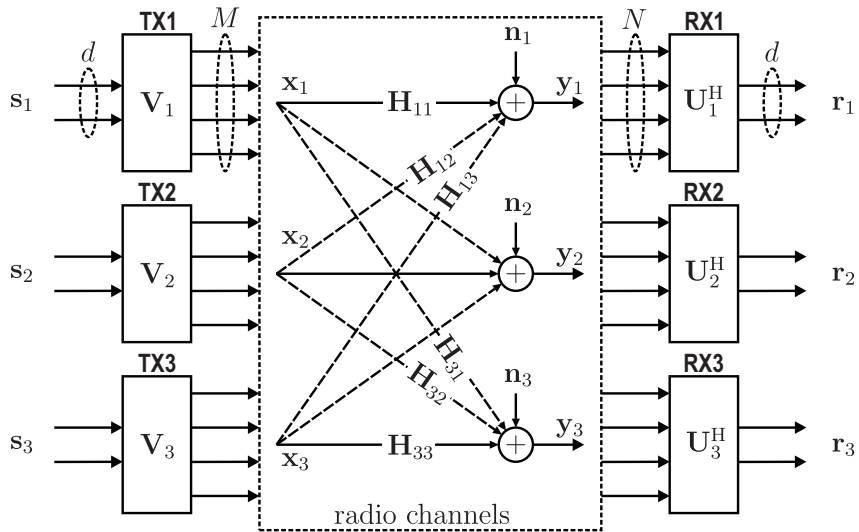


Figure 2.1: $(4 \times 4, 2)^3$ MIMO interference channel

Each transmitter, indexed by $j \in \{1, \dots, K\}$, transmits a data stream $\mathbf{s}_j \in \mathbb{C}^d$ that is beamformed by applying a truncated unitary *precoding matrix* $\mathbf{V}_j \in \mathbb{C}^{M_T \times d}$ according to

$$\mathbf{x}_j = \mathbf{V}_j \mathbf{s}_j, \quad (2.1)$$

where $\mathbf{x}_j \in \mathbb{C}^{M_T}$ constitutes the transmit signal vector. Let $i \in \{1, \dots, K\}$ denote the receiver index. The transmit signal vector is transmitted over the respective channels whose coefficients are stored in channel matrices $\mathbf{H}_{ij} \in \mathbb{C}^{N_R \times M_T}$. At the i^{th} receiver, the noise vector $\mathbf{n}_i \in \mathbb{C}^{N_R}$

is added, which is (for simplicity in the following) assumed to be circularly symmetric complex Gaussian i.i.d.¹ with zero mean and variance $\sigma_{n_i}^2$, $\mathbf{n}_i \sim \mathcal{CN}(\mathbf{0}, \sigma_{n_i}^2 \mathbf{I}_{N_R})$. The receive signal vector $\mathbf{y}_i \in \mathbb{C}^{N_R}$, obtained as

$$\mathbf{y}_i = \sum_{j=1}^K \mathbf{H}_{ij} \underbrace{\mathbf{V}_j \mathbf{s}_j}_{\mathbf{x}_j} + \mathbf{n}_i, \quad (2.2)$$

is then filtered by the truncated unitary *interference suppression matrix* $\mathbf{U}_i \in \mathbb{C}^{N_R \times d}$ according to

$$\mathbf{r}_i = \mathbf{U}_i^H \mathbf{y}_i = \sum_{j=1}^K \mathbf{U}_i^H \mathbf{H}_{ij} \mathbf{V}_j \mathbf{s}_j + \mathbf{U}_i^H \mathbf{n}_i = \underbrace{\mathbf{U}_i^H \mathbf{H}_{ii} \mathbf{V}_i \mathbf{s}_i}_{\text{desired signal}} + \underbrace{\sum_{\substack{j=1 \\ j \neq i}}^K \mathbf{U}_i^H \mathbf{H}_{ij} \mathbf{V}_j \mathbf{s}_j}_{\text{interference}} + \underbrace{\mathbf{U}_i^H \mathbf{n}_i}_{\text{noise}} \quad (2.3)$$

which yields the receive data stream $\mathbf{r}_i \in \mathbb{C}^d$, an estimation of the corresponding transmit data stream \mathbf{s}_i of user i .

The precoding matrices \mathbf{V}_j and interference suppression matrices \mathbf{U}_i are chosen to jointly suppress the interference in Equation (2.3), their calculation is discussed in Section 2.3.2.

2.2 Mutual Information and Degrees of Freedom

Consider a MIMO link with M_T transmit antennas and N_R receive antennas. The receive signal vector is obtained as $\mathbf{y} = \mathbf{H}\mathbf{x} + \mathbf{n}$, with fixed (deterministic) channel realization \mathbf{H} and circularly symmetric complex Gaussian i.i.d. noise vector $\mathbf{n} \sim \mathcal{CN}(\mathbf{0}, \sigma_n^2 \mathbf{I}_{N_R})$. The mutual information² between \mathbf{x} and \mathbf{y} is defined as [11]

$$\mathcal{I}(\mathbf{x}; \mathbf{y}) = \log_2 \det \left(\mathbf{I}_{N_R} + \frac{1}{\sigma_n^2} \mathbf{H} \mathbf{Q} \mathbf{H}^H \right), \quad (2.4)$$

where $\mathbf{Q} \in \mathbb{R}^{M_T \times M_T}$ defines the power allocation at the transmit antennas and $\text{trace}(\mathbf{Q}) = P$ yields the total transmit power constraint. Assuming equal transmit power $\frac{P}{M_T}$ at each antenna,

$$\mathbf{Q} = \frac{P}{M_T} \mathbf{I}_{M_T} \quad (2.5)$$

and Equation (2.4) becomes

$$\mathcal{I}(\mathbf{x}; \mathbf{y}) = \log_2 \det (\mathbf{I}_{N_R} + \gamma \mathbf{H} \mathbf{H}^H) \quad (2.6)$$

with SNR $\gamma = \frac{P}{M_T \sigma_n^2}$. A common approach to investigate MIMO systems is to perform a Singular Value Decomposition (SVD)³ on the channel matrix \mathbf{H} :

$$\mathbf{H} = \mathbf{L} \mathbf{\Sigma} \mathbf{R}^H. \quad (2.7)$$

¹The elements of an i.i.d. random vector are (statistically) independent and identically distributed.

²The mutual information $\mathcal{I}(\mathbf{x}; \mathbf{y})$ can be seen as the reduction in the uncertainty about \mathbf{x} due to the knowledge of \mathbf{y} . In the information theoretic context, it corresponds to rate. Its unit is [bit/s/Hz].

³A singular value decomposition $\mathbf{A} = \mathbf{L} \mathbf{\Sigma} \mathbf{R}^H$ decomposes a matrix $\mathbf{A} \in \mathbb{C}^{N_R \times M_T}$ into a unitary matrix $\mathbf{L} \in \mathbb{C}^{N_R \times N_R}$ containing its left singular vectors, a rectangular diagonal matrix $\mathbf{\Sigma} \in \mathbb{R}^{N_R \times M_T}$ containing its singular values in the main diagonal and a unitary matrix $\mathbf{R}^H \in \mathbb{C}^{M_T \times M_T}$ containing its right singular vectors.

The MIMO transmission is decomposed into N_Σ parallel Single-Input Single-Output (SISO) transmissions, where N_Σ is the number of nonzero singular values in Σ and $N_\Sigma = \min(M_T, N_R)$ if \mathbf{H} has full rank, which is assumed here. Decomposing \mathbf{H} in Equation (2.6) leads to

$$\begin{aligned}
\mathcal{I}(\mathbf{x}; \mathbf{y}) &= \log_2 \det \left(\mathbf{I}_{N_R} + \underbrace{\gamma \mathbf{L} \Sigma \mathbf{R}^H \mathbf{R} \Sigma^T \mathbf{L}^H}_{= \mathbf{I}_{M_T}} \right) \\
&= \log_2 \det (\mathbf{I}_{N_R} + \gamma \mathbf{L} \Sigma \Sigma^T \mathbf{L}^H) \\
&= \log_2 \det (\mathbf{L} \mathbf{L}^H + \gamma \mathbf{L} \Sigma \Sigma^T \mathbf{L}^H) \\
&= \log_2 \det (\mathbf{L} (\mathbf{I}_{N_R} + \gamma \Sigma \Sigma^T) \mathbf{L}^H) \\
&= \log_2 \det (\mathbf{I}_{N_R} + \gamma \Sigma \Sigma^T) \\
&= \sum_{s=1}^{\min(M_T, N_R)} \log_2 (1 + \gamma \lambda_s),
\end{aligned} \tag{2.8}$$

where the squared singular values in $\Sigma \Sigma^T = \text{diag}\{\lambda_1, \dots, \lambda_{\min(M_T, N_R)}\}$ are the eigenvalues of $\mathbf{H} \mathbf{H}^H$, denoted λ_s . The Degrees of Freedom (DoF) are now defined as

$$\begin{aligned}
\text{DoF} &= \lim_{\gamma \rightarrow \infty} \frac{\mathcal{I}(\mathbf{x}; \mathbf{y})}{\log_2 \gamma} \\
&= \sum_{s=1}^{\min(M_T, N_R)} \lim_{\gamma \rightarrow \infty} \frac{\log_2 (1 + \gamma \lambda_s)}{\log_2 \gamma} \\
&= \sum_{s=1}^{\min(M_T, N_R)} \underbrace{\lim_{\gamma \rightarrow \infty} \frac{\gamma}{1 + \gamma}}_{=1} \\
&= \min(M_T, N_R).
\end{aligned} \tag{2.9}$$

In a MIMO system, the DoF are also called multiplexing gain since the link capacity grows linearly with the number of antennas $\min(M_T, N_R)$.

The transition to the interference channel introduced in Section 2.1 is now discussed. Instead of one single MIMO link, K links exist, and each user receives interference on top of the desired signal. Assuming *perfect* IA that nulls the interference terms in Equation (2.3), the receive stream \mathbf{r}_i will be interference free. The resulting transmission of information takes place over the *interference free channel* $\mathbf{U}_i^H \mathbf{H}_{ii} \mathbf{V}_i$ of reduced rank $d < \text{rank}(\mathbf{H}_{ii})$. This way, each link is interference free and can be viewed as stand-alone MIMO link as in the beginning of this section. The link index i is now dropped and the mutual information over an interference aligned link becomes⁴

$$\mathcal{I}(\mathbf{s}; \mathbf{r}) = \log_2 \det \left(\mathbf{I}_d + \frac{1}{\sigma_n^2} (\mathbf{U}^H \mathbf{H} \mathbf{V}) \mathbf{Q} (\mathbf{U}^H \mathbf{H} \mathbf{V})^H \right). \tag{2.10}$$

Taking the same assumptions and steps as in the interference free case, this develops into

$$\mathcal{I}(\mathbf{s}; \mathbf{r}) = \sum_{s=1}^d \log_2 (1 + \gamma \lambda_s). \tag{2.11}$$

⁴Note that $\mathbf{Q} = \frac{P}{d} \mathbf{I}_d$, since power is now allocated on d data streams rather than M_T antennas.

The DoF in the interference aligned case are

$$\text{DoF}^{\text{IA}} = \lim_{\gamma \rightarrow \infty} \frac{\mathcal{I}(\mathbf{s}; \mathbf{r})}{\log_2 \gamma} = d < \min(M_T, N_R). \quad (2.12)$$

IA therefore renders a system interference free at the expense of reduced DoF respectively multiplexing gain. The computation of the mutual information in the non-ideal IA case (i.e. non-perfect channel knowledge) is discussed in Section 4.2.

A capacity characterization for the K -user interference channel is not straight-forward. The following summary relates to K -user interference channels with single antenna nodes (not MIMO). The $K = 2$ -user Gaussian interference channel was studied in [12] and capacity bounds were proposed. In [13], it was shown that the maximum achievable DoF of a network involving $K = 2$ users is one ($\frac{1}{2}$ per user) and they inferred that for K users, it is at most $\frac{K}{2}$ ($\frac{1}{2}$ per user). The landmark paper [1] coincides with that result and characterizes the sum capacity of the K -user interference channel as $C(\gamma) = \frac{K}{2} \log_2(\gamma) + \mathcal{O}(\log_2(\gamma))$, where $\mathcal{O}(\log_2(\gamma))$ is an approximation error. This result is shown to be achievable almost surely in the case of time-varying channel coefficients and beamforming over multiple symbol extensions.

This work focuses on the symmetric square ($M_T = N_R$) $K = 3$ -user MIMO interference channel with quasi-static channel coefficients, since these circumstances are experienced in the measurements (Chapter 5). It was shown in [1] that the sum capacity in this case is characterized (almost surely) as $C(\gamma) = \frac{3}{2} N_R \log_2(1 + \gamma) + \mathcal{O}(1)$. The total DoF are hence $\frac{3}{2} N_R = \frac{K}{2} N_R$, and the per user DoF are $\frac{1}{2} N_R$ which is half the DoF a user could achieve in the absence of interference (see Equation (2.9)). This is a major improvement over classical orthogonalization approaches like TDMA where the per user DoF are given as $\frac{1}{K} N_R$ and are hence decreasing with increasing number of users. This result also holds true⁵ for larger number of users K and is the essence behind the “every user gets half the cake” statement. However, it is only valid at high SNR. The scheme achieving this is called Interference Alignment (IA) and will now be discussed.

⁵Requirements see [1]. A larger number of users K requires a larger signal space.

2.3 Interference Alignment

Interference Alignment (IA) is the scheme proposed to maximize the achievable Degrees of Freedom (DoF) in an interference channel. In a MIMO system, the DoF correspond to the achievable multiplexing gain (see Section 2.2). Considering an interference channel, they can be interpreted as follows:

- The DoF of wireless interference networks represent the number of interference-free signaling dimensions in the network [14].
- The maximum total DoF correspond to the first-order approximation of sum-rate capacity in the high SNR regime [15].

By maximizing the DoF, intuitively the achievable data rate is also maximized. IA is currently seen to be the optimal scheme that approaches the Shannon capacity [16] of interference networks in the high SNR regime.

The realization of IA basically boils down to the computation of precoding matrices \mathbf{V}_j and interference suppression matrices \mathbf{U}_i that jointly suppress the interference (see Equation (2.3)) in the K -user MIMO interference channel introduced in Section 2.1. To that end, following two conditions have to be satisfied simultaneously:

$$\mathbf{U}_i^H \mathbf{H}_{ij} \mathbf{V}_j = \mathbf{0}, \forall j \neq i \quad (2.13a)$$

$$\text{rank}(\mathbf{U}_i^H \mathbf{H}_{ii} \mathbf{V}_i) = d, \forall i \in \{1, \dots, K\}. \quad (2.13b)$$

These conditions already imply that the channel matrices \mathbf{H}_{ij} have to be known in order to compute \mathbf{V}_j , \mathbf{U}_i .

The precoding matrices \mathbf{V}_j applied at transmitters $j = \{1, \dots, K\}$ are designed to maximize the overlap of the interference signal subspaces at each receiver while ensuring that the desired signal vectors at each receiver are linearly independent of the interference subspace [14].

The interference suppression matrices \mathbf{U}_i applied at receivers $i = \{1, \dots, K\}$ perform zero forcing of the interference without zero forcing the desired signal (which is linearly independent of interfering signals).

Figure 2.2 illustrates the signal vectors in a $(2 \times 2, 1)^2$ interference channel. The channel solely rotates the transmit signal vectors \mathbf{x}_j in this toy example. By knowing the channel coefficients, the users are able to come up with a joint precoding scheme that fulfills the IA Conditions (2.13). Imagine a larger number of users K : interference of all interfering transmitters will overlap in the interference dimension and the desired signal that is linearly independent of the interference can be projected onto the desired dimension, thereby nulling all the interference.

The DoF available to every user in the interference free case are basically halved in the interference case, one half for the desired signal and one half for the interference. In the MIMO case, d data streams are mapped onto M_T transmit antennas (Equation (2.1)) and received on N_R receive antennas (Equation (2.2)). The desired data subspace at the receiver therefore has d dimensions, whereas the remaining $N_R - d$ dimensions belong to the interference subspace. Condition (2.13b) ensures that the data transmitted over the effective $d \times d$ MIMO channel $\mathbf{U}_i^H \mathbf{H}_{ii} \mathbf{V}_i$ really retains its d dimensions which also correspond to the DoF of user i (Equation (2.12)).

Feasibility of IA and the constraints on the data stream dimension respectively DoF d will now be discussed.

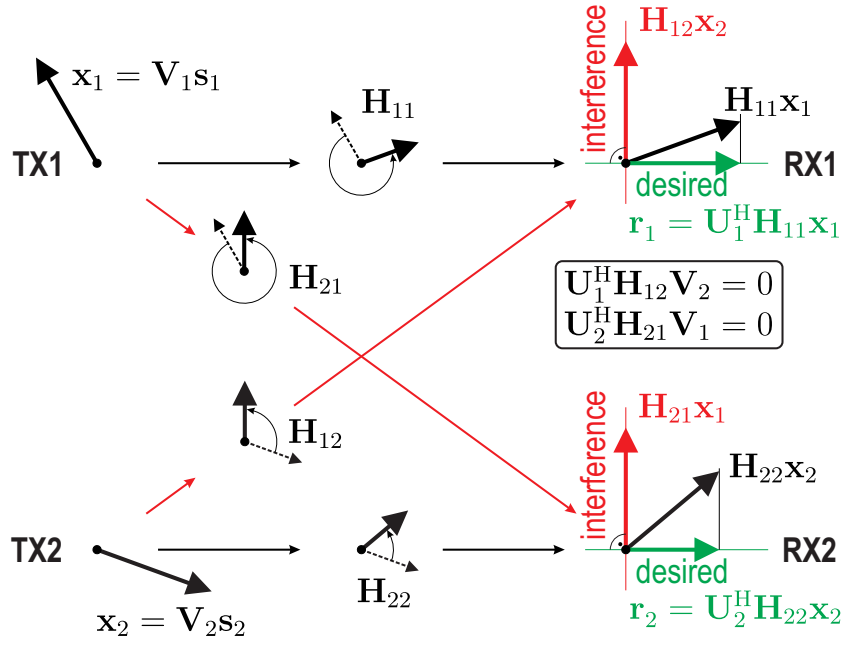


Figure 2.2: Signal vectors in a $(2 \times 2, 1)^2$ interference channel without noise

2.3.1 Feasibility

Feasibility of IA in general was researched in [14] whereas the MIMO symmetric square case was researched in [17]. In [14], IA was found to be (almost surely) feasible if a system is proper. A system is said to be proper if the number of variables is not smaller than the number of equations in Condition (2.13a) (non-overdetermined system of linear equations). In a symmetric $(M_T \times N_R, d)^K$ system, this boils down to following condition [14]:

$$M_T + N_R - (K + 1)d \geq 0. \quad (2.14)$$

Assuming equal number of transmit and receive antennas $M_T = N_R$ (symmetric square case) and generic channel matrices (non-degenerate continuously distributed entries), IA is feasible if and only if [17]

$$N_R \geq \frac{d(K + 1)}{2}. \quad (2.15)$$

Furthermore, for $K \geq 3$ and generic channel matrices, the maximum number of total DoF is given as [17]

$$\text{DoF}_{\max} = \frac{K}{N_R} \left\lfloor \frac{2N_R}{K + 1} \right\rfloor \leq 2 \frac{K}{K + 1}. \quad (2.16)$$

The symmetric square case with $M_T = N_R = 4$ antennas at each node and $K = 3$ users as investigated in this work attains the maximum DoF achievable in a 3-user system:

$$\text{DoF}_{\max} = \underbrace{\frac{3}{4} \left\lfloor \frac{2 \cdot 4}{3 + 1} \right\rfloor}_{=\frac{3}{2}} = 2 \underbrace{\frac{3}{3 + 1}}_{=\frac{3}{2}}. \quad (2.17)$$

2.3.2 Closed Form Solution

The computation of a closed form analytical solution for the IA precoding matrices \mathbf{V}_j and interference suppression matrices \mathbf{U}_i for the symmetric $K = 3$ -user MIMO square case is now elaborated, following [5]. The conditions imposed on these matrices have already been defined in Equation (2.13). The truncated unitary interference suppression matrix \mathbf{U}_i describes an orthonormal basis for the interference free subspace at the i^{th} receiver. The receive signal vector is projected onto this interference free subspace as stated in Equation (2.3). To perform suppression, the received interference must lie in the $N_R - d$ dimensional nullspace of \mathbf{U}_i^H and hence

$$\text{span}(\mathbf{H}_{ij}\mathbf{V}_j) \subseteq \text{null}(\mathbf{U}_i^H), \forall i \neq j, \quad (2.18)$$

which is basically a reformulation of Condition (2.13a), giving more insight into the nature of the problem. To satisfy Conditions (2.13) and Condition (2.18), the precoding matrices might be computed as follows:

$$\mathbf{V}_2 = \nu(\mathbf{H}_{32}^{-1}\mathbf{H}_{31}\mathbf{H}_{21}^{-1}\mathbf{H}_{23}\mathbf{H}_{13}^{-1}\mathbf{H}_{12}), \quad (2.19a)$$

$$\mathbf{V}_1 = \mathbf{H}_{21}^{-1}\mathbf{H}_{23}\mathbf{H}_{13}^{-1}\mathbf{H}_{12}\mathbf{V}_2, \quad (2.19b)$$

$$\mathbf{V}_3 = \mathbf{H}_{13}^{-1}\mathbf{H}_{12}\mathbf{V}_2, \quad (2.19c)$$

where $\nu(\cdot)$ arbitrarily chooses d eigenvectors to compose \mathbf{V}_2 . This solution is clearly not unique due to the arbitrary choice of eigenvectors in Equation (2.19a) and due to the fact that any rotation inside its subspace yields another valid solution.

The corresponding interference suppression matrices are then obtained as:

$$\mathbf{U}_1 = \nu^{\text{left}}(\mathbf{H}_{12}\mathbf{V}_2), \quad (2.20a)$$

$$\mathbf{U}_2 = \nu^{\text{left}}(\mathbf{H}_{21}\mathbf{V}_1), \quad (2.20b)$$

$$\mathbf{U}_3 = \nu^{\text{left}}(\mathbf{H}_{32}\mathbf{V}_2), \quad (2.20c)$$

where $\nu^{\text{left}}(\cdot)$ arbitrarily chooses $N_R - d$ left singular vectors⁶.

The IA solution described above does not maximize the sum rate directly as it solely focuses on nulling the interference and hence maximizing the SIR at the receiver to infinity. Perfect alignment may even *reduce* the SNR as a result of projecting the receive signal vector onto the interference free subspace (see toy example in Figure 2.2). Improved iterative solutions with constraints on maximizing the Signal to Interference and Noise Ratio (SINR) have been proposed in [3, 5].

This work predominantly focuses on showing the feasibility of IA, online on a testbed. The closed form solutions presented above are hence sufficient (and efficient to compute).

⁶Let $\mathbf{A} = \mathbf{L}\mathbf{\Sigma}\mathbf{R}^H$ denote the singular value decomposition of \mathbf{A} . The columns of \mathbf{L} are called left singular vectors of \mathbf{A} .

Chapter 3

Vienna MIMO Testbed

Section 3.1 gives a hardware overview of the Vienna MIMO Testbed (VMTB), and a link to the theoretical discourse in Section 2.1 is drawn. Section 3.2 subsumes the procedures of a measurement cycle. In Section 3.3, the used signals to perform IA measurements are explained in detail and channel estimation is described. Finally, Section 3.4 focuses on the underlying software implementation performing the various measurements and provides understanding over the sequential chain of events.

3.1 Hardware and Deployment

The VMTB in the setup considered here¹ consists of two outdoor transmitter stations TX1 and TX2 located on rooftops, one indoor transmitter station TX3 and one indoor receiver station RX. Both indoor stations are located on the 5th floor of the Institute of Telecommunications at Vienna University of Technology and are within Line of Sight (LOS) of each other. This heterogeneous² setup represents an urban scenario. The deployment of all stations is depicted in Figure 3.1.

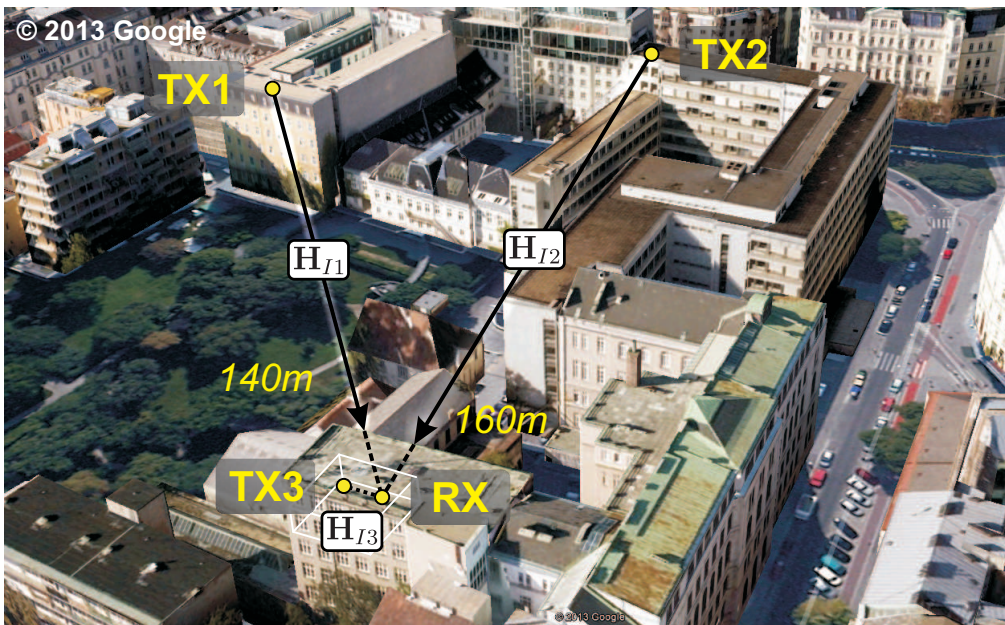


Figure 3.1: Deployment of Vienna MIMO Testbed

¹Contrary to the description in [18], transmitter station TX3 was located indoors throughout this work.

²A heterogeneous scenario in this context contains outdoor to indoor and indoor to indoor radio links.

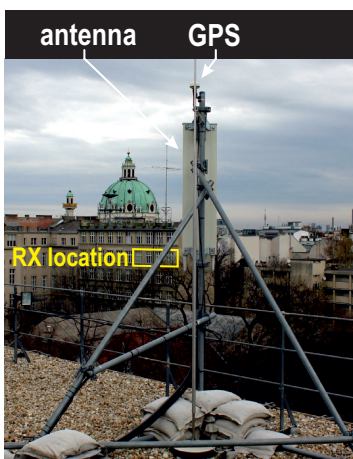


Figure 3.2: TX1 antenna setup

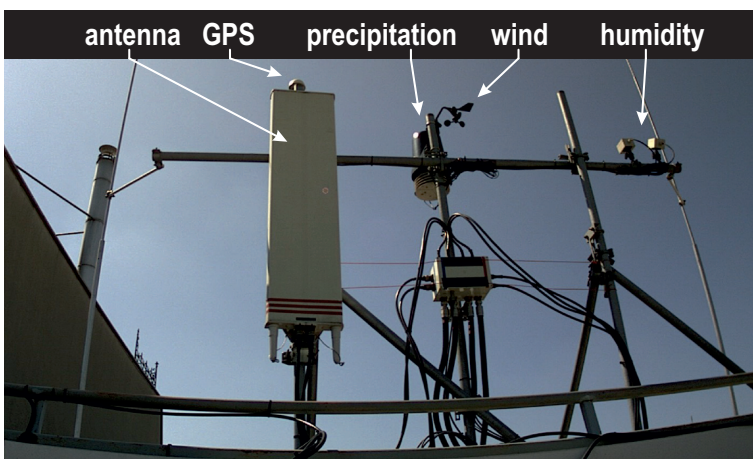


Figure 3.3: TX2 antenna setup with sensors

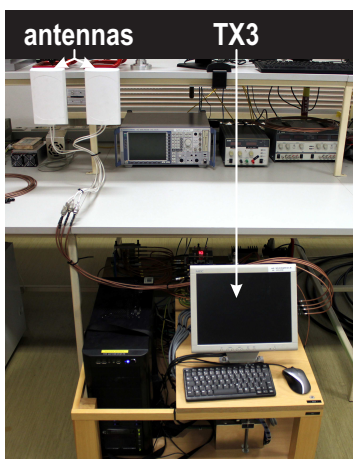


Figure 3.4: TX3 station

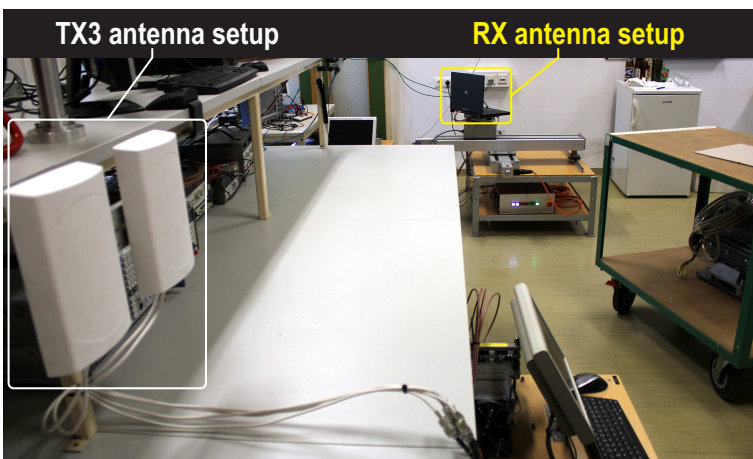


Figure 3.5: TX3 to RX indoor channel

Each station comprises a Personal Computer (PC), RF hardware, synchronization hardware and an antenna setup with 4 antennas. Figure 3.2 and Figure 3.3 show the antenna setup of transmitter TX1 and TX2, respectively. The antenna setup of TX2 employs a variety of sensors to monitor the environmental conditions. Figure 3.4 shows the indoor transmitter station of TX3, Figure 3.5 depicts the indoor LOS channel from TX3 to RX. All PCs are connected via a dedicated fiber network to communicate with each other.

Comparing this setup to the $K = 3$ -user interference channel depicted in Figure 2.1, the absence of two receivers is recognized. RX is chosen as counterpart of the desired transmitter, selectable from $j \in \{1, 2, 3\}$. The resulting *desired link* is denoted as $I \in \{1, 2, 3\}$, where $i = j = I$ on the desired link. For example, the desired transmitter shall be TX1 ($j = 1$). The corresponding receiver therefore is RX1 ($i = 1$). The desired link is $I = 1$, and RX plays the role of RX1. Channels to the remaining two receivers are chosen randomly as defined in Section 3.3.3 to compensate for their absence.

3.1.1 Transmitter

The transmit-hardware included in all three transmitter stations (TX1, TX2 and TX3) is now characterized, subsuming the detailed description in [19]. Figure 3.6 shows the basic structure of a transmitter.

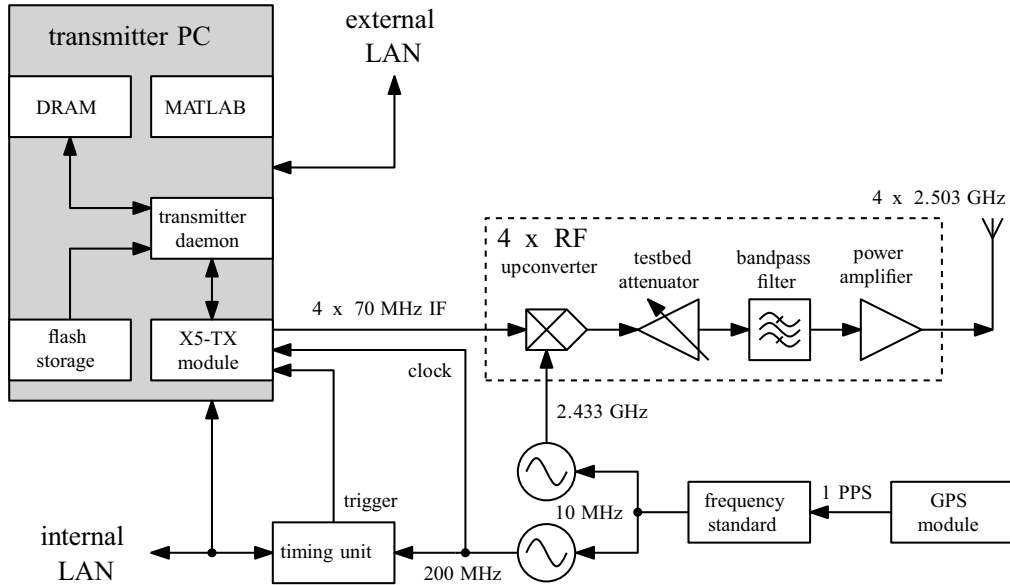


Figure 3.6: Transmitter overview [19]

- Transmitter PC:** Contains an INNOVATIVE INTEGRATION X5-TX FIFO Digital to Analog Conversion (DAC) card that generates transmit samples at 70 MHz Intermediate Frequency (IF). The X5-TX card includes four channels, works at sampling frequency 200 MHz and has a resolution of 16 bit. For the measurements in this work, an efficient C++³ transmit routine was developed (see Section 3.4.2) that generates the IF samples and stores them directly in the DRAM⁴ which results in high transmission rates. Alternatively, the transmit samples can be stored on a flash storage device embodied by a SSD⁵. A MATLAB⁶ daemon that is responsible for start-up and initialization tasks prior to measurements is running on each transmitter PC. All PCs are connected via a dedicated fiber network (LAN⁷). The transmit routine is invoked via LAN.
- RF Hardware:** The RF chain contains an upconverter that filters the 70 MHz IF from the X5-TX module and converts it up to 2.503 GHz transmit frequency. The bandpass filter has a bandwidth of 20 MHz. The maximum output power of the chain is 35 dBm and can be attenuated by an AEROFLEX 4226 digitally programmable attenuator that allows attenuations from 0 dB to 63 dB with 1 dB step size. These attenuators will be used to control the transmit power of each transmitter individually.

³C++ is an object oriented compiled programming language.

⁴DRAM... Dynamic Random Access Memory

⁵SSD... Solid State Drive

⁶MATLAB is a numerical computing environment and programming language developed by MathWorks.

⁷LAN... Local Area Network

- **Synchronization Hardware:** A common timebase for the whole testbed is derived from a TRIMBLE Acutime GPS⁸ module. The so obtained PPS⁹ signal is used by a STANFORD RESEARCH SYSTEM Rubidium FS725 frequency standard to output a precise 10 MHz reference for the oscillators depicted in Figure 3.6. The reference is thereby used to generate the clock for the local oscillator used for upconversion, the X5-TX card and the timing unit. The timing unit responsible for synchronization and triggering the X5-TX module is described in [20].
- **Antenna Setup:** Whereas the transmit hardware described previously is built on a wooden desk mounted on wheels, the antennas might be located elsewhere (still connected with cables). In case of TX1 and TX2, they are outdoors on rooftops as illustrated in Figure 3.2 and Figure 3.3. Every setup comprises $M_T = 4$ antennas. The used antenna types are now listed:

TX1, TX2: KATHREIN Scala Division 60° XX-pol panel antenna (800 10543)

TX3: 2 × KATHREIN Scala Division X-pol directional indoor antenna (800 10677)

3.1.2 Receiver

An overview of the receive hardware of RX is now provided, summarizing the detailed work of [21]. Figure 3.7 shows the basic structure of the receiver.

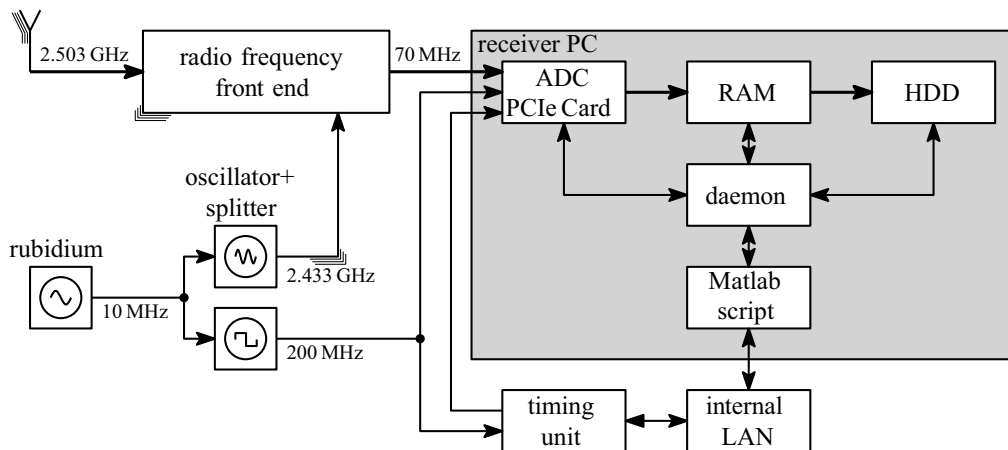


Figure 3.7: Receiver overview [21]

- **Receiver PC:** Contains an INNOVATIVE INTEGRATION X5-RX FIFO Analog to Digital Conversion (ADC) card that fetches the receive samples at 70 MHz IF. Similar to the X5-TX card, it includes four channels, works at sampling frequency 200 MHz and has a resolution of 16 bit. The receive samples are stored on a RAMDrive¹⁰ which allows fast processing. RX is also the control node in the system. Measurement script (see Section 3.4.1) and thus transmissions are invoked from here.

⁸GPS... Global Positioning System

⁹PPS... Pulse Per Second

¹⁰RAMDrive is a virtually generated drive in the random access memory that entails higher reading and writing speeds than conventional hard disk drives.

- **RF Hardware:** The radio frequency front end receives the signal at center frequency 2.503 GHz and includes several filtering operations, downconversion to 70 MHz IF and amplification before the signal is fed into the X5-RX card.
- **Synchronization Hardware:** Essentially the same function as at the transmitters - see Section 3.1.1.
- **Antenna Setup:** The $N_R = 4$ receive antennas of RX are custom built and implemented in the shell of a laptop (see Figure 3.8) that resembles a possible user equipment. This laptop is mounted on a $3\lambda \times 3\lambda \times 360^\circ$ x-y- ϕ positioning table as depicted in Figure 3.9. The antennas are $\frac{\lambda}{2}$ dipoles that have not been fully characterized in a measurement chamber by the time this work was written.

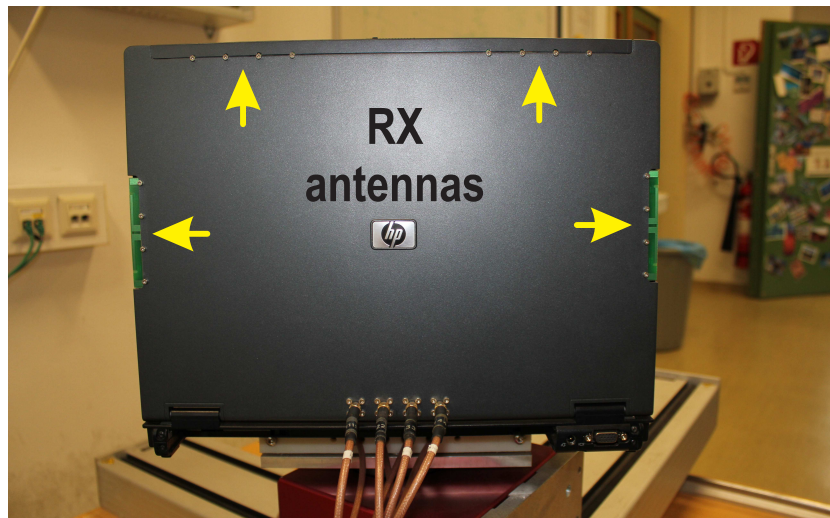


Figure 3.8: RX antennas in laptop shell

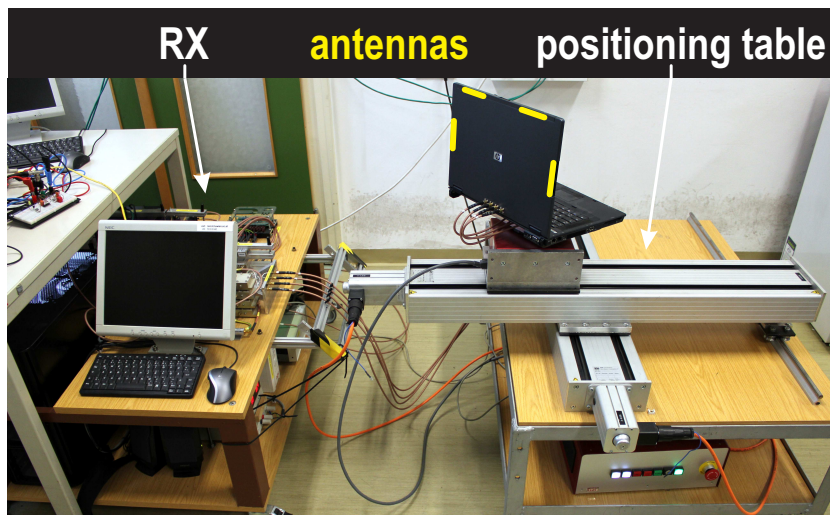


Figure 3.9: RX station

3.2 Measurement Methodology

A measurement cycle entails successive frame transmissions. Each frame contains a pilot preamble and data. Let the frames (and hence transmissions) be indexed by l . The pilot preamble of frame (l) is used to compute the estimated channel matrices $\hat{\mathbf{H}}_{Ij}^{(l)}$, where I denotes the desired link and $j \in \{1, 2, 3\}$ the used transmitters. The estimated channel matrices are used to compute the precoding matrices $\mathbf{V}_j^{(l)}$ and interference suppression matrices $\mathbf{U}_i^{(l)}$. These are then applied on the data of frame ($l + 1$). The process is illustrated in Figure 3.10. IA as used here hence requires constant channels to work perfectly, a requirement that will not be met in the real world. However, by keeping the processing time T_p between two consecutive frames as low as possible, the channels in a quasi-static setup hardly change (the filters \mathbf{U}_i and \mathbf{V}_j computed from frame (l) are suitable but not ideal for the channel realization at frame ($l + 1$)).

Computation of channel estimates, precoding matrices and interference suppression matrices takes place online. The evaluation and validation of IA takes place offline.

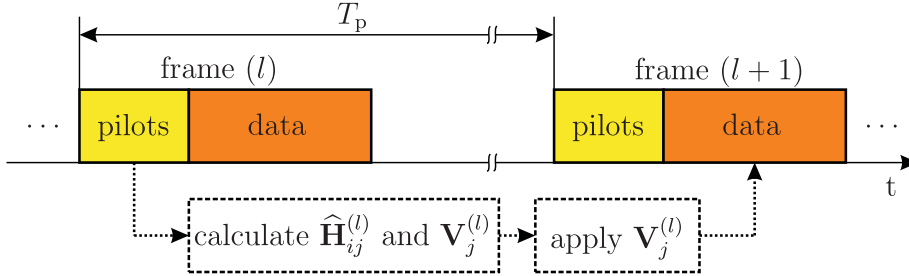


Figure 3.10: Two consecutive transmit frames

3.3 Signals and Channel Estimation

Orthogonal Frequency Division Multiplexing (OFDM) is used as modulation format. The computational complexity increases with the number of subcarriers, since channel estimation and precoder computation has to be performed on each subcarrier individually. To ensure fast processing times between frames (see Figure 3.10), only one subcarrier is used in this work. This is sufficient to show the feasibility of IA. Furthermore, no subcarrier indexation is needed in the description. The general signal specifications are listed in Table 3.1.

| parameter | value |
|------------------------|---------------|
| sampling rate | 200 MHz |
| oversampling factor | 13 |
| subcarrier spacing | 15.02 kHz |
| FFT length | 1024 |
| symbol duration | 66.56 μ s |
| cyclic prefix duration | 4.94 μ s |
| signal constellation | 4 QAM |

Table 3.1: Signal specifications

3.3.1 Transmit Signals

The generation of an OFDM transmit symbol from symbol level to Intermediate Frequency (IF) samples is now discussed. First, the single antenna case with no precoding matrix is explained. The transmit symbols of one OFDM symbol are defined in frequency domain. Up to $C = 1024$ (number of subcarriers) symbols are accommodated in one OFDM symbol. Let c denote the subcarrier index and k the sample index (time). In general, the baseband samples $x^{\text{BB}}[k]$ of one OFDM symbol are obtained by a C -point Inverse Fast Fourier Transform (IFFT) applied on the symbols in frequency domain $S[c]$:

$$x^{\text{BB}}[k] = \frac{1}{C} \sum_{c=0}^{C-1} S[c] \exp\left(j2\pi \frac{tc}{C}\right), \quad 0 \leq k < C. \quad (3.1)$$

This work restricts itself to only one subcarrier, namely the DC subcarrier at 0 Hz. The corresponding symbol is $S = S[0]$, the other symbols are zero. Considering this in Equation (3.1), the resulting baseband samples of one OFDM symbol will just be a repetition of the scaled frequency domain symbol:

$$x^{\text{BB}}[k] = \frac{1}{C} S, \quad 0 \leq k < C. \quad (3.2)$$

The cyclic prefix is attached by inserting a copy of the last $N_{\text{CP}} = 72$ samples before the OFDM symbol. One OFDM symbol contains $C = 1024$ samples, its duration¹¹ is $1024 \cdot 5 \text{ ns} = 5.12 \mu\text{s}$. To increase the duration to $66.56 \mu\text{s}$, upsampling with factor 13 is performed by repeating each sample 13 times. The resulting signal is then upconverted to 70 MHz IF. Furthermore, scaling factors are introduced. The IF transmit samples are:

$$\begin{aligned} x^{\text{IF}}[k] &= \underbrace{C\sqrt{2}}_{\text{scaling}} \Re \left\{ \underbrace{\frac{1}{C} S \exp\left(j2\pi \frac{70}{200} k\right)}_{\text{upconversion}} \right\} \\ &= \sqrt{2} \Re \left\{ S \exp\left(j2\pi \frac{70}{200} k\right) \right\} \\ &= \frac{1}{\sqrt{2}} \left(S \exp\left(j2\pi \frac{70}{200} k\right) + S^* \exp\left(-j2\pi \frac{70}{200} k\right) \right), \quad 0 \leq k < 13(N_{\text{CP}} + C). \end{aligned} \quad (3.3)$$

Since the the X5-TX FIFO DAC card requires 16 bit integer values, samples are scaled with a DAC scaling factor and converted from floating point to integer values:

$$\tilde{x}^{\text{IF}}[k] = \lfloor \text{DACscaling} \cdot x^{\text{IF}}[k] \rfloor, \quad 0 \leq k < 13(N_{\text{CP}} + C). \quad (3.4)$$

These are the final OFDM symbol samples that are ready to be written into memory for transmission.

Advancing to the multiple antenna case with precoding matrix, the symbols are stored in a vector

$$\mathbf{s}[c] = \begin{bmatrix} S_0[c] \\ S_1[c] \\ \vdots \\ S_{d-1}[c] \end{bmatrix}, \quad (3.5)$$

¹¹Sampling frequency of the DAC/ADC cards is fixed at 200 MHz.

where d denotes the number of data streams. The precoding matrix $\mathbf{V} \in \mathbb{C}^{M_T \times d}$ is applied at symbol level. The baseband samples $\mathbf{x}^{\text{BB}}[k] \in \mathbb{C}^{M_T}$ of an OFDM symbol are generally obtained by applying a C -point IFFT on the elements of the symbol vector $\mathbf{s}[c]$ as

$$\mathbf{x}^{\text{BB}}[k] = \frac{1}{C} \sum_{c=0}^{C-1} \mathbf{V}[c] \mathbf{s}[c] \exp\left(j2\pi \frac{tc}{C}\right), \quad 0 \leq k < C. \quad (3.6)$$

Utilizing only the DC subcarrier $c = 0$ and following the same steps as before, the transmit signal vector at 70 MHz IF $\mathbf{x}^{\text{IF}}[k] \in \mathbb{R}^{M_T}$ becomes

$$\mathbf{x}^{\text{IF}}[k] = \sqrt{2} \Re \left\{ \mathbf{V} \mathbf{s} \exp\left(j2\pi k \frac{70}{200}\right) \right\}, \quad 0 \leq k < 13(N_{\text{CP}} + C). \quad (3.7)$$

Finally, conversion to integer values is performed:

$$\tilde{\mathbf{x}}^{\text{IF}}[k] = \lfloor \text{DACscaling} \cdot \mathbf{x}^{\text{IF}}[k] \rfloor, \quad 0 \leq k < 13(N_{\text{CP}} + C). \quad (3.8)$$

These are the final OFDM symbol samples $\tilde{\mathbf{x}}^{\text{IF}}[k] \in \mathbb{N}_{0+}^{M_T}$ that are ready to be written into memory for transmission. $M_T = 4$ channels are utilized on the VMTB.

There is an important difference between the generation of pilot and data samples:

- **Pilots:** *No* precoding matrix is applied, symbols are generated individually for each antenna as described in Section 3.3.3. Symbols stay constant over the whole measurement cycle. IF samples are generated offline for each antenna individually prior to the measurement cycle as in Equation (3.4).
- **Data:** Precoding matrix \mathbf{V} is applied, transmit symbols are generated randomly prior to the measurement cycle by RX and passed to the transmitters during the measurement cycle via the dedicated fiber network. IF samples are generated online at the transmitters as in Equation (3.8). Precoding matrices are calculated online for each transmission and stay constant for one frame.

3.3.2 Receive Signals

First, the interference free single antenna case is discussed. The transmit signal from Equation (3.4) is transmitted over a linear time-invariant channel with baseband impulse response $h[k]$ of length L samples:

$$\tilde{y}^{\text{IF}}[k] = [h^{\text{IF}}[k] * \tilde{x}^{\text{IF}}[k]], \quad (3.9)$$

where $h^{\text{IF}}[k] = 2\Re\{h[k] \exp(j2\pi\frac{70}{200}k)\}$ is the equivalent IF impulse response. The error due to quantization at the receiver is modeled as noise which will be omitted in the following description. The 16 bit integer receive samples at 70 MHz IF $\tilde{y}^{\text{IF}}[k] \in \mathbb{N}_{0+}$ of one time dispersed OFDM symbol (cyclic prefix discarded) are read out from RAMDrive and converted back to floating point values

$$y^{\text{IF}}[k] = \frac{1}{\text{DACscaling}} \cdot \tilde{y}^{\text{IF}}[k], \quad \left\lfloor \frac{L}{2} \right\rfloor + 13N_{\text{CP}} - 1 \leq k < 13(N_{\text{CP}} + C) + \left\lfloor \frac{L}{2} \right\rfloor - 2. \quad (3.10)$$

Scaling and downconversion is then performed on the OFDM symbol samples according to:

$$\begin{aligned} y^{\text{BB,US}}[k] &= \underbrace{\frac{\sqrt{2}}{C}}_{\text{scaling}} y^{\text{IF}}[k] \underbrace{\exp\left(-j2\pi k \frac{70}{200}\right)}_{\text{downconversion}} \\ &= \frac{\sqrt{2}}{C} (h^{\text{IF}}[k] * x^{\text{IF}}[k]) \exp\left(-j2\pi k \frac{70}{200}\right) \\ &= h[k] * x^{\text{BB,US}}[k] + (h[k] * x^{\text{BB,US}}[k])^* \exp\left(-j2\pi k \frac{2 \cdot 70}{200}\right), \\ &\quad \left\lfloor \frac{L}{2} \right\rfloor + 13N_{\text{CP}} - 1 \leq k < 13(N_{\text{CP}} + C) + \left\lfloor \frac{L}{2} \right\rfloor - 2. \end{aligned} \quad (3.11)$$

The baseband OFDM symbol is then downsampled by factor 13. This is done by retaining only every 13th sample in the upsampled baseband symbol samples $y^{\text{BB,US}}[k]$ and applying a lowpass filter that suppresses the frequency component at -140 MHz. A C -point Fast Fourier Transform (FFT) is applied and the received symbols in frequency domain are:

$$R[c] = \sum_{k=0}^{C-1} y[k]^{\text{BB}} \exp\left(-j2\pi \frac{ct}{C}\right), \quad 0 \leq c < C. \quad (3.12)$$

Since only the DC subcarrier $c = 0$ was utilized in the transmission, the received symbol is

$$R = R[0] = H[0]S[0], \quad (3.13)$$

where $H[c]$ is the Fourier transform of the downsampled and filtered impulse response. Due to the usage of a cyclic prefix with $N_{\text{CP}} \geq L$, no inter-symbol interference occurs if more than one OFDM symbol is transmitted.

Advancing to the multiple antenna case with interference, a vector of sample instances at 70 MHz IF $\tilde{\mathbf{y}}^{\text{IF}}[k] \in \mathbb{N}_{0+}^N$ is received whose elements are obtained as

$$\tilde{y}_n^{\text{IF}}[k] = \left[\sum_{m=0}^{KM_{\text{T}}-1} h_{nm}^{\text{IF}}[k] * \tilde{x}_m^{\text{IF}}[k] \right], \quad (3.14)$$

where m denotes the transmit antenna index, n the receive antenna index, $h_{nm}^{\text{IF}}[k]$ the channel impulse response between two antennas at IF and the total number of transmit antennas is

obtained as KM_T since the system as in Figure 2.1 has K transmitters with M_T antennas each. The elements of $\tilde{\mathbf{y}}^{\text{IF}}[k]$ are then converted to floating point values the same way as in Equation 3.10. Scaling, downconversion, downsampling and filtering is performed.

Equivalently to the transmit signals, there is a difference in the receive sample processing of pilots and data:

- **Pilots:** No interference suppression matrix is applied, receive symbols at each antenna are stacked in a vector $\mathbf{r} = [R_0, R_1, \dots, R_{N_R-1}]^T$ which is obtained as

$$\mathbf{r} = \mathbf{H}\mathbf{s} + \mathbf{n}. \quad (3.15)$$

- **Data:** Interference suppression matrix $\mathbf{U} \in \mathbb{C}^{N_R \times d}$ is applied, receive symbols at each data stream are stacked in a vector $\mathbf{r} = [R_0, R_1, \dots, R_{d-1}]^T$ which is obtained as

$$\mathbf{r} = \mathbf{U}^H \mathbf{H} \mathbf{V} \mathbf{s} + \mathbf{U}^H \mathbf{n}. \quad (3.16)$$

This formulation is equivalent to the interference channel formulation in Equation (2.3).

The overall channel matrix $\mathbf{H} \in \mathbb{C}^{N_R \times KM_T}$ contains the complex valued channel coefficients $(\mathbf{H})_{nm}$ from transmit antenna m to receive antenna n . In the case of $K = 3$ transmitters:

$$\begin{aligned} \mathbf{r} &= \mathbf{r}_I, \\ \mathbf{U} &= \mathbf{U}_I, \\ \mathbf{H} &= \begin{bmatrix} \mathbf{H}_{I1} & \mathbf{H}_{I2} & \mathbf{H}_{I3} \end{bmatrix}, \\ \mathbf{V} &= \begin{bmatrix} \mathbf{V}_1 \\ \mathbf{V}_2 \\ \mathbf{V}_3 \end{bmatrix}, \\ \mathbf{s} &= \begin{bmatrix} \mathbf{s}_1 \\ \mathbf{s}_2 \\ \mathbf{s}_3 \end{bmatrix}, \\ \mathbf{n} &= \mathbf{n}_I, \end{aligned} \quad (3.17)$$

where I denotes the desired link index.

3.3.3 Channel Estimation

Channel coefficients $(\mathbf{H})_{nm}$ from every transmit antenna $m = \{0, \dots, KM_T - 1\}$ to every receive antenna $n = \{0, \dots, N_R - 1\}$ are estimated. The channel is assumed to stay constant during one frame. A pilot preamble in every frame contains pilot symbols for channel estimation, see Figure 3.10. Note that in the following, t denotes the OFDM symbol index (time). Orthogonal symbol sequences optimal for multiple antenna systems are used as proposed in [22]. The sequence length depends on the number of transmit antennas. The length 16 QPSK sequence

$$S^P = \{1, 1, 1, 1, 1, j, -1, -j, 1, -1, 1, -1, 1, -j, -1, j\}$$

is used, it is circularly shifted by one symbol for each transmit antenna m :

$$S_m^P[t] = S^P[(t + m) \bmod 16]. \quad (3.18)$$

The sequence is orthogonal to circularly shifted instances of itself, the cyclic autocorrelation function $\rho[q]$ has zero off peaks:

$$\rho_{S^P}[q] = \frac{1}{16} \sum_{t=0}^{15} S^P[t \bmod 16] \cdot (S^P[(t - q) \bmod 16])^* = \delta[q]. \quad (3.19)$$

Therefore, up to 16 orthogonal sequences can be generated from S^P and up to 16 transmit antennas are supported.

Channel Estimation is performed at receiver $I \in \{1, 2, 3\}$ via cross-correlation of the receive symbol sequence $R_n[t]$ with the known transmit symbol sequence $S_m^P[t]$ (Equation (3.18)). Assuming perfect synchronization so that the pilot sequences are received at the same time, the channel coefficient from transmit antenna m to receive antenna n is obtained as

$$\begin{aligned} (\hat{\mathbf{H}})_{nm} &= \rho_{R_n, S_m^P}[0] = \\ &= \frac{1}{16} \sum_{t=0}^{15} \underbrace{\left(\sum_{m'=0}^{KM_T-1} (\mathbf{H})_{nm'} S_{m'}^P[t] + n_n[t] \right)}_{R_n[t]} \cdot (S_m^P[t])^* \\ &= (\mathbf{H})_{nm} \underbrace{\frac{1}{16} \sum_{t=0}^{15} S_m^P[t] \cdot (S_m^P[t])^*}_{=1} + \sum_{\substack{m'=0 \\ m' \neq m}}^{KM_T-1} (\mathbf{H})_{nm'} \underbrace{\frac{1}{16} \sum_{t=0}^{15} S_{m'}^P[t] \cdot (S_m^P[t])^*}_{=0} \\ &\quad + \underbrace{\frac{1}{16} \sum_{t=0}^{15} n_n[t] \cdot (S_m^P[t])^*}_{=\tilde{n}_n} \\ &= (\mathbf{H})_{nm} + \tilde{n}_n. \end{aligned} \quad (3.20)$$

The estimated matrix contains the estimated channel matrices from all transmitters $j \in \{1, 2, 3\}$ to desired receiver I ,

$$\hat{\mathbf{H}} = \begin{bmatrix} \hat{\mathbf{H}}_{I1} & \hat{\mathbf{H}}_{I2} & \hat{\mathbf{H}}_{I3} \end{bmatrix}. \quad (3.21)$$

The remaining channel matrices, called virtual channel matrices, are generated randomly as (full rank) complex Gaussian matrices:

$$\hat{\mathbf{H}}_{ij} \sim \mathcal{CN}(\mathbf{0}, \mathbf{I}_{M_T}), \quad i \in \{1, 2, 3\} \wedge i \neq I, \quad j \in \{1, 2, 3\}. \quad (3.22)$$

They are generated prior to a measurement cycle and stay constant for the whole cycle.

3.4 Software and Control

3.4.1 Measurement

The MATLAB *measurement script* is now explained in detail. The sequence of events is illustrated in Figure 3.13. The description focuses on the main flow of the script rather than explaining every function in detail. The step numbers coincide with the sequence numbers in Figure 3.13.

1. The name of the measurement is defined, for example `dummy`. The default paths are then generated as follows:

`pathTX: D:\hiatus\ ...local on the TX PCs`

`pathRX: G:\hiatus\ ...local on the RX PC, this is the RAMDrive`

`pathMeasurement: S:\30_HIATUS\Measurements\dummy\ ...on testbed server`

2. Settings are loaded. To that end, the `loadSettings('settings')` function is executed. It contains predefined settings for the measurement selected by the parameter string `'settings'`.
3. Pilot symbols are generated according to `'settings'`. Then, OFDM symbol samples are created (see Section 3.3.1 for details). The parameter `settings.OFDMTrainingSequence` contains the used pilot sequence. Default value is: `settings.OFDMTrainingSequence = TrainingSequence16`. This is a 4 QAM sequence that is orthogonal to circularly shifted versions of itself (find details in Section 3.3.3). It supports channel estimation with up to 16 transmit antennas. `TrainingSequence16 = [1,1,1,1,1,1i,-1,-1i,1,-1,1,-1,1,-1i,-1,1i]`
4. Data symbols for all transmissions are generated according to `'settings'`. Since 4 QAM symbols entail a finite alphabet, it suffices to store the symbol indices as depicted in Table 3.2. “Zero symbols” (0) are also possible. For each transmission, the data symbol indices are sent to the respective transmitters via the fiber network included in an UDP¹² message.

| symbol | index |
|----------|-------|
| 0 | 0 |
| $1 + j$ | 1 |
| $-1 + j$ | 2 |
| $-1 - j$ | 3 |
| $1 - j$ | 4 |

Table 3.2: Transmit symbol indices of 4 QAM alphabet

5. Initial transmit signal samples are created. Figure 3.11 shows the basic composition of a transmit signal. The zero padding is used for transmitter synchronization (see step 7) and

¹²UDP... User Datagram Protocol

to measure the noise variance. At the initial stage, the data is all zero. The position of the first data sample and the total length of the signal is important. `ZeroPaddingEnd` is calculated so that the total number of samples is a multiple of 512 which is a requirement of the X5-TX FIFO card.



Figure 3.11: Basic transmit signal of a single transmission

6. Loop over all selected transmitters indexed by j . The parameter vector `settings.usedTransmitters` defines which transmitters are used in the measurement. Default value is:
`settings.usedTransmitters = [1,2,3]`.
7. $[j]$ ¹³ The initial transmit signal samples are circularly shifted, for each transmitter individually. The goal is to compensate for the different propagation delays on sample basis¹⁴. The receiver expects samples at the synchronization trigger. By circularly shifting the transmit signals to the left, the propagation delays are compensated and the signals are received concurrently at the trigger instance, keeping the pilot sequences orthogonal. Figure 3.12 illustrates this process. Because neither the employed transmitters nor the receiver moves (except for the receive table whose movement is negligible in terms of synchronization), the sample delays are constant and no synchronization sequences are needed. The parameter vector `settings.sampleDelay` defines the sample offsets. Default value is:
`settings.sampleDelay = [710,730,630]`.

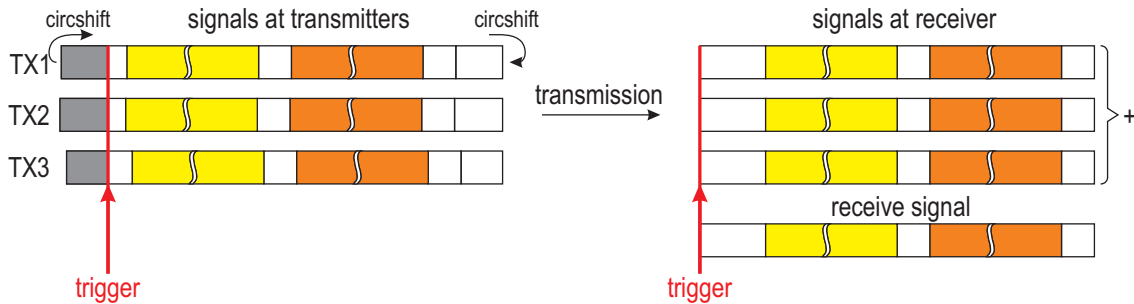


Figure 3.12: Compensation of propagation delays

8. $[j]$ Circularly shifted initial transmit signal samples are stored on the SSD of the respective transmitter.
9. Testbed is initialized. This process encompasses following steps:
 - bind required UDP sockets
 - ping transmitters, check ARP, check GPS, check Rubidium

¹³ $[variable...]$ this symbol denotes being in a loop with counting index $variable$

¹⁴Sampling rate is 200MHz. Sample duration therefore is 5ns.

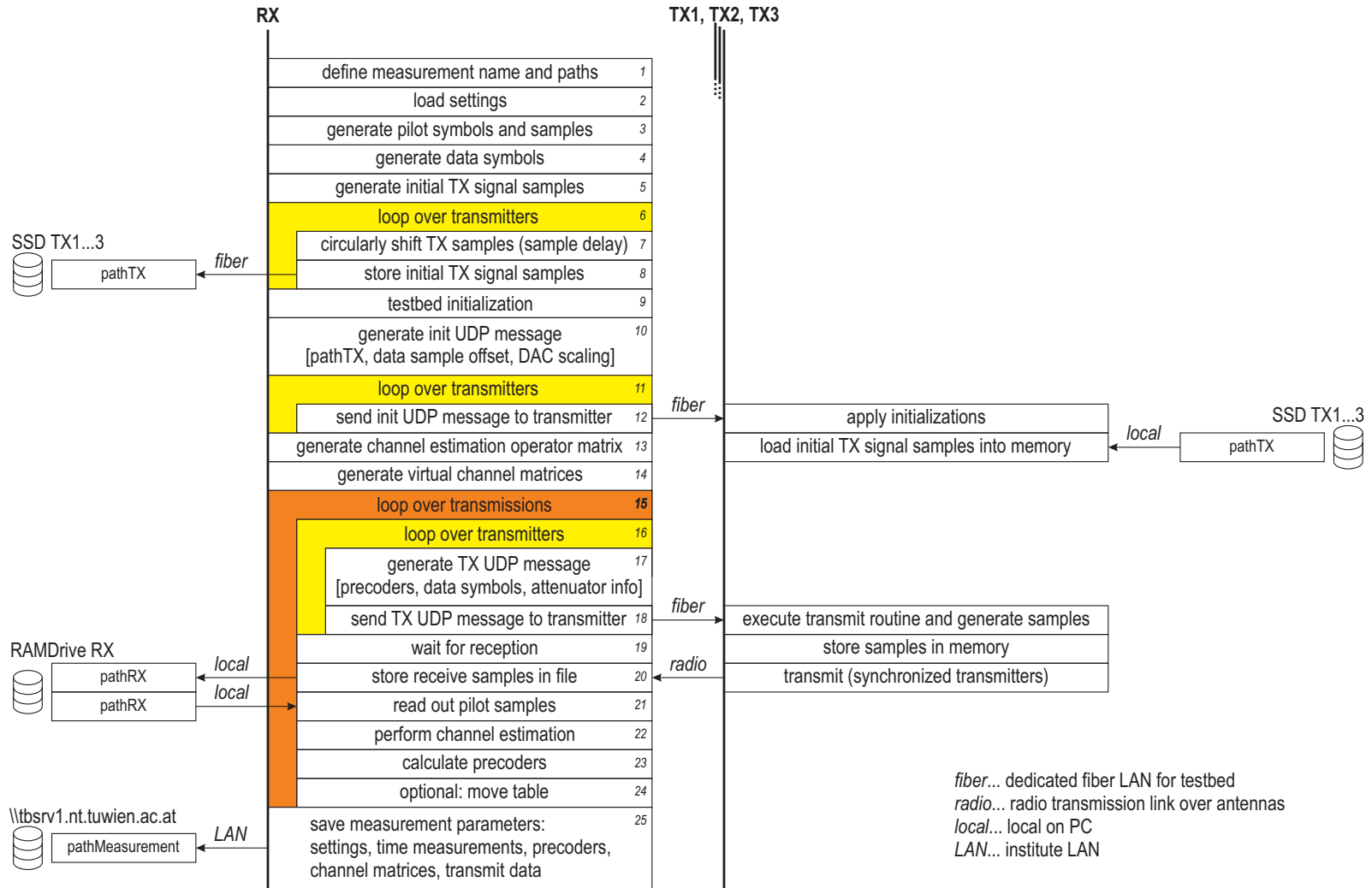
- calibrate DACs
 - initialize synchronization units
10. Initial UDP message is created. It is intended to pass initial information to the transmitters, such as:
 - `pathTX`: Tells the transmitters where the initial data is stored.
 - data sample offset: Tells the transmitters where the data samples begin in the total transmit signal. This is important later on because the transmit routine that generates the data samples online has to know where to write them into the memory.
 - DAC scaling: The DAC works with 16 bit integer values (all samples that are loaded into the X5-TX FIFO card memory have to be in that format). The transmit signal samples have to be converted from floating point to 16 bit integer according to Equation (3.4). Default value is:
`settings.DACscaling = 214.3/settings.numTxAntennasTotal`.
 11. Loop over all selected transmitters indexed by j .
 12. \lceil_j Initial UDP message created in step 10 is sent to the transmitters via dedicated fiber network.
 13. The channel estimation operator matrix \mathbf{Z} is generated. Channel estimation (see Section 3.3.3 for details) is thereby reduced to a multiplication of the pilot receive samples \mathbf{y}_p with the estimation operator matrix:

$$\hat{\mathbf{H}} = \begin{bmatrix} \hat{\mathbf{H}}_{I1} & \hat{\mathbf{H}}_{I2} & \hat{\mathbf{H}}_{I3} \end{bmatrix} = \mathbf{y}_p \mathbf{Z}.$$

14. Virtual channel matrices for the non-existing receivers are generated according to Equation (3.22).
15. Loop over transmissions indexed by l . One measurement cycle entails `settings.numTransmissions` transmissions.
16. \lceil_l Loop over transmitters indexed by j .
17. $\lceil_l \lceil_j$ Generate transmit UDP message for each transmitter individually. The message contains:
 - precoders: these are the precoding matrices \mathbf{V}_j
 - data symbols: 4 QAM symbol indices as generated in step 4
 - attenuator info: 6 bit hardware attenuator value
18. $\lceil_l \lceil_j$ Send transmit UDP message. The respective transmitter then executes the C++ transmit routine to generate the transmit data samples (see Section 3.4.2).
19. \lceil_l While the transmitters are generating the samples and store them in the memory of their X5-TX FIFO card, the receiver RX is waiting.
20. \lceil_l Transmission is triggered and samples are received and stored on the RAMDrive of RX.

21. [l When transmission is over and receiver is ready, the pilot samples are read out from the RAMDrive. The remaining signal samples, namely data and noise samples, are used in the offline evaluation.
22. [l Channel estimation is performed according to step 13.
23. [l The precoders \mathbf{V}_j and interference suppression matrices \mathbf{U}_i are calculated with the closed form solution defined in Section 2.3.2.
24. [l Optional: table is repositioned.
25. The measurement cycle is finished and the parameters are stored:
 - `settings` → `pathMeasurement\dummy_settings.mat`
used settings of the measurement
 - `time measurements` → `pathMeasurement\dummy_Measurements.mat`
timing measurements
 - `precoders` → `pathMeasurement\dummy_UV_stored.mat`
precoding matrices and interference suppression matrices of each transmission
 - `channel matrices` → `pathMeasurement\dummy_H_stored.mat`
channel matrices of each transmission (estimated and virtually created ones)
 - `transmit data` → `pathMeasurement\dummy_TxData.mat`
transmitted data symbols of each transmission

Figure 3.13: Measurement script



3.4.2 Transmit Routine

For each frame, the C++ transmit routine newly generates data samples out of the number encoded data symbols that are passed from RX to the transmitters. This has to be done in an efficient manner to keep the processing time T_p between frame transmissions low. To that end, Equation (3.3) is studied and following aspects lead to an efficient implementation:

- Equation (3.3) can further be decomposed:

$$x^{\text{IF}}[k] = \sqrt{2}S_{\text{re}}\cos\left(2\pi\frac{70}{200}k\right) - \sqrt{2}S_{\text{im}}\sin\left(2\pi\frac{70}{200}k\right), \quad 0 \leq k < 13(N_{\text{CP}} + C),$$

where S_{re} and S_{im} denote the real and imaginary part of symbol S , respectively.

- The upconversion multipliers $\cos\left(2\pi\frac{70}{200}k\right)$ and $\sin\left(2\pi\frac{70}{200}k\right)$ have a periodicity of 20 samples. Two tables, each containing 20 values, can be computed in advance.
- The baseband samples of one OFDM symbol are constant because only the DC subcarrier is used (see Equation (3.2)). Therefore, the OFDM symbol samples are just a repetition of the upconversion table values multiplied with the symbol value.
- Cyclic prefix length N_{CP} is chosen in order to make the total number of samples of the OFDM symbol including cyclic prefix a multiple of 20:

$$13(N_{\text{CP}} + C) \bmod 20 = 0.$$

This way, concatenation of OFDM symbols does not lead to phase jumps in the upconversion multipliers.

- Finally, assuming $M_{\text{T}} = 4$ and $d = 2$, the elements of the transmit signal vector $\mathbf{x}^{\text{IF}}[k]$ including precoding as in Equation (3.7) are obtained as:

$$\begin{aligned} x_0^{\text{IF}}[k] &= \sqrt{2} (V_{00,\text{re}}S_{0,\text{re}}[k] - V_{00,\text{im}}S_{0,\text{im}}[k] + V_{01,\text{re}}S_{1,\text{re}}[k] - V_{01,\text{im}}S_{1,\text{im}}[k]) \cos\left(2\pi\frac{70}{200}k\right) \\ &\quad - \sqrt{2} (V_{00,\text{re}}S_{0,\text{im}}[k] + V_{00,\text{im}}S_{0,\text{re}}[k] + V_{01,\text{re}}S_{1,\text{im}}[k] + V_{01,\text{im}}S_{1,\text{re}}[k]) \sin\left(2\pi\frac{70}{200}k\right), \\ x_1^{\text{IF}}[k] &= \sqrt{2} (V_{10,\text{re}}S_{0,\text{re}}[k] - V_{10,\text{im}}S_{0,\text{im}}[k] + V_{11,\text{re}}S_{1,\text{re}}[k] - V_{11,\text{im}}S_{1,\text{im}}[k]) \cos\left(2\pi\frac{70}{200}k\right) \\ &\quad - \sqrt{2} (V_{10,\text{re}}S_{0,\text{im}}[k] + V_{10,\text{im}}S_{0,\text{re}}[k] + V_{11,\text{re}}S_{1,\text{im}}[k] + V_{11,\text{im}}S_{1,\text{re}}[k]) \sin\left(2\pi\frac{70}{200}k\right), \\ x_2^{\text{IF}}[k] &= \sqrt{2} (V_{20,\text{re}}S_{0,\text{re}}[k] - V_{20,\text{im}}S_{0,\text{im}}[k] + V_{21,\text{re}}S_{1,\text{re}}[k] - V_{21,\text{im}}S_{1,\text{im}}[k]) \cos\left(2\pi\frac{70}{200}k\right) \\ &\quad - \sqrt{2} (V_{20,\text{re}}S_{0,\text{im}}[k] + V_{20,\text{im}}S_{0,\text{re}}[k] + V_{21,\text{re}}S_{1,\text{im}}[k] + V_{21,\text{im}}S_{1,\text{re}}[k]) \sin\left(2\pi\frac{70}{200}k\right), \\ x_3^{\text{IF}}[k] &= \sqrt{2} (V_{30,\text{re}}S_{0,\text{re}}[k] - V_{30,\text{im}}S_{0,\text{im}}[k] + V_{31,\text{re}}S_{1,\text{re}}[k] - V_{31,\text{im}}S_{1,\text{im}}[k]) \cos\left(2\pi\frac{70}{200}k\right) \\ &\quad - \sqrt{2} (V_{30,\text{re}}S_{0,\text{im}}[k] + V_{30,\text{im}}S_{0,\text{re}}[k] + V_{31,\text{re}}S_{1,\text{im}}[k] + V_{31,\text{im}}S_{1,\text{re}}[k]) \sin\left(2\pi\frac{70}{200}k\right), \end{aligned}$$

where

$$\mathbf{V} = \begin{bmatrix} V_{00,\text{re}} & V_{01,\text{re}} \\ V_{10,\text{re}} & V_{11,\text{re}} \\ V_{20,\text{re}} & V_{21,\text{re}} \\ V_{30,\text{re}} & V_{31,\text{re}} \end{bmatrix} + j \begin{bmatrix} V_{00,\text{im}} & V_{01,\text{im}} \\ V_{10,\text{im}} & V_{11,\text{im}} \\ V_{20,\text{im}} & V_{21,\text{im}} \\ V_{30,\text{im}} & V_{31,\text{im}} \end{bmatrix},$$

$$\mathbf{x}^{\text{IF}}[k] = \begin{bmatrix} x_0^{\text{IF}}[k] \\ x_1^{\text{IF}}[k] \\ x_2^{\text{IF}}[k] \\ x_3^{\text{IF}}[k] \end{bmatrix}.$$

Considering one OFDM symbol including cyclic prefix, the samples in $\mathbf{x}^{\text{IF}}[k]$ are computed for $k = 0, 1, \dots, 19$ (one period), the resulting chunks are repeated until the desired length is reached.

Chapter 4

Evaluation and Quantities of Interest

This section introduces performance measures to evaluate the measurements. Evaluation takes place offline after the measurement and utilizes the stored receive samples. Section 4.1 discusses assumptions on the involved signals and explains the detailed frame structure. Data covariance matrices are introduced. Section 4.2 then describes two different means to compute the mutual information. Section 4.3 introduces a measure for interference suppression and finally, Section 4.4 defines measured powers, SNR and SIR.

4.1 Assumptions and Detailed Frame Structure

Based upon the $K = 3$ -user MIMO interference channel model introduced in Section 2.1, details regarding signals and noise as encountered on the VMTB are now discussed.

Analogous to Equation (2.3), the receive signal vector at RX decomposes into three components:

$$\mathbf{y}_I = \sum_{j=1}^K \mathbf{H}_{Ij} \mathbf{V}_j \mathbf{s}_j + \mathbf{n}_I = \underbrace{\mathbf{H}_{II} \mathbf{V}_I \mathbf{s}_I}_{\text{desired signal}} + \underbrace{\sum_{\substack{j=1 \\ j \neq I}}^K \mathbf{H}_{Ij} \mathbf{V}_j \mathbf{s}_j}_{\text{interference}} + \underbrace{\mathbf{n}_I}_{\text{noise}}. \quad (4.1)$$

These components can be summarized as follows:

- **desired signal:** signal of interest from desired transmitter TX I , $I \in \{1, 2, 3\}$ denotes the desired link index
- **interference:** signals from interfering transmitters TX j , $j \in \{1, 2, 3\} \wedge j \neq I$
- **noise:** additive noise at RX

All three components are assumed to be *statistically independent*. The transmit data streams $\mathbf{s}_j \in \mathcal{S}^d$ contain 4QAM symbols picked from the symbol alphabet

$$\mathcal{S} = \{S^{(1)}, S^{(2)}, S^{(3)}, S^{(4)}\} = \frac{1}{\sqrt{2}}\{1 + j, -1 + j, -1 - j, 1 - j\}.$$

The transmit symbols are equally likely and hence uniformly distributed:

$$P\{S^{(1)}\} = P\{S^{(2)}\} = P\{S^{(3)}\} = P\{S^{(4)}\} = \frac{1}{4}.$$

The additive Gaussian noise is not spatially white as assumed in Section 2.1 and is generally distributed according to $\mathbf{n}_I \sim \mathcal{CN}(0, \mathbf{Q}_{\mathbf{n}_I})$, where $\mathbf{Q}_{\mathbf{n}_I} \in \mathbb{C}^{N_R \times N_R}$ denotes the noise covariance matrix.

The detailed frame structure as introduced in Section 3.2 is now discussed. The covariance matrix of the receive signal vector at the receiver of desired link I

$$\begin{aligned} \mathbf{Q}_{\mathbf{y}_I} &= \mathbb{E} \{ \mathbf{y}_I \mathbf{y}_I^H \} \\ &= \underbrace{\mathbf{H}_{II} \mathbf{V}_I \mathbf{V}_I^H \mathbf{H}_{II}^H}_{\mathbf{Q}_S} + \underbrace{\sum_{\substack{j=1 \\ j \neq I}}^K \mathbf{H}_{Ij} \mathbf{V}_j \mathbf{V}_j^H \mathbf{H}_{Ij}^H}_{\mathbf{Q}_I} + \underbrace{\mathbf{Q}_N}_{\mathbf{Q}_N} \end{aligned} \quad (4.2)$$

decomposes into the respective covariance matrices of the signal of interest \mathbf{Q}_S , interference \mathbf{Q}_I and noise \mathbf{Q}_N . In order to compute the mutual information and other quantities of interest, three stages are imposed on the data as illustrated in Figure 4.1, where the desired link is $I = 1$. White boxes correspond to “zero symbols” and indicate that nothing is transmitted.

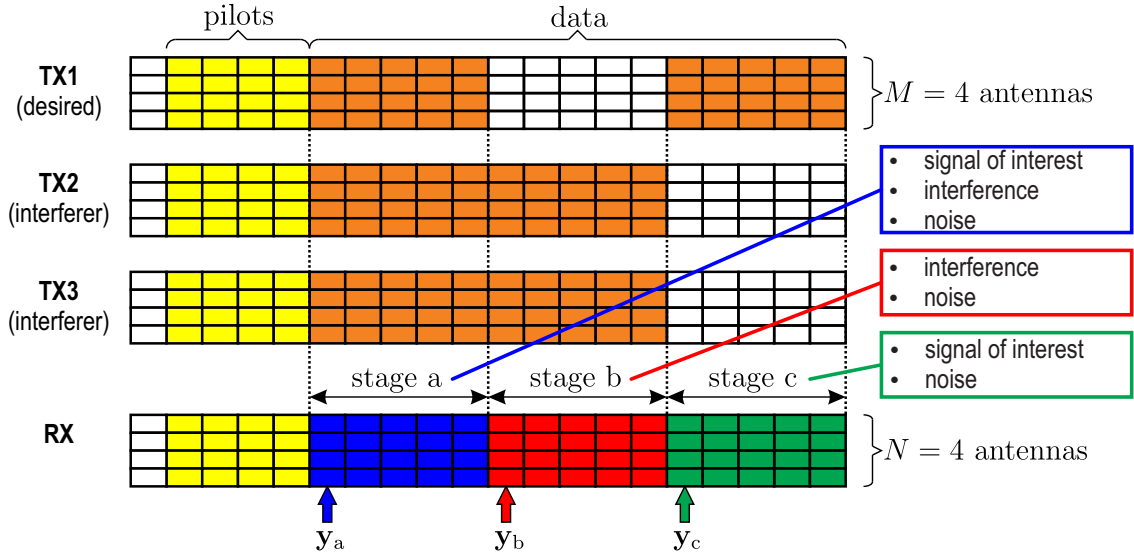


Figure 4.1: Detailed frame structure

- During *stage a*, all three transmitters transmit concurrently and the receive signal vector \mathbf{y}_a is observed. The corresponding sample covariance matrix $\hat{\mathbf{Q}}_a \in \mathbb{C}^{N_R \times N_R}$ estimates the true covariance matrix

$$\mathbf{Q}_a = \mathbb{E} \{ \mathbf{y}_a \mathbf{y}_a^H \} = \mathbf{Q}_S + \mathbf{Q}_I + \mathbf{Q}_N. \quad (4.3)$$

- During *stage b*, only interferers transmit and the receive signal vector \mathbf{y}_b is observed. The corresponding sample covariance matrix $\hat{\mathbf{Q}}_b \in \mathbb{C}^{N_R \times N_R}$ estimates the true covariance matrix

$$\mathbf{Q}_b = \mathbb{E} \{ \mathbf{y}_b \mathbf{y}_b^H \} = \mathbf{Q}_I + \mathbf{Q}_N. \quad (4.4)$$

- During *stage c*, only the desired transmitter transmits and the receive signal vector \mathbf{y}_c is observed. The corresponding sample covariance matrix $\hat{\mathbf{Q}}_c \in \mathbb{C}^{N_R \times N_R}$ estimates the true covariance matrix

$$\mathbf{Q}_c = \mathbb{E} \{ \mathbf{y}_c \mathbf{y}_c^H \} = \mathbf{Q}_S + \mathbf{Q}_N. \quad (4.5)$$

The covariance matrices above are estimated with respect to the number of receive signal vectors during a *stage*, for each receive frame individually. In front of each frame, a noise symbol is introduced where no transmitter transmits data and only noise is received. Each receive frame hence yields one noise symbol, and the sample noise covariance matrix $\hat{\mathbf{Q}}_N$ is estimated over all received frames at a fixed receiver position (moving the receiver might redistribute the noise contributions at each receive antenna). The difference in estimation is justified because the noise statistic does not change between frame transmissions at fixed receiver position, whereas the signal and interference statistics might change due to different channel realizations and precoders.

4.2 Measured Mutual Information

In Section 2.2, mutual information as a measure of data rate was introduced for ideal Interference Alignment (IA) (i.e. perfect channel knowledge) and assuming white Gaussian noise at the receiver. During measurement, following aspects lead to impaired IA performance:

- **Noisy channel estimation:**
 - Additive noise leads to noisy receive pilot sequences.
 - Impact of noise depends on receive signal strength.
- **Outdated channel knowledge:**
 - Channels are subject to time dependent fading (e.g. trees moving in the wind).
 - Channel coefficients are outdated by processing time T_p (see Section 3.2).
- **Correlated channels:**
 - They might lead to rank deficient channel matrices and decreased DoF.
 - This is not an issue on VMTB.

The assumptions in Section 2.2 are hence not realistic for measurements. Section 4.2.1 introduces a realistic formulation for mutual information computation based upon the estimated channel matrices. Section 4.2.2 describes an alternative way of computing the mutual information utilizing the receive data covariance matrices introduced in Section 4.1, which allows to crosscheck the results and used methods.

4.2.1 Mutual Information from Channel Estimates

The mutual information between transmit signal vector \mathbf{x}_I and receive signal vector \mathbf{y}_I over desired link I computed from the estimated channel matrices $\hat{\mathbf{H}}_{Ij}$ is obtained as¹

$$\mathcal{I}_{\hat{\mathbf{H}}}(\mathbf{x}_I; \mathbf{y}_I) = \log_2 \det \left(\mathbf{I}_{N_R} + \hat{\mathbf{H}}_{II} \hat{\mathbf{H}}_{II}^H \left(\sum_{\substack{j=1 \\ j \neq I}}^K \hat{\mathbf{H}}_{Ij} \hat{\mathbf{H}}_{Ij}^H + \hat{\mathbf{Q}}_N \right)^{-1} \right). \quad (4.6)$$

Note that *no pre- or post-processing* of data via linear filtering is performed. Allowing for precoders \mathbf{V}_j , the mutual information between transmit data stream \mathbf{s}_I and receive signal

¹ $\mathcal{I}_{\hat{\mathbf{H}}}$ denotes mutual information *computed from* channel estimates $\hat{\mathbf{H}}$.

vector \mathbf{y}_I is obtained as

$$\mathcal{I}_{\hat{\mathbf{H}}}(\mathbf{s}_I; \mathbf{y}_I) = \log_2 \det \left(\mathbf{I}_{N_R} + \hat{\mathbf{H}}_{II} \mathbf{V}_I (\hat{\mathbf{H}}_{II} \mathbf{V}_I)^H \left(\sum_{\substack{j=1 \\ j \neq I}}^K \hat{\mathbf{H}}_{Ij} \mathbf{V}_j (\hat{\mathbf{H}}_{Ij} \mathbf{V}_j)^H + \hat{\mathbf{Q}}_N \right)^{-1} \right). \quad (4.7)$$

If IA precoders are used, interference is aligned at the receiver. Finally including the receive filters \mathbf{U}_i as well, the mutual information between transmit data stream \mathbf{s}_I and receive data stream \mathbf{r}_I is obtained as

$$\mathcal{I}_{\hat{\mathbf{H}}}(\mathbf{s}_I; \mathbf{r}_I) = \log_2 \det \left(\mathbf{I}_d + \mathbf{U}_I^H \hat{\mathbf{H}}_{II} \mathbf{V}_I (\mathbf{U}_I^H \hat{\mathbf{H}}_{II} \mathbf{V}_I)^H \left(\sum_{\substack{j=1 \\ j \neq I}}^K \mathbf{U}_I^H \hat{\mathbf{H}}_{Ij} \mathbf{V}_j (\mathbf{U}_I^H \hat{\mathbf{H}}_{Ij} \mathbf{V}_j)^H + \mathbf{U}_I^H \hat{\mathbf{Q}}_N \mathbf{U}_I \right)^{-1} \right). \quad (4.8)$$

If IA receive filters (i.e. interference suppression matrices) are used, the previously aligned interference is suppressed.

In order to compare IA to other schemes, the precoding matrices and receive filters can be chosen accordingly. A natural approach is to perform a Singular Value Decomposition (SVD) (introduced in Equation (2.7)) on the channel estimates

$$\hat{\mathbf{H}}_{Ij} = \mathbf{L}_I \boldsymbol{\Sigma}_{Ij} \mathbf{R}_j^H \quad (4.9)$$

and use the right singular vectors as precoders $\mathbf{V}_{j,\text{SVD}} = \mathbf{R}_j$ and the left singular vectors as receive filters $\mathbf{U}_{I,\text{SVD}} = \mathbf{L}_I$. The transmit signal is thereby aligned along the N_Σ (number of singular values) independent directions of the channel, decomposing the vector channel into N_Σ independent scalar channels:

$$\mathbf{U}_{I,\text{SVD}}^H \hat{\mathbf{H}}_{Ij} \mathbf{V}_{j,\text{SVD}} = \mathbf{L}_I^H \mathbf{L}_I \boldsymbol{\Sigma}_{Ij} \mathbf{R}_j^H \mathbf{R}_j = \boldsymbol{\Sigma}_{Ij}. \quad (4.10)$$

Additionally, power allocation could be performed at the transmitters, considering the strength of each ‘‘channel direction’’ (not done in this work). The mutual information computed from channel estimates using SVD filters is denoted $\mathcal{I}_{\hat{\mathbf{H}},\text{SVD}}$.

The mutual information over link I in the *interference free case* (single link) can be calculated by setting the sums in Equation (4.6), Equation (4.7) and Equation (4.8) to zero. The mutual information computed from channel estimates in the absence of interference is denoted $\mathcal{I}_{\hat{\mathbf{H}},\text{noInt}}$.

The method of mutual information computation from channel estimation matrices is similar to emulation of IA with measured channels (transmission of pilot sequence would suffice). The method of truly transmitting data and compute the mutual information from the measured receive data covariance matrices is now discussed.

4.2.2 Mutual Information from Receive Data Covariance

A measure for the mutual information based upon the sample covariance matrices introduced in Section 4.1 is now derived. Utilizing *stage a* and *stage b* as introduced in Section 4.1, the mutual information between \mathbf{s}_I and \mathbf{y}_I is computed as² [11]

$$\mathcal{I}_{\mathbf{Q}}(\mathbf{s}_I; \mathbf{y}_I) = \log_2 \det(\mathbf{I}_{N_R} + \mathbf{Q}_S(\mathbf{Q}_I + \mathbf{Q}_N)^{-1}) = \log_2 \det(\mathbf{Q}_a \mathbf{Q}_b^{-1}). \quad (4.11)$$

The mutual information $\mathcal{I}(\mathbf{s}_I; \mathbf{r}_I)$ between transmit data stream \mathbf{s}_I and receive data stream \mathbf{r}_I as introduced in Equation (2.10) is obtained equivalently, focusing on the interference suppressed receive data stream $\mathbf{r}_I = \mathbf{U}_I^H \mathbf{y}_I$ rather than the receive signal vector \mathbf{y}_I in Equation (4.2). The covariance matrix $\mathbf{Q}_{\mathbf{r}_I}$ similarly decomposes into signal, interference and noise covariance. Note that in general,

$$\mathcal{I}(\mathbf{s}_I; \mathbf{r}_I) \leq \mathcal{I}(\mathbf{s}_I; \mathbf{y}_I) \quad (4.12)$$

because interference suppression by \mathbf{U}_I^H might decrease the SNR as described in Section 2.3.2.

Stage c allows to measure an upper bound on the mutual information with the given precoders to determine how interference actually impairs the data transmission. The mutual information (during *stage c*) in the absence of interference but using IA precoders is obtained as

$$\mathcal{I}_{\mathbf{Q}, \text{noInt}}(\mathbf{s}_I; \mathbf{y}_I) = \log_2 \det(\mathbf{I}_{N_R} + \mathbf{Q}_S \mathbf{Q}_N^{-1}) = \log_2 \det(\mathbf{Q}_c \mathbf{Q}_N^{-1}). \quad (4.13)$$

During measurement, only a finite number of receive signal vectors is observed and the measured (estimated) mutual information is

$$\mathcal{I}_{\hat{\mathbf{Q}}}(\mathbf{s}_I; \mathbf{y}_I) = \log_2 \det(\hat{\mathbf{Q}}_a \hat{\mathbf{Q}}_b^{-1}), \quad (4.14)$$

$$\mathcal{I}_{\hat{\mathbf{Q}}}(\mathbf{s}_I; \mathbf{r}_I) = \log_2 \det\left(\mathbf{U}^H \hat{\mathbf{Q}}_a \mathbf{U} \left(\mathbf{U}^H \hat{\mathbf{Q}}_b \mathbf{U}\right)^{-1}\right), \quad (4.15)$$

$$\mathcal{I}_{\hat{\mathbf{Q}}, \text{noInt}}(\mathbf{s}_I; \mathbf{y}_I) = \log_2 \det(\hat{\mathbf{Q}}_c \hat{\mathbf{Q}}_N^{-1}). \quad (4.16)$$

Many channel realizations are encountered, and the *average mutual information* is of interest:

$$\bar{\mathcal{I}} = \mathbb{E}\{\mathcal{I}\}, \quad (4.17)$$

where the expectation is with respect to the number of received frames.

² $\mathcal{I}_{\mathbf{Q}}$ denotes mutual information computed from receive data covariance \mathbf{Q} .

4.3 Interference Suppression

Observing *stage b* as illustrated in Figure 4.1 over many frames, the estimated covariance matrices $\widehat{\mathbf{Q}}_b$ yield information about the average alignment effort achieved by the precoding matrices. The aim of IA is to restrict the interference in a $N_R - d$ dimensional subspace at the receiver, which translates into $\text{rank}(\mathbf{Q}_b) = N_R - d$ in the absence of noise, because only interference is received during *stage b*. A measure for this is now derived.

The concatenation of the interference suppression matrix \mathbf{U}_I and its orthogonal complement $\mathbf{U}_I^\perp \in \mathbb{C}^{N_R \times N_R - d}$ yields a unitary matrix

$$\mathbf{M} = \begin{bmatrix} \mathbf{U}_I & \mathbf{U}_I^\perp \end{bmatrix}. \quad (4.18)$$

Remember that the received interference lies in the nullspace of \mathbf{U}_I^H (Equation (2.18)) and therefore in the column space of its orthogonal complement:

$$\text{span}(\mathbf{H}_{Ij} \mathbf{V}_j) \subseteq \text{span}\left(\left(\mathbf{U}_I^\perp\right)^H\right), \forall I \neq j. \quad (4.19)$$

Utilizing $\mathbf{M}\mathbf{M}^H = \mathbf{I}_{N_R}$ and Condition (2.13a) in Equation (4.4) gives

$$\begin{aligned} \mathbf{Q}_b &= \mathbf{M}\mathbf{M}^H \underbrace{\sum_{\substack{j=1 \\ j \neq I}}^K \mathbf{H}_{Ij} \mathbf{V}_j \mathbf{V}_j^H \mathbf{H}_{Ij}^H}_{\mathbf{Q}_I} \mathbf{M}\mathbf{M}^H + \mathbf{M}\mathbf{M}^H \mathbf{Q}_N \\ &= \mathbf{M} \left(\mathbf{M}^H \left(\sum_{\substack{j=1 \\ j \neq I}}^K \mathbf{H}_{Ij} \mathbf{V}_j \mathbf{V}_j^H \mathbf{H}_{Ij}^H \right) \mathbf{M} + \mathbf{Q}_N \right) \mathbf{M}^H \\ &= \mathbf{M} \left(\sum_{\substack{j=1 \\ j \neq I}}^K \begin{bmatrix} \underbrace{\mathbf{U}_I^H \mathbf{H}_{Ij} \mathbf{V}_j \mathbf{V}_j^H \mathbf{H}_{Ij}^H \mathbf{U}_I}_{=0} & \underbrace{\mathbf{U}_I^H \mathbf{H}_{Ij} \mathbf{V}_j \mathbf{V}_j^H \mathbf{H}_{Ij}^H \mathbf{U}_I^\perp}_{\neq 0} \\ \underbrace{\left(\mathbf{U}_I^\perp\right)^H \mathbf{H}_{Ij} \mathbf{V}_j \mathbf{V}_j^H \mathbf{H}_{Ij}^H \mathbf{U}_I}_{=0} & \underbrace{\left(\mathbf{U}_I^\perp\right)^H \mathbf{H}_{Ij} \mathbf{V}_j \mathbf{V}_j^H \mathbf{H}_{Ij}^H \mathbf{U}_I^\perp}_{\neq 0} \end{bmatrix} + \mathbf{Q}_N \right) \mathbf{M}^H \\ &= \mathbf{M} \left(\begin{bmatrix} 0 & 0 \\ 0 & \left(\mathbf{U}_I^\perp\right)^H \mathbf{Q}_I \mathbf{U}_I^\perp \end{bmatrix} + \mathbf{Q}_N \right) \mathbf{M}^H. \end{aligned} \quad (4.20)$$

An eigenvalue decomposition is performed on the interference covariance term

$$\left(\mathbf{U}_I^\perp\right)^H \mathbf{Q}_I \mathbf{U}_I^\perp = \tilde{\mathbf{E}} \tilde{\mathbf{\Lambda}} \tilde{\mathbf{E}}^H, \quad (4.21)$$

where $\tilde{\mathbf{E}} \in \mathbb{C}^{N_R - d \times N_R - d}$ is unitary and $\tilde{\mathbf{\Lambda}} = \text{diag}\{\tilde{\lambda}_1, \dots, \tilde{\lambda}_{N_R - d}\}$ contains the $N_R - d$ eigenvalues that correspond to the interference subspace in non-decreasing order. Incorporating these results in an eigenvalue decomposition of \mathbf{Q}_b in Equation (4.20) finally yields

$$\mathbf{Q}_b = \underbrace{\mathbf{M} \begin{bmatrix} \mathbf{I}_d & \mathbf{0} \\ \mathbf{0} & \tilde{\mathbf{E}} \end{bmatrix}}_{\mathbf{E}} \underbrace{\left(\begin{bmatrix} \mathbf{0} & \mathbf{0} \\ \mathbf{0} & \tilde{\mathbf{\Lambda}} \end{bmatrix} + \mathbf{\Lambda}_N \right)}_{\mathbf{\Lambda}} \underbrace{\begin{bmatrix} \mathbf{I}_d & \mathbf{0} \\ \mathbf{0} & \tilde{\mathbf{E}} \end{bmatrix}^H}_{\mathbf{E}^H} \mathbf{M}^H, \quad (4.22)$$

where $\mathbf{\Lambda}_N = \text{diag}\{\sigma_1^2, \sigma_2^2, \dots, \sigma_N^2\}$ contains the eigenvalues of the noise covariance matrix \mathbf{Q}_N . The eigenvalues of \mathbf{Q}_b are therefore obtained as

$$\begin{aligned}\mathbf{\Lambda} &= \text{diag}\{\lambda_1, \dots, \lambda_N\} \\ &= \text{diag}\{\underbrace{\sigma_1^2, \dots, \sigma_d^2}_d, \underbrace{\tilde{\lambda}_1 + \sigma_{d+1}^2, \dots, \tilde{\lambda}_{N_R-d} + \sigma_N^2}_{N_R-d}\}.\end{aligned}\quad (4.23)$$

If interference is aligned perfectly by the precoders \mathbf{V}_j , the first d eigenvalues of \mathbf{Q}_b that correspond to the desired signal subspace contain only noise. The eigenvectors corresponding to the remaining $N_R - d$ eigenvalues span the interference subspace as stated in Equation (4.19). Interference at the receiver can only be suppressed perfectly by \mathbf{U}_i^H if it is aligned perfectly. If alignment is imperfect, interference leaks into the desired signal subspace and the first d eigenvalues grow. A measure for interference suppression is thus given by the separation between the smallest eigenvalue corresponding to the interference subspace λ_{d+1} and the largest eigenvalue corresponding to the desired signal subspace λ_d according to

$$I_{\text{supp}} = 10 \log_{10} \left(\frac{\lambda_{d+1}}{\lambda_d} \right) \text{ dB} \stackrel{(d=2)}{=} 10 \log_{10} \left(\frac{\lambda_3}{\lambda_2} \right) \text{ dB}.\quad (4.24)$$

During measurement, several frames are observed and the average interference suppression is computed according to

$$\bar{I}_{\text{supp}} = 10 \log_{10} \left(\mathbb{E} \left\{ \frac{\lambda_{d+1}}{\lambda_d} \right\} \right) \text{ dB},\quad (4.25)$$

where the expectation is with respect to the number of received frames.

4.4 Power, SNR and SIR

The respective powers of signal, interference and noise are now defined in two ways, one is based upon the sample covariance matrices introduced in Section 4.1, the other one utilizes the estimated channel matrices. Then, SNR and SIR which are computed from these powers are defined.

The power of the *desired* signal at the receiver is obtained as

$$P_{\hat{\mathbf{Q}},S} = \text{trace}(\hat{\mathbf{Q}}_S) = \text{trace}(\hat{\mathbf{Q}}_c - \hat{\mathbf{Q}}_N). \quad (4.26)$$

In theory, the power of the desired signal can also be computed as $P_{\hat{\mathbf{Q}},S} = \text{trace}(\hat{\mathbf{Q}}_a - \hat{\mathbf{Q}}_b)$. However, this leads to bad estimations in practice, especially if the interfering signals are a lot stronger than the desired signal. The desired signal “vanishes” in the much stronger interference. The power of the *interference* at the receiver is obtained as

$$P_{\hat{\mathbf{Q}},I} = \text{trace}(\hat{\mathbf{Q}}_I) = \text{trace}(\hat{\mathbf{Q}}_b - \hat{\mathbf{Q}}_N), \quad (4.27)$$

the power of the *noise* at the receiver is

$$P_{\hat{\mathbf{Q}},N} = \text{trace}(\hat{\mathbf{Q}}_N). \quad (4.28)$$

An alternative method of power computation considers the estimated channel matrices $\hat{\mathbf{H}}_{Ij}$. The receive power contribution from transmitter j to receiver I is computed as

$$P_{Ij} = \text{trace}(\hat{\mathbf{H}}_{Ij} \hat{\mathbf{H}}_{Ij}^H) = \left\| \hat{\mathbf{H}}_{Ij} \right\|_F^2. \quad (4.29)$$

Note that this formulation considers the *pure channel* without filters \mathbf{V}_j , \mathbf{U}_I . Also note that controlled transmit power variations realized via the programmable RF attenuators are included in the estimated channel matrices (RF attenuators are part of the channel). A measure that compares to the powers defined in Equation (4.26) and Equation (4.27) needs to include the precoders (transmit filters), since they are implicitly contained in the sample covariance matrices. Furthermore, the impact of the interference suppression matrices (receive filters) can also be investigated by including them in the formulation. The receive power contribution of the *desired* transmitter, for each of the three cases, is defined as

$$P_{\hat{\mathbf{H}},S} = \left\| \hat{\mathbf{H}}_{II} \right\|_F^2, \quad (4.30a)$$

$$P_{\hat{\mathbf{H}}\mathbf{V},S} = \left\| \hat{\mathbf{H}}_{II} \mathbf{V}_I \right\|_F^2, \quad (4.30b)$$

$$P_{\mathbf{U}\hat{\mathbf{H}}\mathbf{V},S} = \left\| \mathbf{U}_I^H \hat{\mathbf{H}}_{II} \mathbf{V}_I \right\|_F^2. \quad (4.30c)$$

Similarly, the receive power contribution of the interfering transmitters (*interference power*), for each of the three cases, is defined as

$$P_{\hat{\mathbf{H}},I} = \sum_{\substack{j=1 \\ j \neq I}}^K \left\| \hat{\mathbf{H}}_{Ij} \right\|_F^2, \quad (4.31a)$$

$$P_{\hat{\mathbf{H}}\mathbf{V},I} = \sum_{\substack{j=1 \\ j \neq I}}^K \left\| \hat{\mathbf{H}}_{Ij} \mathbf{V}_j \right\|_F^2, \quad (4.31b)$$

$$P_{\mathbf{U}\hat{\mathbf{H}}\mathbf{V},I} = \sum_{\substack{j=1 \\ j \neq I}}^K \left\| \mathbf{U}_I \hat{\mathbf{H}}_{Ij} \mathbf{V}_j \right\|_F^2. \quad (4.31c)$$

Many frames are observed and the *mean power* is of interest:

$$\bar{P} = \mathbb{E}\{P\}, \quad (4.32)$$

where the expectation is with respect to the number of received frames. Note that the sample covariance matrices and the channel estimation matrices are estimated on frame basis (i.e. each frame yields a matrix). The only exception is the noise covariance matrix, which is estimated over all frames at a fixed receiver position, because each frame contains only one noise symbol. The SNR is now computed as

$$\text{SNR}_{\hat{\mathbf{Q}}} = 10 \log_{10} \left(\frac{\bar{P}_{\hat{\mathbf{Q}},S}}{\bar{P}_{\hat{\mathbf{Q}},N}} \right) \text{dB}, \quad (4.33)$$

the SIR as

$$\text{SIR}_{\hat{\mathbf{Q}}} = 10 \log_{10} \left(\frac{\bar{P}_{\hat{\mathbf{Q}},S}}{\bar{P}_{\hat{\mathbf{Q}},I}} \right) \text{dB}. \quad (4.34)$$

An alternative SNR computation utilizing the channel estimation matrices is given by

$$\text{SNR}_{\hat{\mathbf{H}}} = 10 \log_{10} \left(\frac{\bar{P}_{\hat{\mathbf{H}},S}}{\bar{P}_{\hat{\mathbf{Q}},N}} \right) \text{dB}, \quad (4.35a)$$

$$\text{SNR}_{\hat{\mathbf{H}}\mathbf{V}} = 10 \log_{10} \left(\frac{\bar{P}_{\hat{\mathbf{H}}\mathbf{V},S}}{\bar{P}_{\hat{\mathbf{Q}},N}} \right) \text{dB}, \quad (4.35b)$$

$$\text{SNR}_{\mathbf{U}\hat{\mathbf{H}}\mathbf{V}} = 10 \log_{10} \left(\frac{\bar{P}_{\mathbf{U}\hat{\mathbf{H}}\mathbf{V},S}}{\bar{P}_{\hat{\mathbf{Q}},N}} \right) \text{dB}. \quad (4.35c)$$

Similarly, SIR is computed from the channel estimation matrices according to

$$\text{SIR}_{\hat{\mathbf{H}}} = 10 \log_{10} \left(\frac{\bar{P}_{\hat{\mathbf{H}},S}}{\bar{P}_{\hat{\mathbf{H}},I}} \right) \text{dB}, \quad (4.36a)$$

$$\text{SIR}_{\hat{\mathbf{H}}\mathbf{V}} = 10 \log_{10} \left(\frac{\bar{P}_{\hat{\mathbf{H}}\mathbf{V},S}}{\bar{P}_{\hat{\mathbf{H}}\mathbf{V},I}} \right) \text{dB}, \quad (4.36b)$$

$$\text{SIR}_{\mathbf{U}\hat{\mathbf{H}}\mathbf{V}} = 10 \log_{10} \left(\frac{\bar{P}_{\mathbf{U}\hat{\mathbf{H}}\mathbf{V},S}}{\bar{P}_{\mathbf{U}\hat{\mathbf{H}}\mathbf{V},I}} \right) \text{dB}. \quad (4.36c)$$

$\text{SNR}_{\hat{\mathbf{Q}}}$ compares to $\text{SNR}_{\hat{\mathbf{H}}\mathbf{V}}$ and $\text{SIR}_{\hat{\mathbf{Q}}}$ compares to $\text{SIR}_{\hat{\mathbf{H}}\mathbf{V}}$, which will be proven by measurements in Section 5.2.1 and Section 5.3.1.

For the following, keep in mind that SNR and SIR are implicitly averaged over all transmissions, which usually include many receiver positions to average over small scale fading. A certain SNR or SIR value is achieved *on average* over all transmissions.

Chapter 5

Measurements

Section 5.1 shows the feasibility of IA at fixed SNR and SIR and explains how the subsequent measurements are performed. Section 5.2 investigates how the performance measures introduced in Chapter 4 depend on variable SNR at fixed SIR. Section 5.3 does the same for variable SIR, keeping the SNR fixed.

5.1 Validation of Interference Alignment

The feasibility of IA on the Vienna MIMO Testbed (VMTB) is now shown utilizing the performance measures introduced in Chapter 4. This section establishes the basic methodology for the subsequent measurements in Section 5.2 and Section 5.3. All three links are desired once to compare the results. Figure 5.1 subsumes the measurement process.

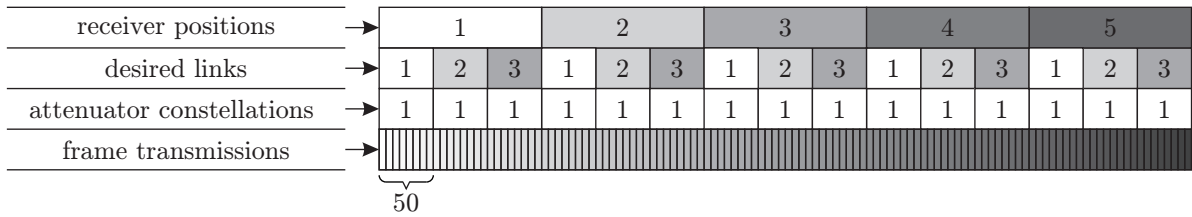


Figure 5.1: Validation: measurement process

Note following aspects of the illustration:

- **receiver positions:** 5 receiver positions (RX antennas positioned in x - y - ϕ) were realized.
- **desired links:** At each position, transmitters $I = \{1, 2, 3\}$ were desired once.
- **attenuator constellations:** For each desired link, one RF transmit-attenuator constellation was utilized to achieve $SIR = -3$ dB.
- **frame transmissions:** 50 frames were transmitted at one attenuator constellation of one receiver position.

The layer-order coincides with the actual measurement process - receiver repositioning is the “outer loop” of the measurement. Table 5.1 depicts the parameters of the validation measurement.

Figure 5.2, Figure 5.3 and Figure 5.4 (one figure for each desired link) show the eigenvalues of $\hat{\mathbf{Q}}_b$ and $\hat{\mathbf{Q}}_N$, denoted $\{\lambda_1, \dots, \lambda_4\}$ and $\{\sigma_1^2, \dots, \sigma_4^2\}$, respectively. Remember that each point corresponds to one frame evaluation, and that $\hat{\mathbf{Q}}_b$ is estimated during *stage b* where only the interferers transmit. The eigenvalues are plotted logarithmically and normalized so that λ_2 lies at 0 dB on average. Ideally, λ_1 and λ_2 that correspond to the desired signal subspace would

| parameter | value | comments |
|---------------------------------------|-------|--|
| receiver positions | 5 | represent channel realizations |
| attenuator constellations | 1 | only one target SNR/SIR |
| transmissions per constellation | 50 | at one receiver position |
| total transmissions per constellation | 250 | considering all receiver positions |
| data symbols per frame | 2×45 | 2 streams, 15 symbol vectors per stage |
| measured SNR | 55 dB | averaged over all transmissions |
| anticipated SIR | −3 dB | all transmitters received equally strong |
| processing time T_P between frames | 70 ms | averaged over all transmissions |

Table 5.1: Validation: parameters

coincide with the noise variances σ_1^2 and σ_2^2 on average, since no desired signal is transmitted during *stage b* (details see Section 4.3). Due to imperfect alignment and leakage, these eigenvalues are only lower bounded by the noise variances. The average interference suppression (see Equation (4.25)) is highest over link $I = 1$. Measurements were done at five fixed receiver positions. After 50 successive transmissions, the receive antennas move and rotate into a new position and another 50 transmissions take place. The first frame after receiver movement is discarded¹, because precoders based on the channel estimates of the previous receiver position are generally not suitable for the new position.

Figure 5.5, Figure 5.6 and Figure 5.7 (one figure for each desired link) depict several measured mutual information curves. Each receiver position yields a different average mutual information due to small scale fading and different channel realizations. It is therefore imperative to average the results over many receiver positions in the subsequent measurements. Ultimately, only the average mutual information $\bar{\mathcal{I}}$ is of interest. The results show that the mutual information computed from channel estimates $\mathcal{I}_{\hat{\mathbf{H}}}(\mathbf{s}_I; \mathbf{r}_I)$ and the one computed from the receive data covariance $\mathcal{I}_{\hat{\mathbf{Q}}}(\mathbf{s}_I; \mathbf{r}_I)$ practically coincide, confirming that both methods are suitable. The mutual information between transmit signal vector \mathbf{x}_I and receive signal vector \mathbf{y}_I , $\mathcal{I}_{\hat{\mathbf{H}}}(\mathbf{x}_I; \mathbf{y}_I)$, without linear filtering (i.e. no IA) is clearly impaired (reduced) by interference. The interference free case $\mathcal{I}_{\hat{\mathbf{H}}, \text{noInt}}(\mathbf{x}_I; \mathbf{y}_I)$ constitutes the upper bound, attained by exploiting the multiplexing gain respectively DoF of four antennas. IA achieves half the mutual information in the best case (“half the cake”), since only half the DoF are available for the desired signal. The average mutual information is highest over link $I = 1$, confirming that the link with the highest interference suppression also yields the highest mutual information.

Figure 5.8, Figure 5.9 and Figure 5.10 (one figure for each desired link) illustrate the receive power contribution (see Equation (4.29)) from each transmitter individually. At fixed receiver position, the outdoor to indoor channels P_{I1} and P_{I2} vary more than the indoor to indoor channel P_{I3} . This behaviour results from environmental influences like a large tree in front of the laboratory that moves with the wind. No moving objects were situated indoors, therefore the indoor channel is almost constant at fixed receiver position. Movement and rotation of the receive antennas change the receive power contributions due to small scale fading. All three figures show similar behaviour but are not identical due to time dependent fading. In the

¹Actually, 51 frames are received at fixed receiver position, but only 50 are retained as “valid”.

subsequent measurements, the average (over all frames) receive power contributions are calculated and the programmable RF transmit-attenuators are chosen to control the SNR and SIR accordingly. In this measurement, the three transmitters were received about equally strong on average, hence $\text{SIR} \approx -3$ dB as the interference is twice as strong as the desired signal. Overall, the channels are very static at fixed receiver position.

The results show that IA works and interference is aligned at the receiver. The better the alignment, the higher the interference suppression (separation between λ_2 and λ_3) and the higher the mutual information. Channels are quasi-static at fixed receiver position. For the subsequent measurements where SNR and SIR are varied, the results are averaged over all frames of a specific *attenuator constellation*, which includes several receiver positions to average over small scale fading. Attenuator constellation refers to a specific choice of the RF transmit-attenuators, in the following just called attenuators, chosen to achieve a certain SNR or SIR value.

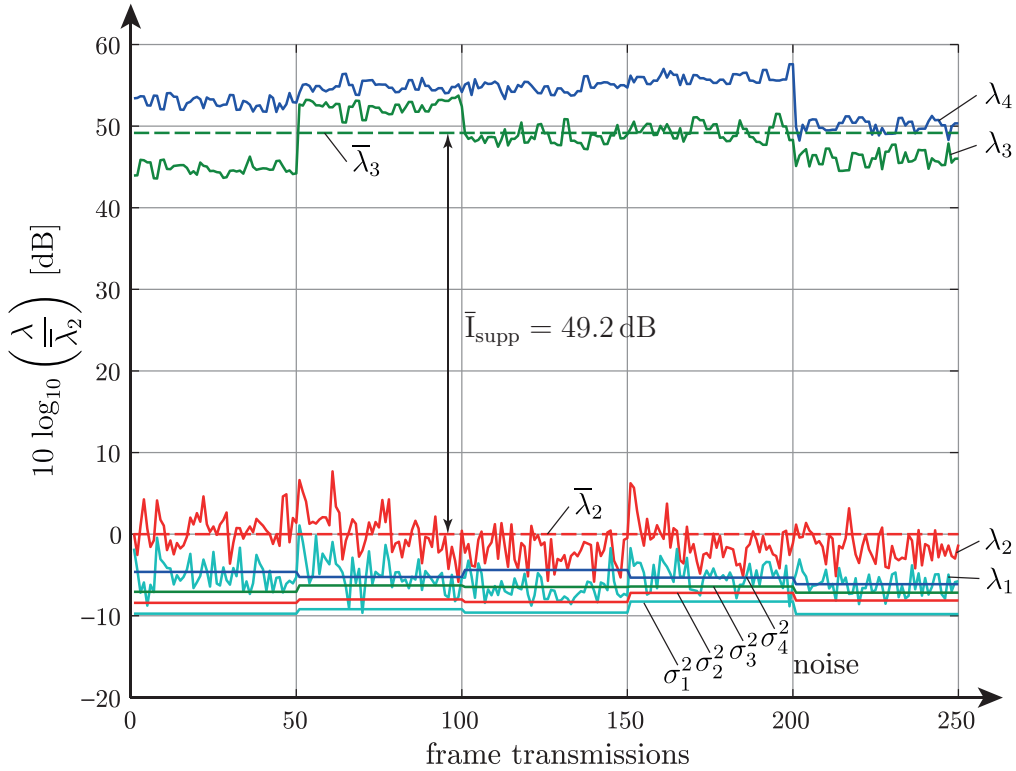


Figure 5.2: Validation: eigenvalues of $\hat{\mathbf{Q}}_b$ and $\hat{\mathbf{Q}}_N$ (desired link $I = 1$)

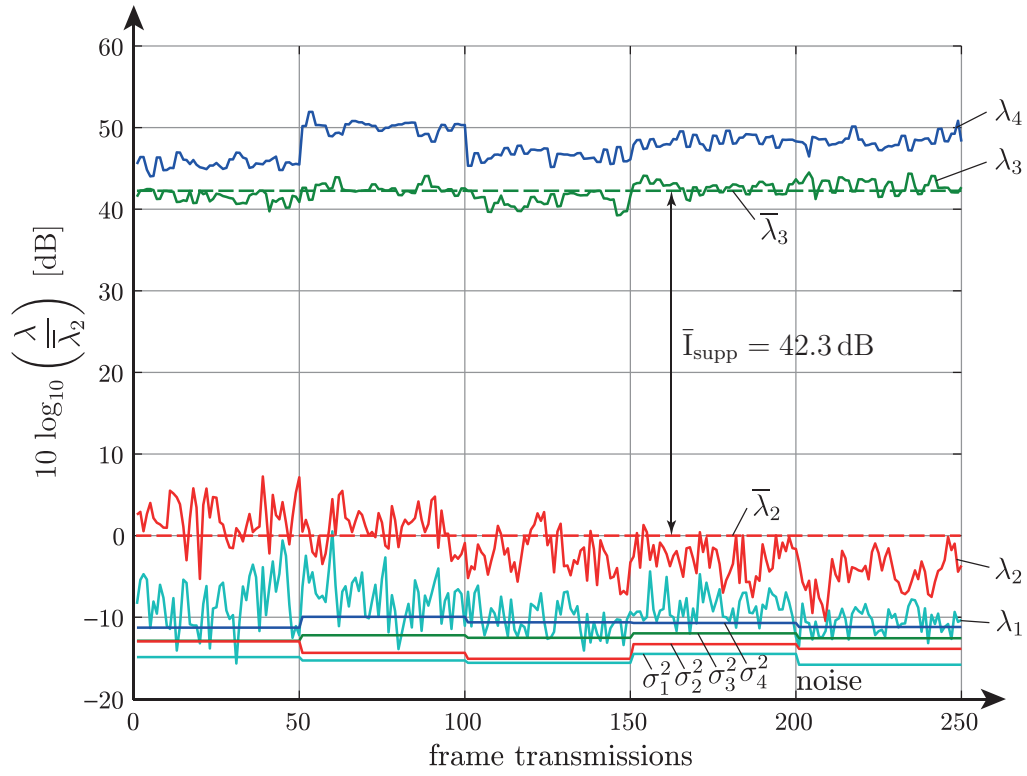


Figure 5.3: Validation: eigenvalues of $\hat{\mathbf{Q}}_b$ and $\hat{\mathbf{Q}}_N$ (desired link $I = 2$)

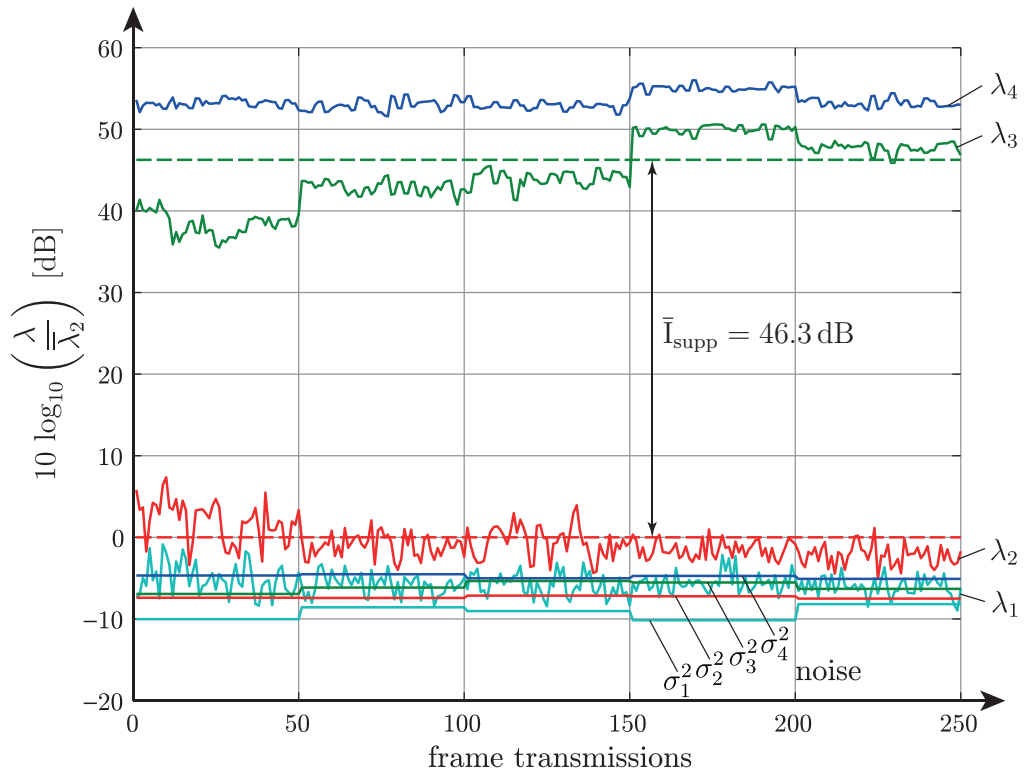


Figure 5.4: Validation: eigenvalues of $\hat{\mathbf{Q}}_b$ and $\hat{\mathbf{Q}}_N$ (desired link $I = 3$)

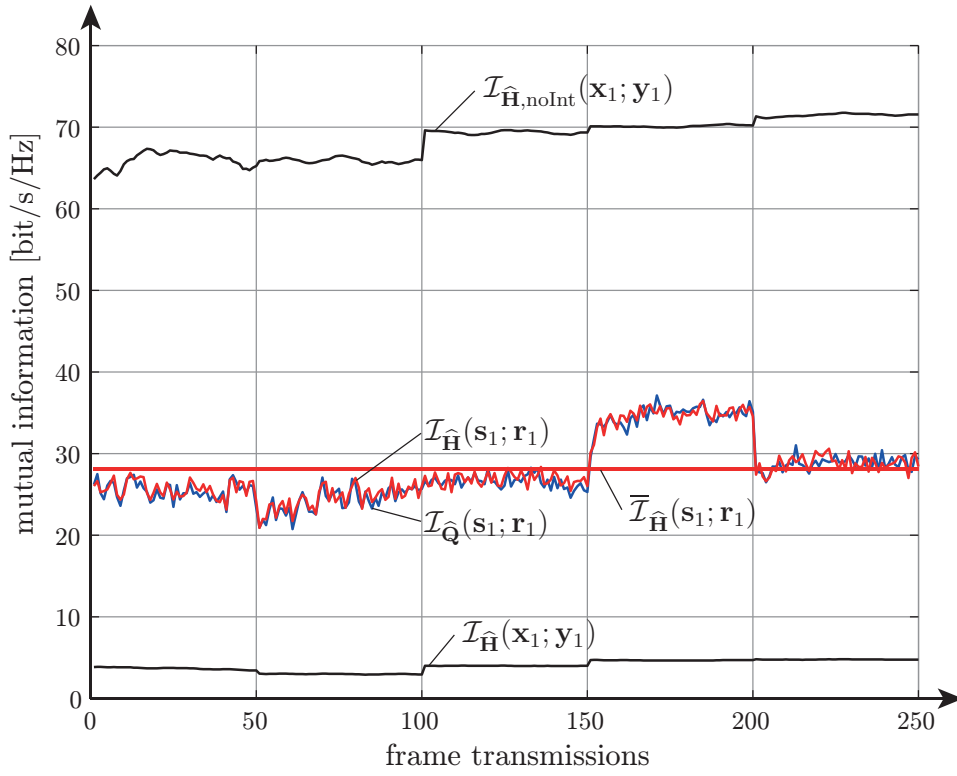


Figure 5.5: Validation: mutual information comparison (desired link $I = 1$)

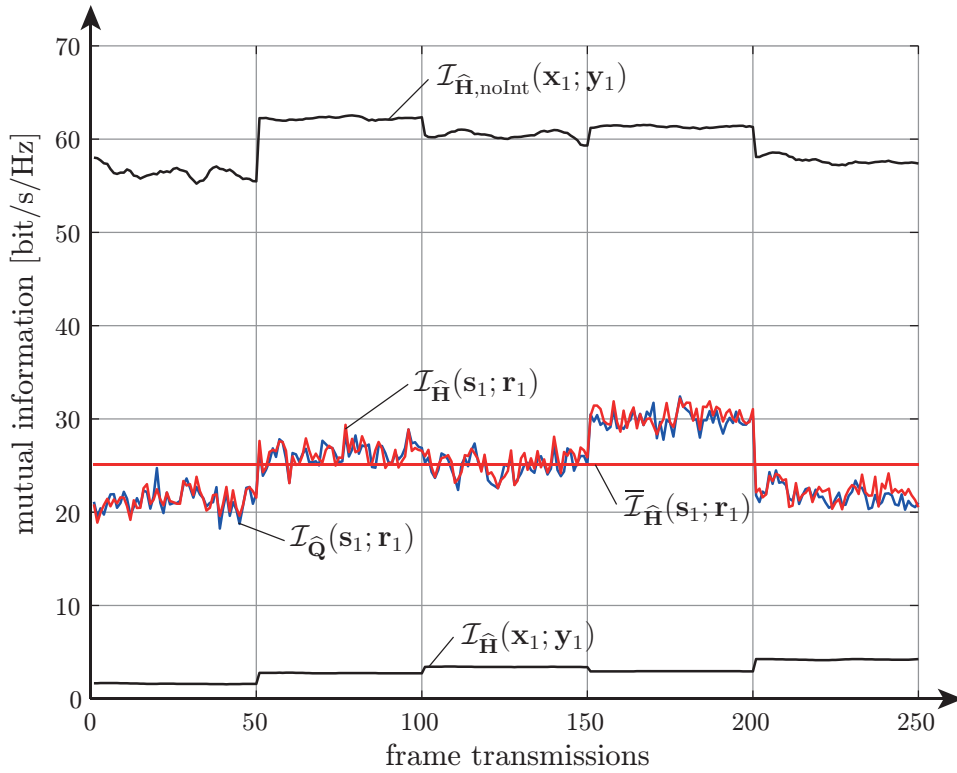


Figure 5.6: Validation: mutual information comparison (desired link $I = 2$)

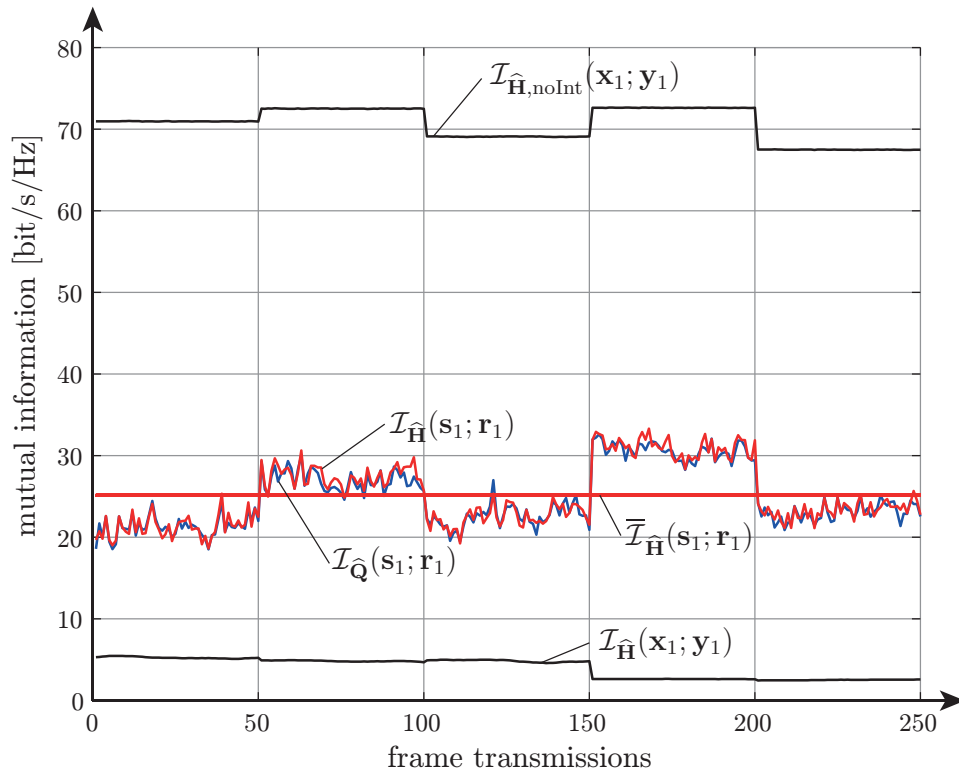


Figure 5.7: Validation: mutual information comparison (desired link $I = 3$)

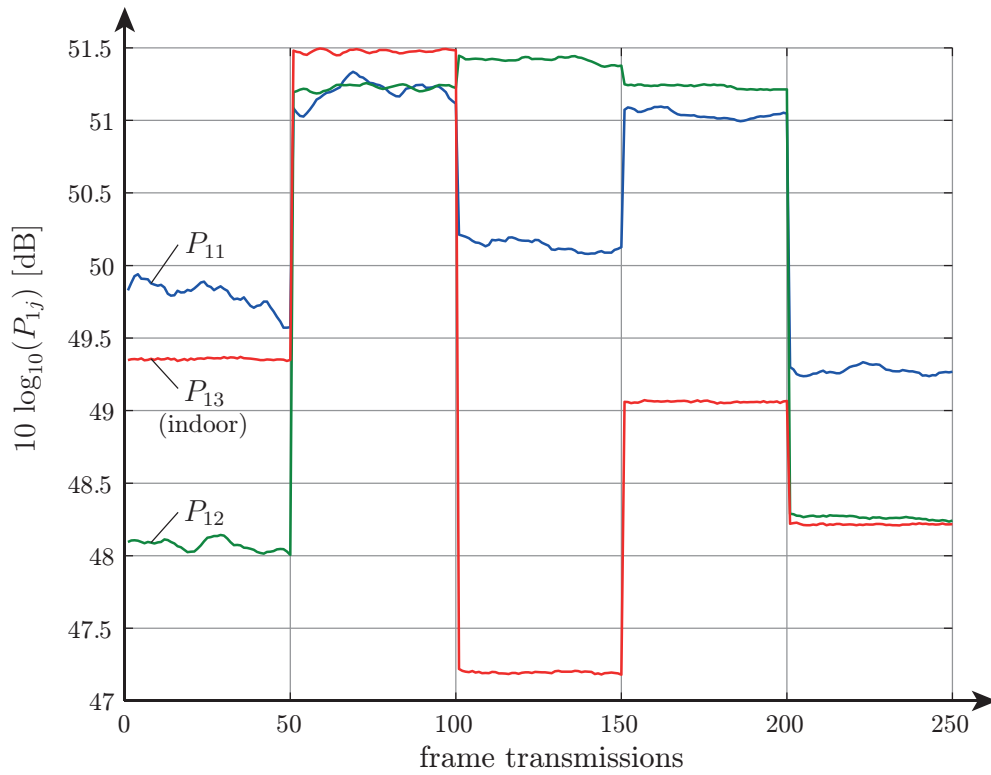


Figure 5.8: Validation: receive power contributions (desired link $I = 1$)

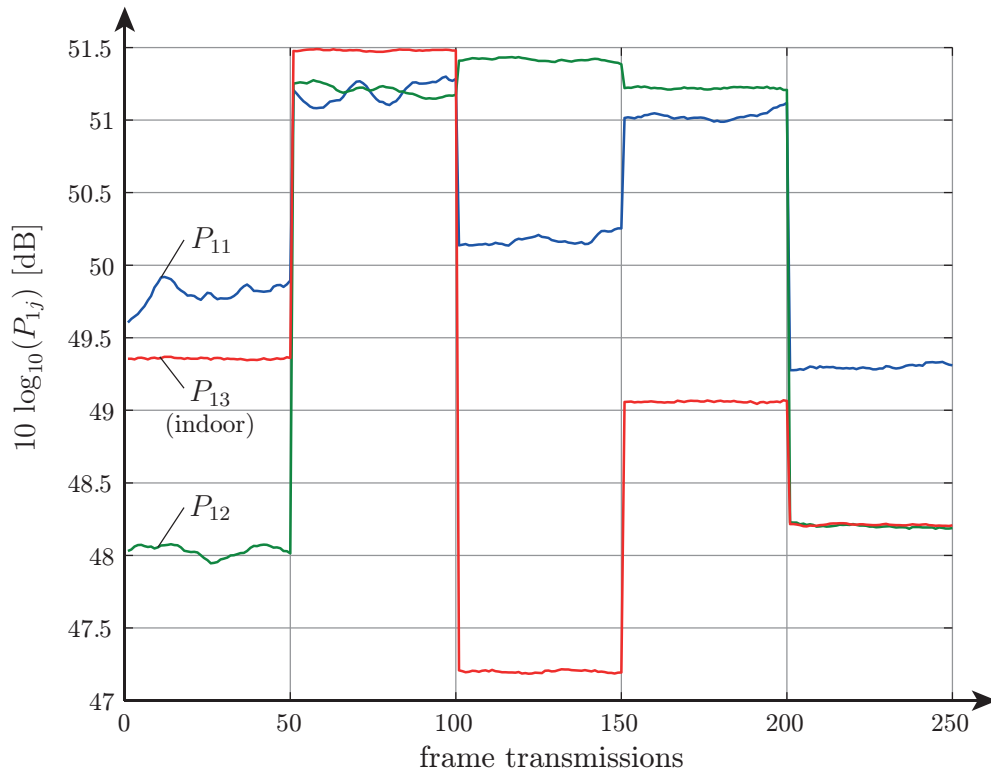


Figure 5.9: Validation: receive power contributions (desired link $I = 2$)

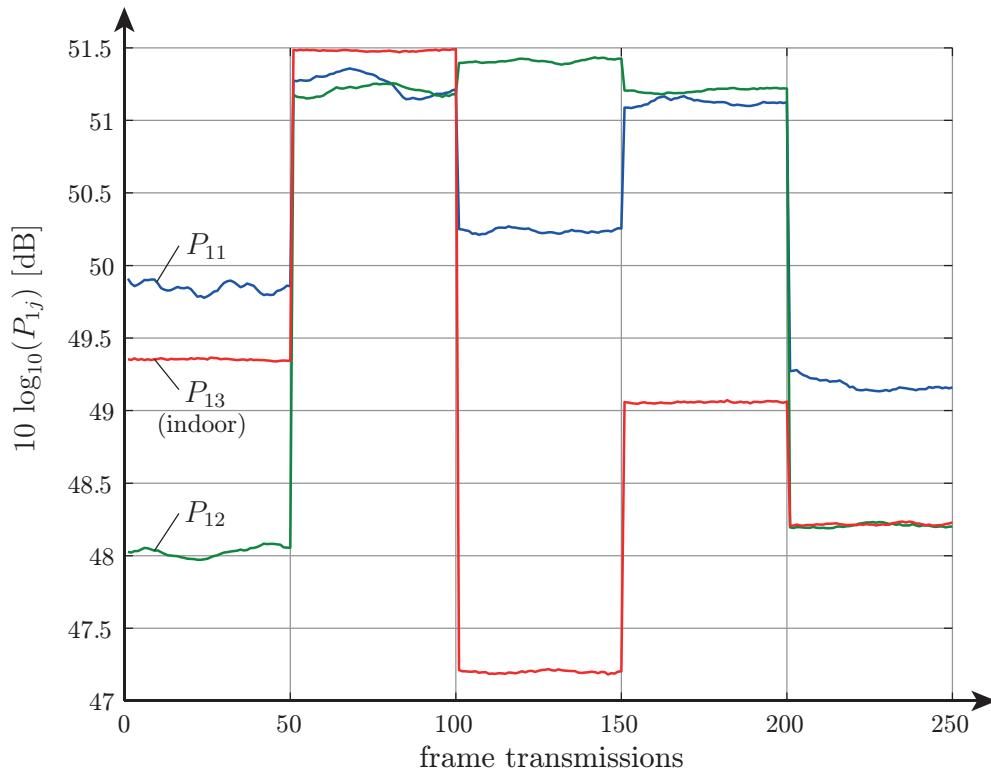


Figure 5.10: Validation: receive power contributions (desired link $I = 3$)

5.2 Variable SNR at Fixed SIR

The dependence of mutual information and other measures on SNR at fixed SIR = -3 dB is now investigated. The necessary *transmit power calibration* can be summarized as follows:

1. Measure the average receive power contributions \bar{P}_{Ij} according to Equation (4.29) over all receiver positions at lowest possible attenuator values $\alpha_{j,\text{init}} = 0$ dB.
2. Consider the lowest average channel power:

$$\bar{P}_{\min} = \min_j \bar{P}_{Ij}, \quad j = \{1, 2, 3\}.$$

3. Compute the attenuator increments according to:

$$\Delta\alpha_j = \left\lceil 10 \log_{10} \left(\frac{\bar{P}_{Ij}}{\bar{P}_{\min}} \right) \right\rceil \text{ dB}.$$

4. Compute the final attenuator values according to:

$$\alpha_j = \alpha_{j,\text{init}} + \Delta\alpha_j.$$

5. Reduce SNR by increasing all attenuator values simultaneously by a certain stepsize.

This results in constant average SIR = -3 dB, since all three transmitters are received equally strong (within +/- 1 dB) on average. Figure 5.11 illustrates the measurement process.

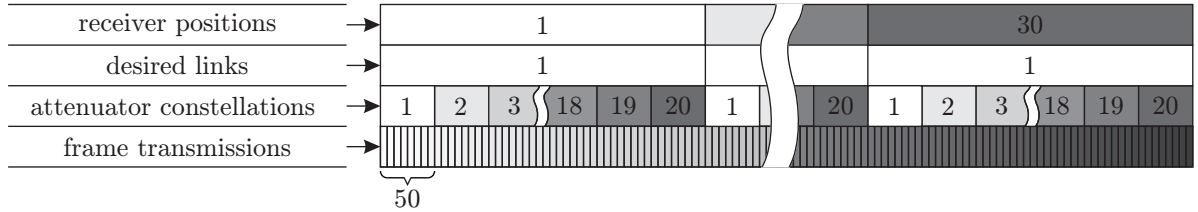


Figure 5.11: Variable SNR: measurement process

The parameters of the the measurement are summarized in Table 5.2.

| parameter | value | comments |
|---------------------------------------|------------|--|
| receiver positions | 30 | represent channel realizations |
| attenuator constellations | 20 | relative attenuator values: 0, 3, ..., 57 dB |
| transmissions per constellation | 50 | at one receiver position |
| total transmissions per constellation | 1500 | considering all receiver positions |
| data symbols per frame | 2×60 | 2 streams, 20 symbol vectors per stage |
| anticipated SNR | 16...73 dB | |
| anticipated SIR | -3 dB | all transmitters received equally strong |
| processing time T_P between frames | 70 ms | averaged over all transmissions |

Table 5.2: Variable SNR: parameters

5.2.1 Measured Powers, SNR and SIR

To verify that the controlled SNR increases as expected while the SIR stays constant, the measured powers introduced in Section 4.4 are now investigated. The measurement encompasses 20 attenuator constellations. Starting at lowest attenuation (highest SNR), the attenuator values α_j are increased simultaneously by 3 dB stepsize at each attenuator constellation, thereby steadily decreasing the SNR while keeping the SIR constant.

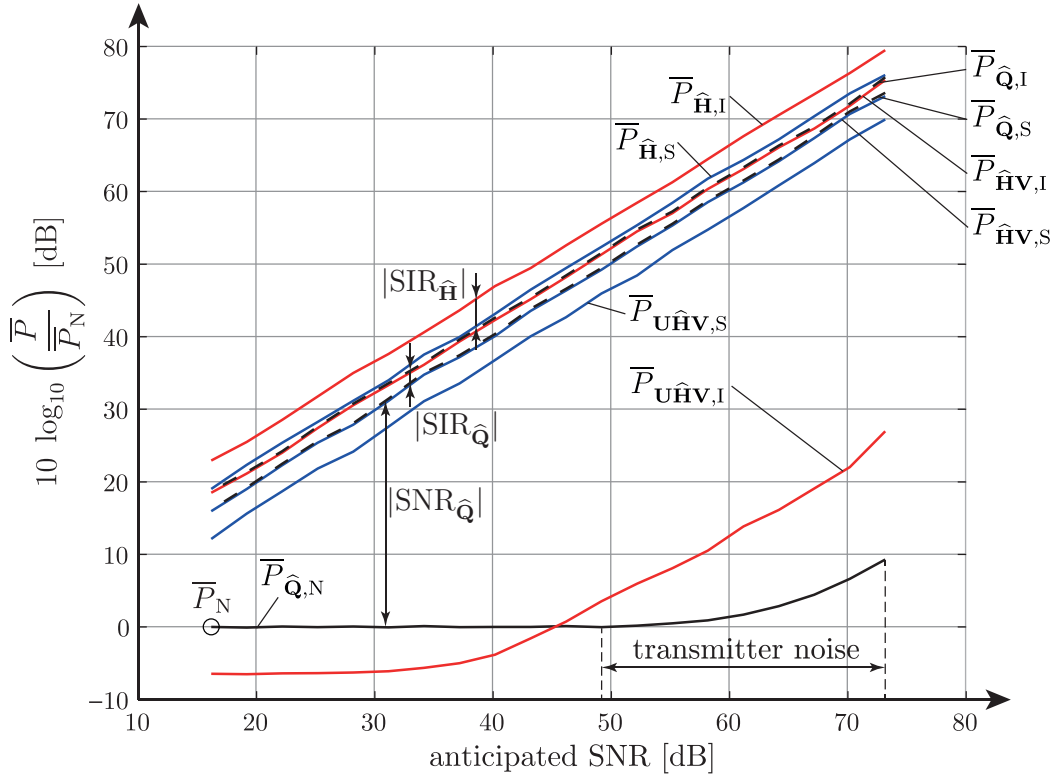


Figure 5.12: Variable SNR: measured powers

Figure 5.12 illustrates the measured powers that are used to compute SNR and SIR. The measured noise power $\bar{P}_{\hat{Q},N}$ at highest attenuation (lowest SNR) is called *anticipated noise power* \bar{P}_N and is expected to stay constant during the whole measurement. The corresponding *anticipated SNR* is obtained by taking the initial value of $\text{SNR}_{\hat{Q}}$ computed at highest attenuation and increasing it with the 3 dB stepsize for each attenuator constellation.

- At low transmitter attenuation (high SNR), the noise power unexpectedly grows and becomes larger than \bar{P}_N . This is a result of *transmitter noise* that is no longer suppressed by the attenuators.
- The powers computed from the sample covariance matrices, $\bar{P}_{\hat{Q},S}$ and $\bar{P}_{\hat{Q},I}$, coincide with the corresponding powers computed from the channel estimation matrices, $\bar{P}_{\hat{H}V,S}$ and $\bar{P}_{\hat{H}V,I}$, thus confirming that both power computation methods yield equivalent results.

Following behaviour is observed:

$$\bar{P}_{\hat{H},S} \stackrel{(a)}{>} \bar{P}_{\hat{H},S} \stackrel{(b)}{>} \bar{P}_{U\hat{H}V,S} \text{ and } \bar{P}_{\hat{H},I} \stackrel{(c)}{>} \bar{P}_{\hat{H}V,I} \stackrel{(d)}{\gg} \bar{P}_{U\hat{H}V,I}.$$

This can be explained as follows:

- (a) Precoding (see Equation 2.1) performs a basis transformation on the transmit data stream and arranges the $d = 2$ signal dimensions in a $M_T = 4$ dimensional space. The precoding matrix \mathbf{V}_j is a *truncated unitary* matrix of dimension $M_T \times d$. The product $\hat{\mathbf{H}}_{II} \mathbf{V}_I$ has the property

$$P_{\hat{\mathbf{H}}\mathbf{V},S} = \left\| \hat{\mathbf{H}}_{II} \mathbf{V}_I \right\|_F^2 < \left\| \hat{\mathbf{H}}_{II} \right\|_F^2 = P_{\hat{\mathbf{H}},S}, \quad (5.1)$$

assuming $\hat{\mathbf{H}}_{II}$ has full rank.

Proof (indices are dropped): The truncated unitary matrix \mathbf{V} can be written as the product of a true unitary matrix \mathbf{V}' and a truncated identity matrix according to

$$\mathbf{V} = \mathbf{V}' \begin{bmatrix} \mathbf{I}_d \\ \mathbf{0} \end{bmatrix}.$$

Furthermore,

$$\hat{\mathbf{H}}\mathbf{V}' = \begin{bmatrix} \hat{\mathbf{H}}_d & \hat{\mathbf{H}}_{M_T-d} \end{bmatrix} \text{ and } \left\| \hat{\mathbf{H}} \right\|_F^2 = \left\| \hat{\mathbf{H}}\mathbf{V}' \right\|_F^2.$$

Considering this in the left hand side of Equation (5.1):

$$P_{\hat{\mathbf{H}}\mathbf{V},S} = \left\| \hat{\mathbf{H}}\mathbf{V} \right\|_F^2 = \left\| \hat{\mathbf{H}}\mathbf{V}' \begin{bmatrix} \mathbf{I}_d \\ \mathbf{0} \end{bmatrix} \right\|_F^2 = \left\| \begin{bmatrix} \hat{\mathbf{H}}_d & \hat{\mathbf{H}}_{M_T-d} \end{bmatrix} \begin{bmatrix} \mathbf{I}_d \\ \mathbf{0} \end{bmatrix} \right\|_F^2 = \left\| \hat{\mathbf{H}}_d \right\|_F^2.$$

The right hand side of Equation (5.1) is treated similarly:

$$\begin{aligned} P_{\hat{\mathbf{H}},S} &= \left\| \hat{\mathbf{H}} \right\|_F^2 = \left\| \hat{\mathbf{H}}\mathbf{V}' \right\|_F^2 = \left\| \begin{bmatrix} \hat{\mathbf{H}}_d & \hat{\mathbf{H}}_{M_T-d} \end{bmatrix} \right\|_F^2 \\ &= \text{trace} \left(\begin{bmatrix} \hat{\mathbf{H}}_d & \hat{\mathbf{H}}_{M_T-d} \end{bmatrix} \begin{bmatrix} \hat{\mathbf{H}}_d^H \\ \hat{\mathbf{H}}_{M_T-d}^H \end{bmatrix} \right) \\ &= \text{trace} \left(\hat{\mathbf{H}}_d \hat{\mathbf{H}}_d^H \right) + \text{trace} \left(\hat{\mathbf{H}}_{M_T-d} \hat{\mathbf{H}}_{M_T-d}^H \right) \\ &= \left\| \hat{\mathbf{H}}_d \right\|_F^2 + \left\| \hat{\mathbf{H}}_{M_T-d} \right\|_F^2. \end{aligned}$$

Comparing both sides:

$$P_{\hat{\mathbf{H}}\mathbf{V},S} = \left\| \hat{\mathbf{H}}_d \right\|_F^2 < \left\| \hat{\mathbf{H}}_d \right\|_F^2 + \left\| \hat{\mathbf{H}}_{M_T-d} \right\|_F^2 = P_{\hat{\mathbf{H}},S}.$$

This proves that *precoding reduces the power*.

- (b) Interference suppression lowers the power of the desired signal. As mentioned in Section 2.3.2, the closed form computation of the IA filters has no constraint on maximizing the SNR. A reasoning similar to (a) applies (\mathbf{U}_I is a truncated unitary matrix).
- (c) Each interferer uses precoding matrices, interference power is hence also reduced by precoding. The same reasoning as in (a) applies.
- (d) Interference suppression tries to suppress the interference power completely (remember Equation 2.18). Ideally, $\bar{P}_{\mathbf{U}\hat{\mathbf{H}}\mathbf{V},I}$ would be zero at all times. Above 40 dB SNR, $\bar{P}_{\mathbf{U}\hat{\mathbf{H}}\mathbf{V},I}$ starts to grow and is constantly 50 dB lower than $\bar{P}_{\hat{\mathbf{H}},I}$ - the (non-ideal) IA filters are able to lower the interference power by approximately 50 dB. The effect of growing interference power will be further studied in Section 5.2.2.

Note that $\text{SIR}_{\hat{\mathbf{H}}}$ is used as reference to control the SIR (via attenuators), since it considers the “true” power contribution from each transmitter without transmit or receive filters.

Figure 5.13 shows the measured SNR and SIR curves.

- $\text{SNR}_{\hat{\mathbf{Q}}}$ follows the anticipated SNR line nicely until it is lowered by the received transmitter noise, noticeable above 60 dB SNR.
- $\text{SNR}_{\hat{\mathbf{H}}} > \text{SNR}_{\hat{\mathbf{Q}}} (\approx \text{SNR}_{\hat{\mathbf{H}\mathbf{V}}}) > \text{SNR}_{\mathbf{U}\hat{\mathbf{H}}\mathbf{V}}$, evident from explanations (a) and (b) above.
- $\text{SIR}_{\hat{\mathbf{H}}}$ follows the anticipated SIR line (-3 dB) nicely since it was used as reference for transmit power calibration.
- $\text{SIR}_{\mathbf{U}\hat{\mathbf{H}}\mathbf{V}}$ is the actual SIR after interference suppression and shows impressive results.

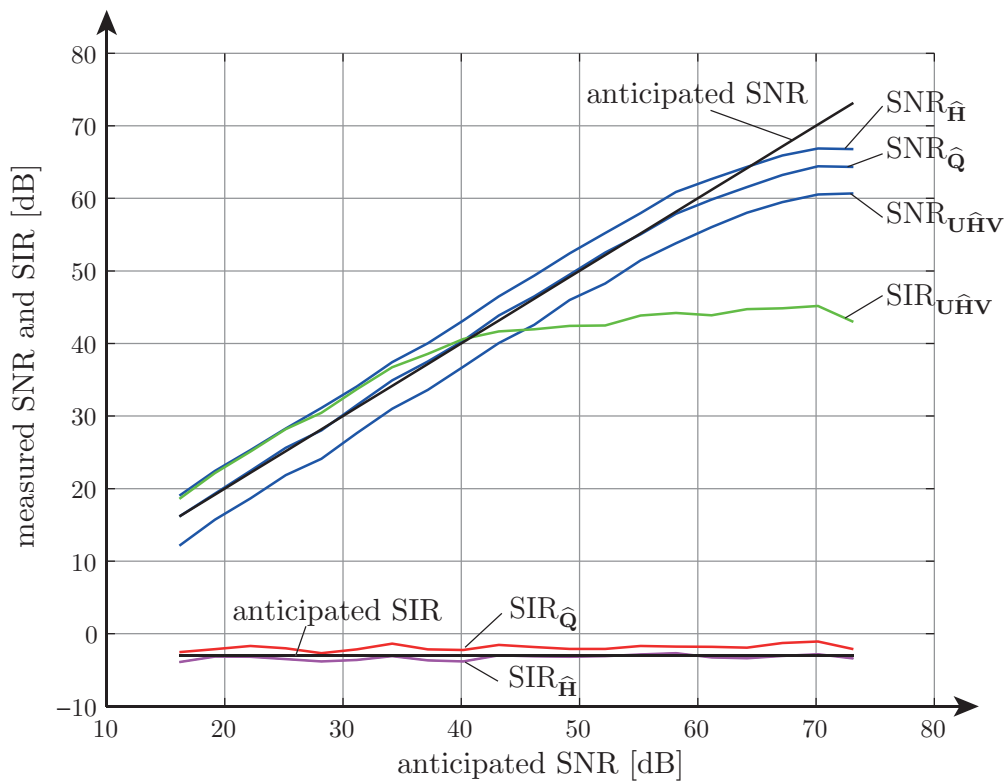


Figure 5.13: Variable SNR: measured SNR and SIR

5.2.2 Interference Suppression

Figure 5.14 depicts the average interference suppression as defined in Equation (4.25). The measured $\text{SNR}_{\hat{\mathbf{Q}}}$ is also plotted for comparison. In Figure 5.12, it was confirmed that signal and interference power steadily increase with increasing SNR. Increasing interference power corresponds to growing eigenvalues λ_3 and λ_4 of \mathbf{Q}_b , and the associated \bar{I}_{supp} would ideally also increase in the same manner. However, it peaks out at around 60 dB SNR and then even decreases. Intuitively, this could be caused by received transmitter noise or by *leakage* of the interference (λ_3 and λ_4) into the desired signal subspace (λ_1 and λ_2) as a result of bad alignment.

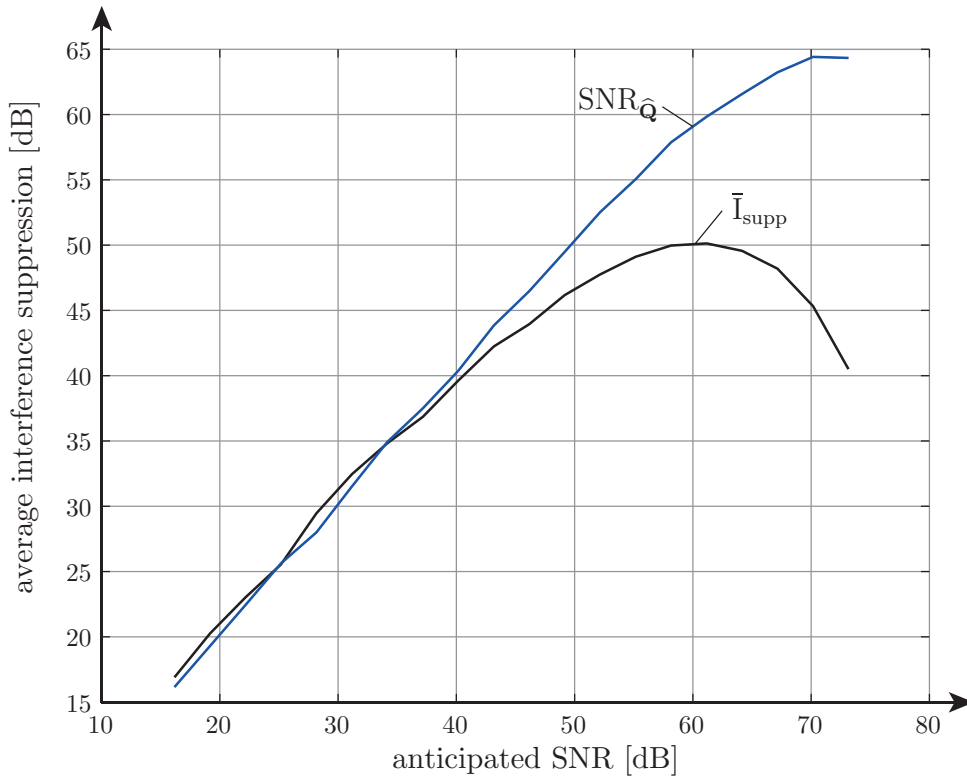


Figure 5.14: Variable SNR: average interference suppression

Figure 5.15 shows the eigenvalues of $\hat{\mathbf{Q}}_b$ (denoted $\{\lambda_1, \dots, \lambda_4\}$) and $\hat{\mathbf{Q}}_N$ (denoted $\{\sigma_1^2, \dots, \sigma_4^2\}$), averaged over all transmissions and plotted for each attenuator constellation (SNR realization). It becomes apparent that the effect of growing noise (received transmitter noise) at high SNR is not the only cause of the reduced interference suppression, as it starts at around 60 dB SNR whereas the leakage phenomenon starts already around 40 dB SNR. The increased leakage is caused by outdated precoders that are computed from the channel estimates of “the last frame rather than the actual frame” (see Section 3.2). This is a systematic error in the measurement methodology that can not be circumvented. Due to the sequential nature of channel estimation \rightarrow filter computation \rightarrow filter feedback, filters are always outdated by $T_p = 70$ ms. An interference suppression of 50 dB is “as good as it gets” considering the used measurement methodology and the experienced channel fluctuations. If ideal precoders (from perfect channel knowledge) would be used, leakage would not occur.

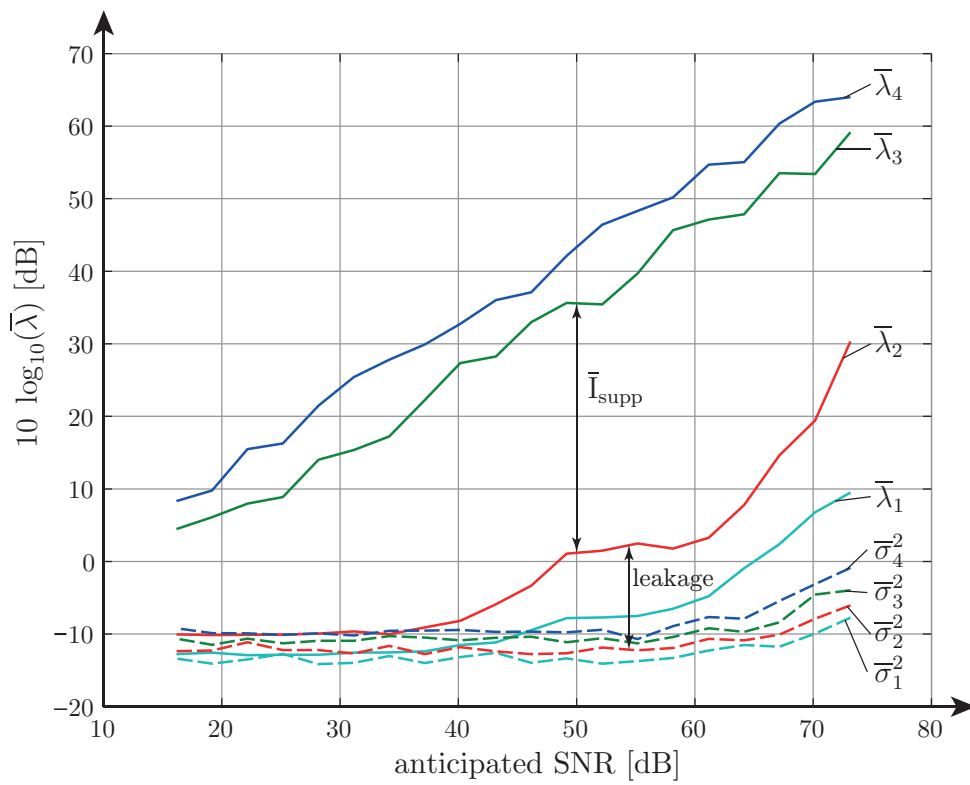


Figure 5.15: Variable SNR: average eigenvalues of $\hat{\mathbf{Q}}_b$ and $\hat{\mathbf{Q}}_N$

5.2.3 Mutual Information

Figure 5.16 illustrates various measured mutual information curves. The upper bound is constituted by $\bar{\mathcal{I}}_{\hat{\mathbf{H}},\text{noInt}}(\mathbf{x}_1; \mathbf{y}_1)$, which coincides with $\bar{\mathcal{I}}_{\hat{\mathbf{H}},\text{SVD},\text{noInt}}(\mathbf{s}_1; \mathbf{r}_1)$ (not plotted here) and is only achievable in the absence of interference by exploiting all four DoF provided by four antenna MIMO transmission. The lowest mutual information is given by $\bar{\mathcal{I}}_{\hat{\mathbf{H}}}(\mathbf{x}_1; \mathbf{y}_1)$, which coincides with $\bar{\mathcal{I}}_{\hat{\mathbf{H}},\text{SVD}}(\mathbf{s}_1; \mathbf{y}_1)$ (not plotted here) and heavily suffers from interference. It is not visibly affected by SNR variations, because the interference power is the dominant power throughout the whole measurement ($P_1 \gg P_N$). In between, IA tries to optimally exploit its two DoF and would ideally attain “half the cake”, meaning half of the the upper bound. This seems to be true only in the low SNR regime of the plot, as the gap between mutual information with and without interference present grows with increasing SNR. The worsened mutual information at high SNR is a result of the leakage phenomenon discovered in Section 5.2.2.

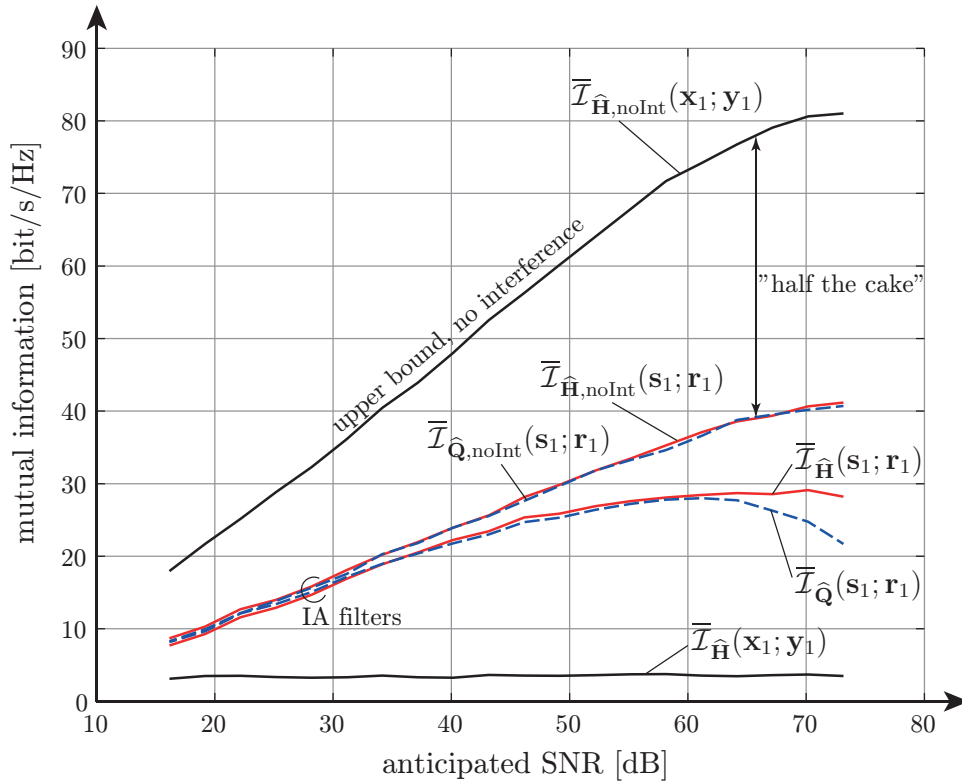


Figure 5.16: Variable SNR: mutual information (overview)

Figure 5.17 focuses on mutual information in the presence of interference. The lower curves show the mutual information with SVD filters as defined in Section 4.2.1. Note that these filters utilize all four DoF but are computed as if no interference is present (each user assumes a single link). Using IA filters (i.e. IA precoding and interference suppression matrices), the results are improved considerably. Apparently, mutual information is lowered by receive filtering. For IA, this behaviour was already mentioned in Section 2.3.2 and in Section 5.2.1. Imagine that interference is aligned in a subspace at the receiver. This subspace is linearly independent of the desired signal subspace, but not necessarily orthogonal to it. Interference suppression that projects the desired signal onto a subspace that is orthogonal to the interference subspace therefore lowers the SNR. Another interpretation considers the mutual information. The receive signal vector \mathbf{y}_I contains a certain amount of information about the transmit signal

stream \mathbf{s}_I , but interference is still present. Part of this information is “cut away” in the process of interference suppression and is missing in the receive symbol stream \mathbf{r}_I .

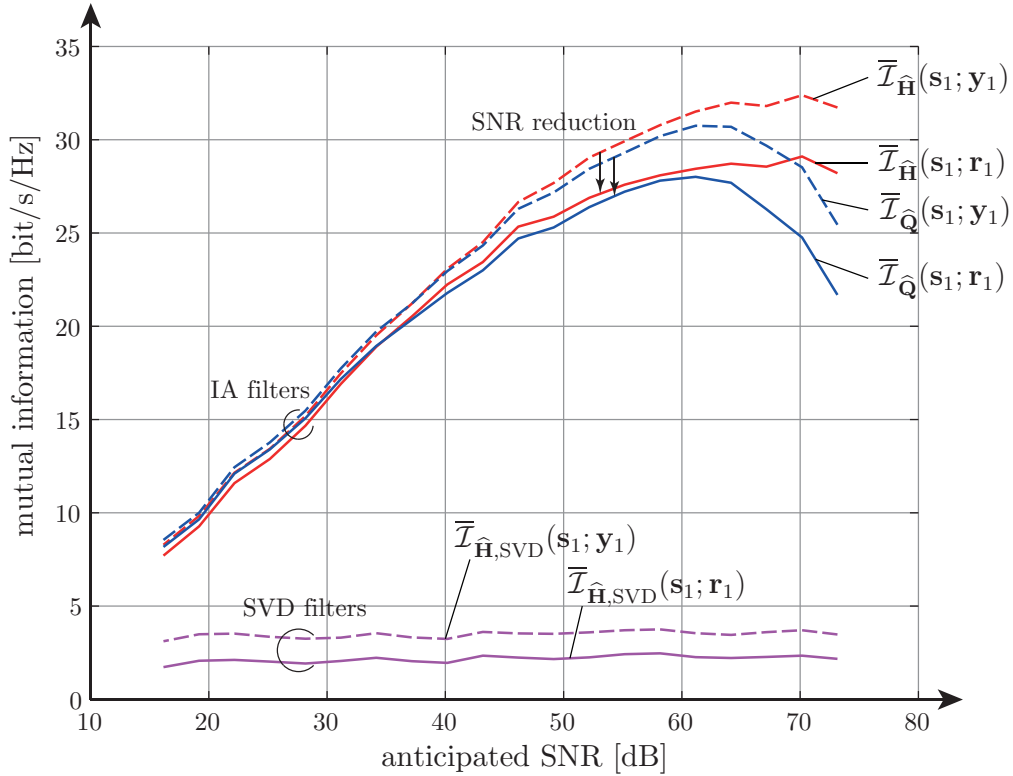


Figure 5.17: Variable SNR: mutual information

The measurements above demonstrated that in the low SNR regime of the plots, IA works as expected in theory and achieves superb results. Note that the low SNR regime actually considers relatively high SNR values. The focus of the measurements was clearly set on high SNR values, provoking hardware-induced effects which diminish the IA performance. In order to realize lower SNR values, the “DACscaling” (see Equation (3.4)) has to be lowered, which in turn introduces heightened quantization noise. This exceeds the focus of this work.

5.3 Variable SIR at Fixed SNR

The dependence of the performance measures on SIR at fixed SNR = 37 dB is now investigated. The *transmit power calibration* is performed similarly to the method described in Section 5.2, only step 5 is altered in order to vary the SIR. With the final attenuator values as obtained in step 4, all transmitters are received equally strong (SNR = -3 dB) and have maximum power (lowest attenuation). The desired transmitter attenuator α_I is then increased to obtain a certain (fixed) SNR value. Finally, the interfering transmitter attenuators α_j , $j \neq I$, are jointly increased in order to increase the SIR. An *example* will illuminate the process:

1. Final attenuator values after transmit power calibration (see Section 5.2):

$$[\alpha_1, \alpha_2, \alpha_3] = [0, 2, 6] \text{ dB} \xrightarrow{\text{accomplish}} \text{SNR} = 73 \text{ dB}, \text{ SIR} = -3 \text{ dB}.$$

2. Increase desired transmitter attenuator α_1 (desired link $I = 1$) by 36 dB in order to obtain SNR = 37 dB:

$$[\alpha_1 + 36, \alpha_2, \alpha_3] = [36, 2, 6] \text{ dB} \rightarrow \text{SNR} = 73 - 36 = 37 \text{ dB}, \text{ SIR} = -3 - 36 = -39 \text{ dB}.$$

3. Assuming 3 dB increment of α_2 and α_3 (interfering transmitter attenuators) at each attenuator constellation, this results in following *anticipated* SIR range:

attenuator constellation 1: [36, 2, 6] dB → SNR = 37 dB, SIR = -39 dB,
attenuator constellation 2: [36, 5, 9] dB → SNR = 37 dB, SIR = -36 dB,
attenuator constellation 3: [36, 8, 12] dB → SNR = 37 dB, SIR = -33 dB,
⋮
attenuator constellation 20: [36, 59, 63] dB → SNR = 37 dB, SIR = 18 dB.

Figure 5.11 illustrates the measurement process. In this measurement, all three links were desired once.

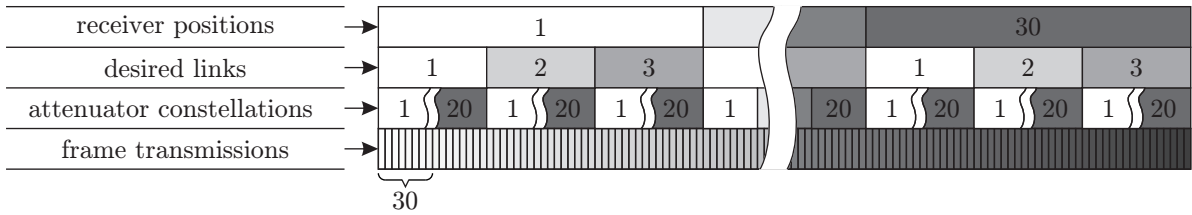


Figure 5.18: Variable SIR: measurement process

The parameters of the the measurement are summarized in Table 5.3.

5.3.1 Measured Powers, SNR and SIR

To verify that the controlled SIR increases as expected while the SNR stays constant, the measured powers are now investigated. The measurement encompasses 20 attenuator constellations.

Figure 5.19 illustrates the measured powers that are used to compute SNR and SIR. The measured noise power $\bar{P}_{\hat{Q},N}$ at highest interferer attenuation (highest SIR) is called *anticipated noise power* \bar{P}_N and is expected to stay constant during the whole measurement. The corresponding *anticipated* SNR is also expected to stay constant at 37 dB, $\text{SNR}_{\hat{Q}}$ constitutes its

| parameter | value | comments |
|---------------------------------------|-------------|--|
| receiver positions | 30 | represent channel realizations |
| attenuator constellations | 20 | relative attenuator values: 0, 3, ..., 57 dB |
| transmissions per constellation | 30 | at one receiver position |
| total transmissions per constellation | 1500 | considering all receiver positions |
| data symbols per frame | 2×60 | 2 streams, 20 symbol vectors per stage |
| anticipated SNR | 37 dB | |
| anticipated SIR | −39...18 dB | |
| processing time T_P between frames | 70 ms | averaged over all transmissions |

Table 5.3: Variable SIR: parameters

measured value. The *anticipated* SIR is obtained by taking the initial value of $\text{SIR}_{\hat{\mathbf{H}}}$ computed at highest interferer attenuation (corresponding to attenuator constellation 20 in the introductory example) and decreasing it by the 3 dB stepsize for each attenuator constellation until the lowest possible SIR is obtained (attenuator constellation 1 in the introductory example).

- Interference power is steadily decreasing with increasing interference attenuators, while the signal power stays constant. $\bar{P}_{\hat{\mathbf{H}},S}$ and $\bar{P}_{\hat{\mathbf{H}},I}$ intersect at 0 dB SIR as expected.
- At high interferer attenuation (low SIR), the noise power unexpectedly grows and becomes larger than \bar{P}_N . This is a result of *transmitter noise* that is received at RX (and is no longer suppressed by the attenuators).
- The powers computed from the sample covariance matrices, $\bar{P}_{\hat{\mathbf{Q}},S}$ and $\bar{P}_{\hat{\mathbf{Q}},I}$, coincide with the corresponding powers computed from the channel estimation matrices, $\bar{P}_{\hat{\mathbf{H}},S}$ and $\bar{P}_{\hat{\mathbf{H}},I}$, thus confirming that both power computation methods yield equivalent results. This was already confirmed in Section 5.2.1.

The measured powers compare the same way as in Section 5.2.1, the same reasoning applies.

Figure 5.20 shows a power-comparison of all three desired links. It confirms that the same signal and interference power, $\bar{P}_{\hat{\mathbf{H}},S}$ and $\bar{P}_{\hat{\mathbf{H}},I}$, is experienced by all three links. Including the IA filters, the powers begin to behave differently for each desired link, especially considering the power after interference suppression $\bar{P}_{\mathbf{U}\hat{\mathbf{H}},I}$. The best interference power suppression seems to be achieved over desired link one.

Figure 5.21 depicts the measured SNR and SIR curves.

- $\text{SNR}_{\hat{\mathbf{Q}}}$ follows the anticipated SNR line nicely until it is lowered by the received transmitter noise, noticeable below −20 dB SIR.
- $\text{SNR}_{\hat{\mathbf{H}}} > \text{SNR}_{\hat{\mathbf{Q}}} (\approx \text{SNR}_{\hat{\mathbf{H}}\mathbf{V}}) > \text{SNR}_{\mathbf{U}\hat{\mathbf{H}}\mathbf{V}}$, evident from explanations (a) and (b) in Section 5.2.1.
- $\text{SIR}_{\hat{\mathbf{H}}}$ follows the anticipated SIR line nicely since it was used as reference for transmit power calibration.
- $\text{SIR}_{\mathbf{U}\hat{\mathbf{H}}\mathbf{V}}$ is the actual SIR after interference suppression and shows impressive results.

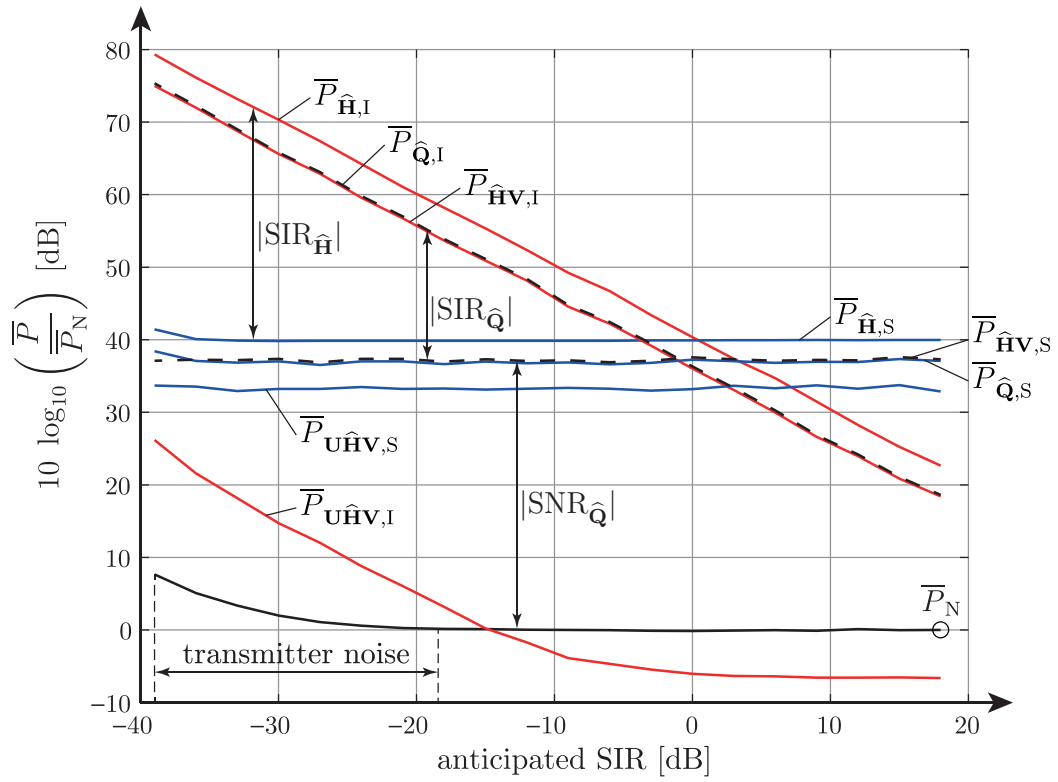


Figure 5.19: Variable SIR: measured powers (desired link $I = 1$)

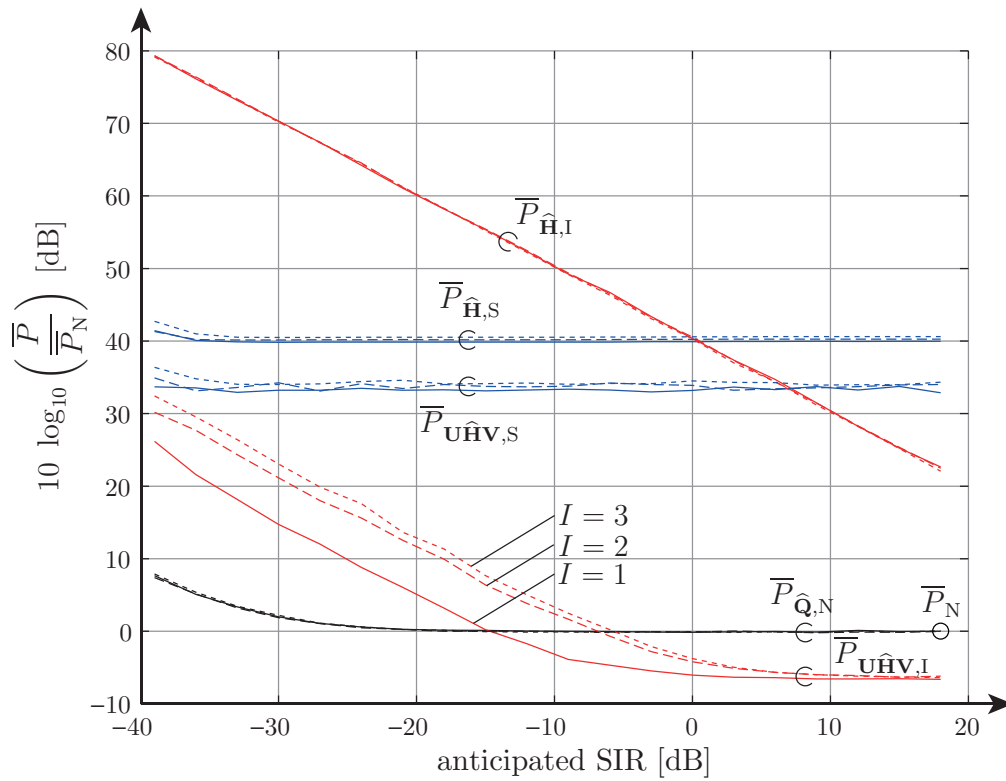


Figure 5.20: Variable SIR: measured powers (desired link $I = \{1, 2, 3\}$)

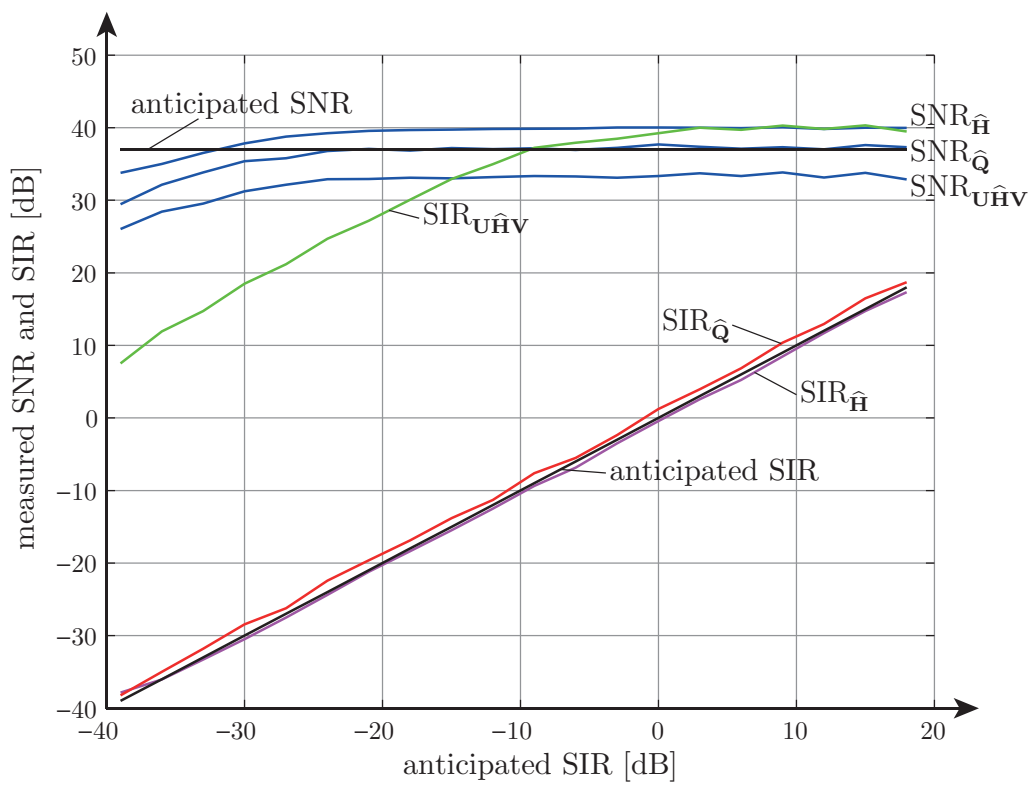


Figure 5.21: Variable SIR: measured SNR and SIR (desired link $I = 1$)

5.3.2 Interference Suppression

Figure 5.22 depicts the average interference suppression as defined in Equation (4.25), for each link individually. It behaves as expected at moderate and high SIR - growing interference power results in growing interference suppression. It peaks out at around -25 dB SIR and even decreases for smaller SIR. Two effects have to be considered:

- The leakage phenomenon, discovered in Section 5.2.2, will also occur at low SIR (strong interference). It is mainly caused by outdated precoders (see Section 3.2). Similar to Section 5.2.2, an interference suppression of 50 dB is “as good as it gets”.
- Below -20 dB SIR, received transmitter noise becomes noticeable.

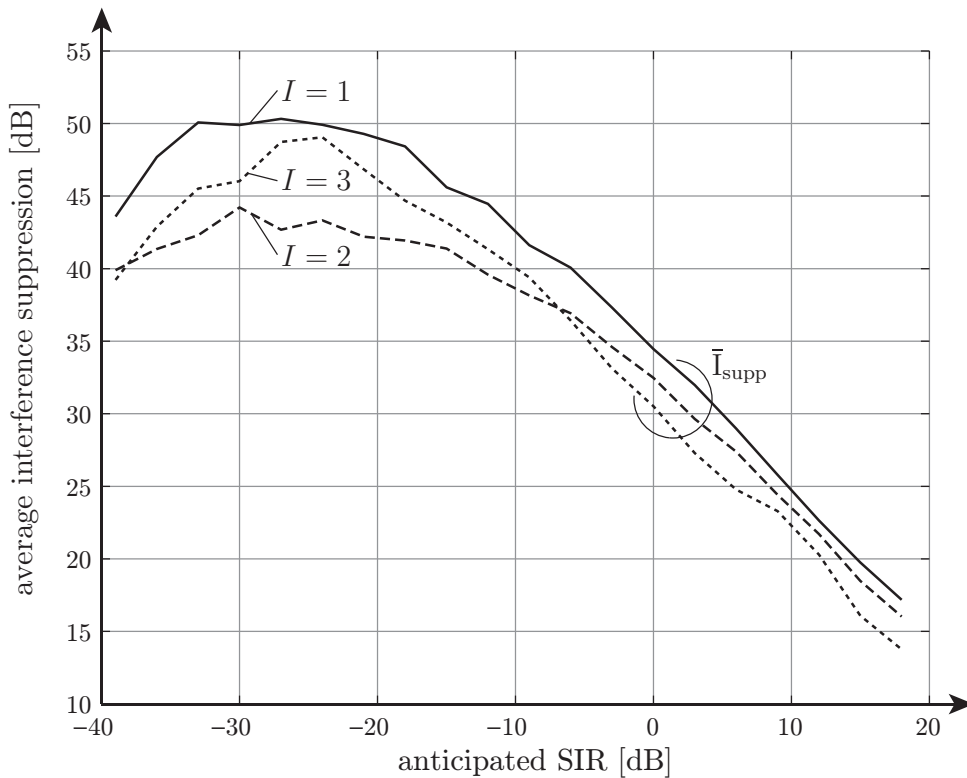


Figure 5.22: Variable SIR: average interference suppression (desired link $I = \{1, 2, 3\}$)

Figure 5.23, Figure 5.24 and Figure 5.25 show the eigenvalues of $\hat{\mathbf{Q}}_b$ (denoted $\{\lambda_1, \dots, \lambda_4\}$) and $\hat{\mathbf{Q}}_N$ (denoted $\{\sigma_1^2, \dots, \sigma_4^2\}$) averaged over all transmissions and plotted for each attenuator constellation (SIR realization), for each link individually. This allows to investigate the leakage that lowers the interference suppression. The lowest leakage is experienced over link one, link two is the worst. This supports the findings from Figure 5.22.

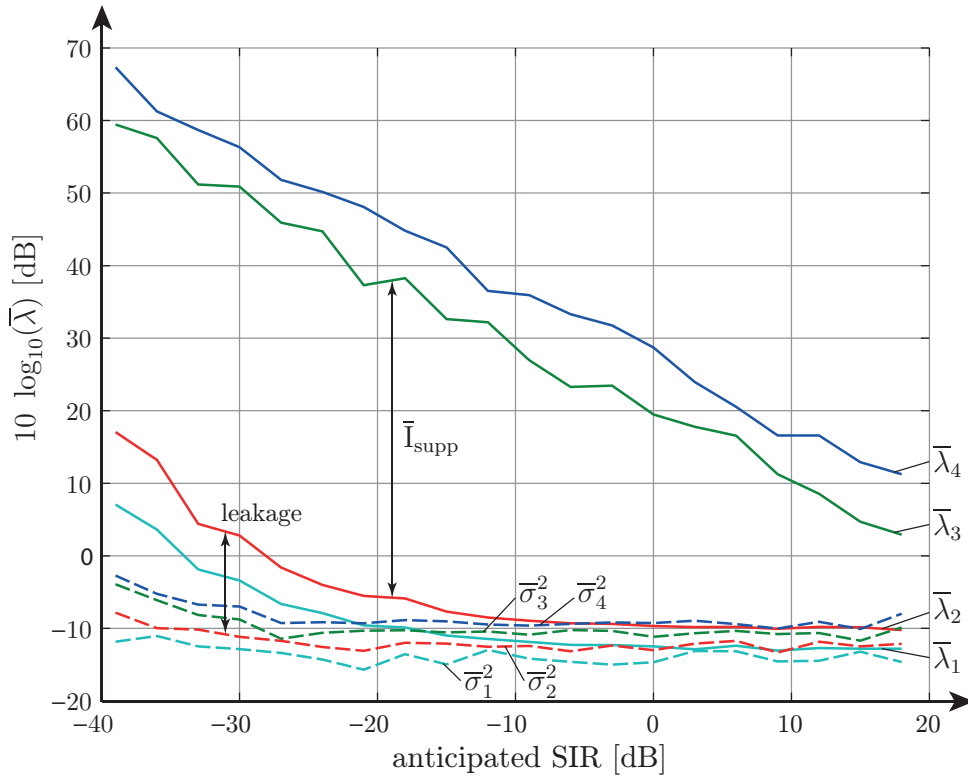


Figure 5.23: Variable SIR: average eigenvalues of $\hat{\mathbf{Q}}_b$ and $\hat{\mathbf{Q}}_N$ (desired link $I = 1$)

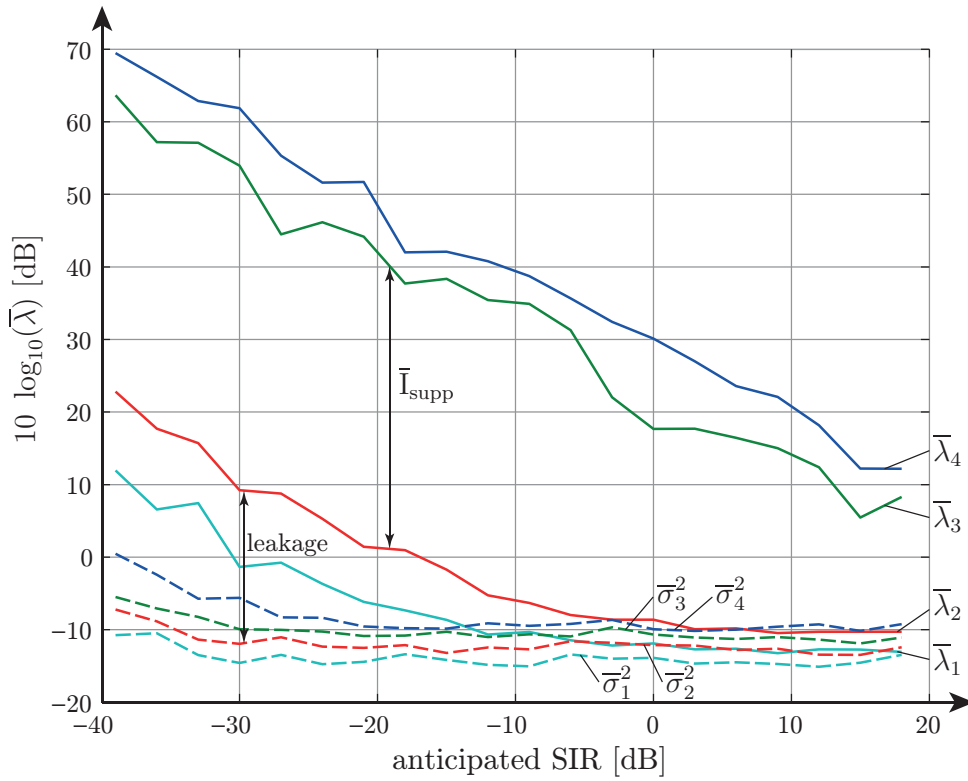


Figure 5.24: Variable SIR: average eigenvalues of $\hat{\mathbf{Q}}_b$ and $\hat{\mathbf{Q}}_N$ (desired link $I = 2$)

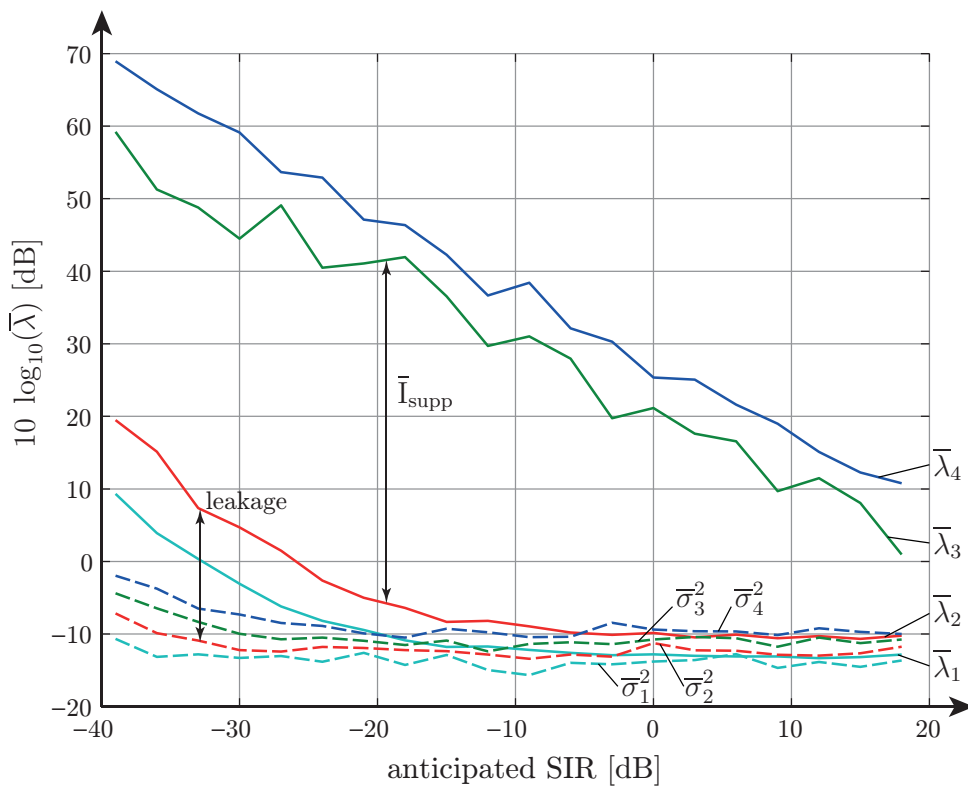


Figure 5.25: Variable SIR: average eigenvalues of $\hat{\mathbf{Q}}_b$ and $\hat{\mathbf{Q}}_N$ (desired link $I = 3$)

5.3.3 Mutual Information

Figure 5.27 illustrates various measured mutual information curves. The upper bound is constituted by $\bar{I}_{\hat{\mathbf{H}},\text{noInt}}(\mathbf{x}_1; \mathbf{y}_1)$, which is only achievable in the absence of interference by exploiting all four DoF provided by four antenna MIMO transmission. The lowest mutual information is given by $\bar{I}_{\hat{\mathbf{H}}}(\mathbf{x}_1; \mathbf{y}_1)$, which coincides with $\bar{I}_{\hat{\mathbf{H}},\text{SVD}}(\mathbf{s}_1; \mathbf{y}_1)$ (not plotted here) and heavily suffers from interference at low SIR. IA tries to optimally exploit its two DoF and would ideally attain half of the the upper bound. Mutual information stays constantly high above -10 dB SIR and decreases below. The reasons for this behaviour were pointed out in Section 5.3.2.

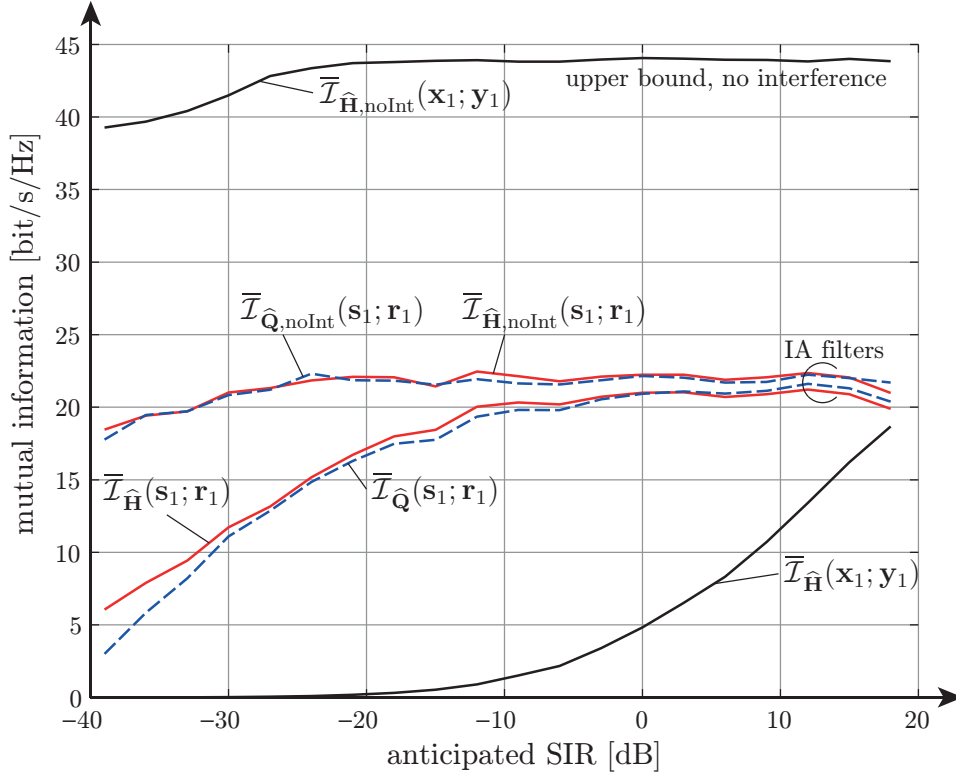


Figure 5.26: Variable SIR: mutual information (overview, desired link $I = 1$)

Figure 5.27 focuses on mutual information in the presence of interference. The relation between the various displayed mutual information curves has been described in Section 5.2.3. The lower curves show the mutual information with SVD filters as defined in Section 4.2.1. IA strongly improves the results below 20 dB SIR. Above (at high SIR), interference is low enough for the SVD filters to “catch up” and improve over IA. Remember that SVD filters utilize all four DoF provided by MIMO transmission, whereas IA can only exploit two DoF for the desired signal transmission.

Figure 5.28 compares the mutual information for all three desired links. The results show that in the absence of interference, the highest mutual information is achieved over link three (indoor channel), followed by link one and link two. With interference present, the SVD case draws a similar picture. Considering desired link three, SVD filtering exceeds IA in terms of mutual information above 13 dB SIR. For desired link one, this occurs around 18 dB SIR.

Above measurements have shown that IA performs well, even during strong interference. A considerable gain in mutual information is experienced at low and moderate SIR, despite the occurrence of leakage and received transmitter noise at low SIR.

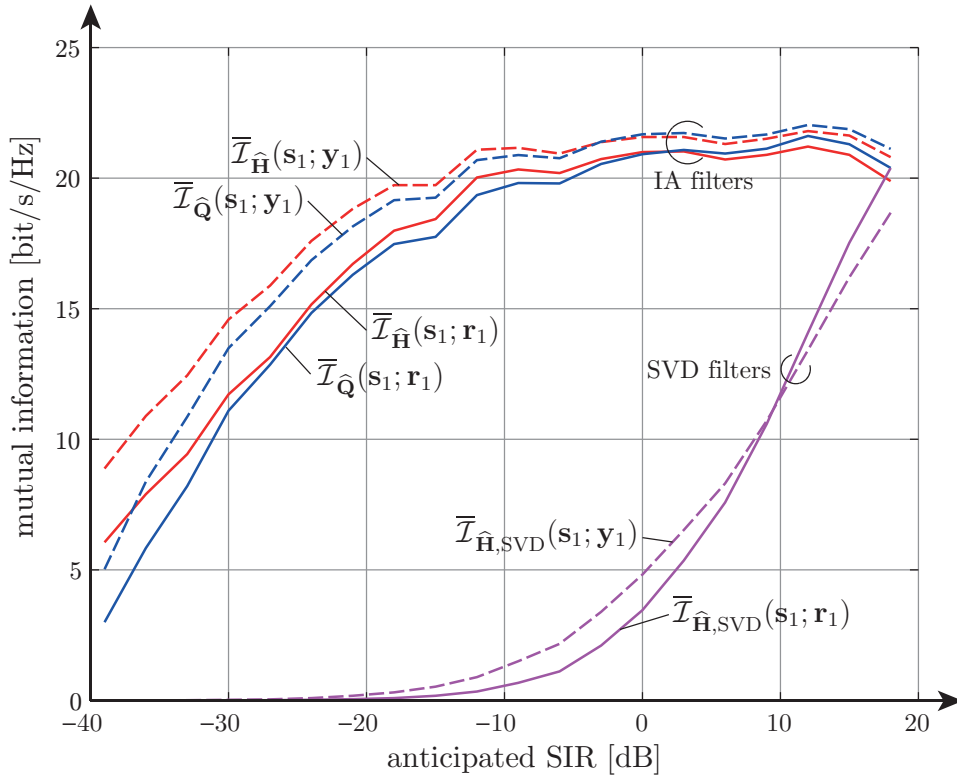


Figure 5.27: Variable SIR: mutual information (desired link $I = 1$)

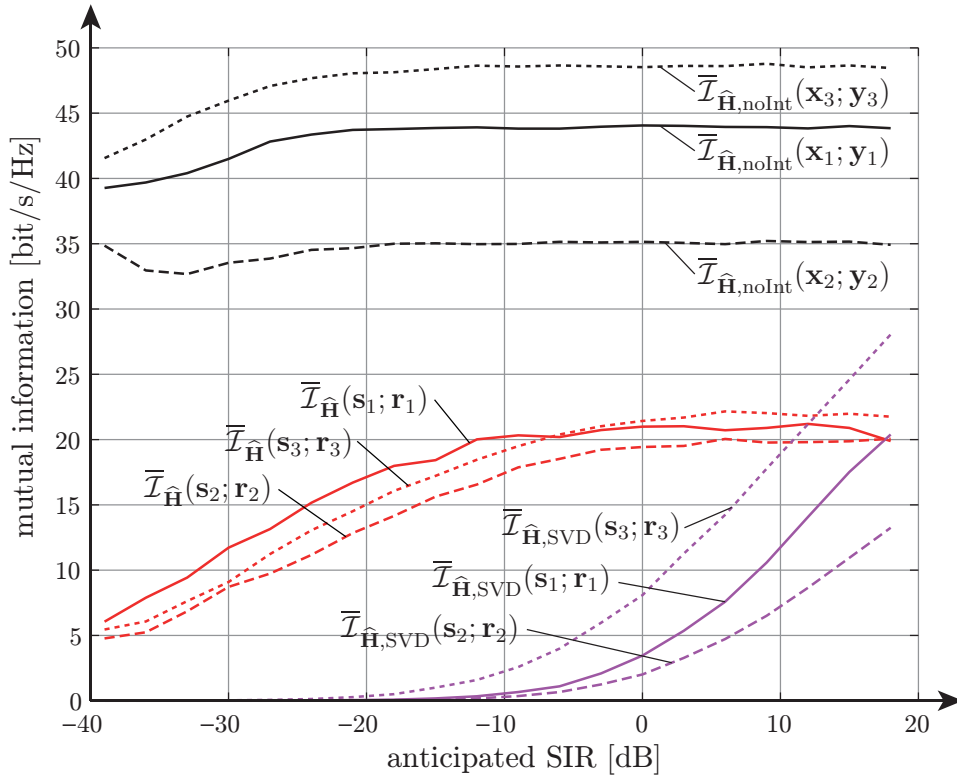


Figure 5.28: Variable SIR: mutual information (desired link $I = \{1, 2, 3\}$)

Chapter 6

Conclusion and Outlook

Throughout this work, an interference mitigation technique for wireless multi-user networks called Interference Alignment (IA) was investigated and implemented on the Vienna MIMO Testbed (VMTB). Theoretical aspects such as the mathematical background and feasibility were discussed. The VMTB was utilized to perform a measurement based analysis. Necessary augmentations in hardware, software and signal generation that make IA possible were described. Performance measures to investigate and compare the alignment quality were introduced.

The first measurement dealt with feasibility of IA at fixed SNR and SIR. It was shown, for each of the three possible links individually, that interference is aligned at the receiver. The mutual information, representative of data rate, was thereby strongly improved. Further measurements investigated the impact of variable SNR and variable SIR, respectively. It was shown that IA reaches “half the cake” in terms of data rate, namely half of the mutual information that could be achieved in the absence of interference. However, the results were aggravated by hardware influences such as unsuppressed transmitter noise and by outdated filters that caused leakage.

This work restricted itself to quasi-static channels with no deliberate movement (measurements took place at fixed receiver positions, no moving scatterers were placed intentionally). Another thesis [23] utilizes the same testbed and investigates how spatially outdated IA filters affect the alignment.

Many aspects of the system could be investigated in the future, the most relevant are:

- **Low SNR:** How does IA perform at low SNR (below 10 dB)?
 - *Noisy* channel estimates might impair the alignment.
- **Feedback:** An ideal feedback link constituted by a dedicated fiber network was used.
 - *Limited* feedback is more realistic.
 - *Quantized* feedback is usually used and has already been investigated in theory.
- **Channels:** The virtual channels to the non-existing receivers are full rank and constant.
 - *Measured* channels,
 - *spatially correlated* channels,
 - *time varying* channels (simulated or measured) could be investigated.
- **Schemes:** An efficient closed form solution for the IA filters was used.
 - *IA with constraints* on e.g. SINR maximization is of interest.
 - *Iterative* algorithms have been proposed in literature.
 - *Coordinated multipoint* is a prominent alternative to IA.

- **Implementation:** A more realistic implementation could be considered.
 - *Frame structure* according to a standard (e.g. LTE or WLAN).

To conclude this work: IA was shown to be feasible on a real world testbed. Difficulties in implementation will arise in more realistic systems with moving receivers and moving scatterers, where the filter computation-time becomes a more pressing issue. Performing optimal feedback and synchronization in more realistic scenarios is an open problem that is currently investigated.

The author of this work sees a possible incorporation of IA in the further progression of WLAN or LTE, particularly in applications where neither the transmitters nor the receivers move considerably. This mitigates the synchronization issue and the filter computation-time issue.

The thorough investigation of various IA aspects is currently subject of several research projects whose outcome will determine the viability of IA and how it compares to competitive schemes. An efficient interference management scheme would pave the way for wireless multi-user networks with substantially increased spectral efficiency and data throughput.

Interference Alignment might be that scheme.

List of Figures

| | | |
|------|--|----|
| 1.1 | Basic principle of TDMA in the three user case | 3 |
| 1.2 | Basic principle of IA in the three user case | 3 |
| 2.1 | $(4 \times 4, 2)^3$ MIMO interference channel | 6 |
| 2.2 | Signal vectors in a $(2 \times 2, 1)^2$ interference channel without noise | 11 |
| 3.1 | Deployment of Vienna MIMO Testbed | 13 |
| 3.2 | TX1 antenna setup | 14 |
| 3.3 | TX2 antenna setup with sensors | 14 |
| 3.4 | TX3 station | 14 |
| 3.5 | TX3 to RX indoor channel | 14 |
| 3.6 | Transmitter overview [19] | 15 |
| 3.7 | Receiver overview [21] | 16 |
| 3.8 | RX antennas in laptop shell | 17 |
| 3.9 | RX station | 17 |
| 3.10 | Two consecutive transmit frames | 18 |
| 3.11 | Basic transmit signal of a single transmission | 25 |
| 3.12 | Compensation of propagation delays | 25 |
| 3.13 | Measurement script | 28 |
| 4.1 | Detailed frame structure | 32 |
| 5.1 | Validation: measurement process | 40 |
| 5.2 | Validation: eigenvalues of $\hat{\mathbf{Q}}_b$ and $\hat{\mathbf{Q}}_N$ (desired link $I = 1$) | 42 |
| 5.3 | Validation: eigenvalues of $\hat{\mathbf{Q}}_b$ and $\hat{\mathbf{Q}}_N$ (desired link $I = 2$) | 43 |
| 5.4 | Validation: eigenvalues of $\hat{\mathbf{Q}}_b$ and $\hat{\mathbf{Q}}_N$ (desired link $I = 3$) | 43 |
| 5.5 | Validation: mutual information comparison (desired link $I = 1$) | 44 |
| 5.6 | Validation: mutual information comparison (desired link $I = 2$) | 44 |
| 5.7 | Validation: mutual information comparison (desired link $I = 3$) | 45 |
| 5.8 | Validation: receive power contributions (desired link $I = 1$) | 45 |
| 5.9 | Validation: receive power contributions (desired link $I = 2$) | 46 |
| 5.10 | Validation: receive power contributions (desired link $I = 3$) | 46 |
| 5.11 | Variable SNR: measurement process | 47 |
| 5.12 | Variable SNR: measured powers | 48 |
| 5.13 | Variable SNR: measured SNR and SIR | 50 |
| 5.14 | Variable SNR: average interference suppression | 51 |
| 5.15 | Variable SNR: average eigenvalues of $\hat{\mathbf{Q}}_b$ and $\hat{\mathbf{Q}}_N$ | 52 |
| 5.16 | Variable SNR: mutual information (overview) | 53 |
| 5.17 | Variable SNR: mutual information | 54 |
| 5.18 | Variable SIR: measurement process | 55 |
| 5.19 | Variable SIR: measured powers (desired link $I = 1$) | 57 |
| 5.20 | Variable SIR: measured powers (desired link $I = \{1, 2, 3\}$) | 57 |

| | | |
|------|--|----|
| 5.21 | Variable SIR: measured SNR and SIR (desired link $I = 1$) | 58 |
| 5.22 | Variable SIR: average interference suppression (desired link $I = \{1, 2, 3\}$) | 59 |
| 5.23 | Variable SIR: average eigenvalues of $\hat{\mathbf{Q}}_b$ and $\hat{\mathbf{Q}}_N$ (desired link $I = 1$) | 60 |
| 5.24 | Variable SIR: average eigenvalues of $\hat{\mathbf{Q}}_b$ and $\hat{\mathbf{Q}}_N$ (desired link $I = 2$) | 60 |
| 5.25 | Variable SIR: average eigenvalues of $\hat{\mathbf{Q}}_b$ and $\hat{\mathbf{Q}}_N$ (desired link $I = 3$) | 61 |
| 5.26 | Variable SIR: mutual information (overview, desired link $I = 1$) | 62 |
| 5.27 | Variable SIR: mutual information (desired link $I = 1$) | 63 |
| 5.28 | Variable SIR: mutual information (desired link $I = \{1, 2, 3\}$) | 63 |

Bibliography

- [1] Viveck R. Cadambe and Syed A. Jafar. Interference Alignment and Degrees of Freedom of the K-User Interference Channel. *IEEE Transactions on Information Theory*, 54, August 2008.
- [2] Omar El Ayach, Steven W Peters, and RW Heath. Real World Feasibility of Interference Alignment using MIMO-OFDM Channel Measurements. In *Military Communications Conference, 2009. MILCOM 2009. IEEE*, pages 1–6. IEEE, 2009.
- [3] Viveck R. Cadambe Krishna Gomadam and Syed A. Jafar. Approaching the Capacity of Wireless Networks through Distributed Interference Alignment. In *Global Telecommunications Conference, 2008. IEEE GLOBECOM 2008. IEEE*, pages 1–6. IEEE, 2008.
- [4] Steven W Peters and Robert W Heath. Interference Alignment via Alternating Minimization. In *Acoustics, Speech and Signal Processing, 2009. ICASSP 2009. IEEE International Conference on*, pages 2445–2448. IEEE, 2009.
- [5] Omar El Ayach, Steven W Peters, and Robert W Heath. The Feasibility of Interference Alignment Over Measured MIMO-OFDM Channels. *Vehicular Technology, IEEE Transactions on*, 59(9):4309–4321, 2010.
- [6] O González, D Ramirez, I Santamaria, JA Garcia-Naya, and L Castedo. Experimental Validation of Interference Alignment Techniques using a Multiuser MIMO Testbed. In *Smart Antennas (WSA), 2011 International ITG Workshop on*, pages 1–8. IEEE, 2011.
- [7] Roland Tresch and Maxime Guillaud. Cellular Interference Alignment with Imperfect Channel Knowledge. In *Communications Workshops, 2009. ICC Workshops 2009. IEEE International Conference on*, pages 1–5. IEEE, 2009.
- [8] JA Garcia-Naya, L Castedo, O González, D Ramirez, and I Santamaria. Experimental Evaluation of Interference Alignment Under Imperfect Channel State Information. *Proc. EUSIPCO 2011*, 2011.
- [9] Per Zetterberg and Nima N Moghadam. An Experimental Investigation of SIMO, MIMO, Interference-Alignment (IA) and Coordinated Multi-Point (CoMP). In *Systems, Signals and Image Processing (IWSSIP), 2012 19th International Conference on*, pages 211–216. IEEE, 2012.
- [10] Martin Mayer, Gerald Artner, Gabor Hannak, Martin Lerch, and Maxime Guillaud. Measurement Based Evaluation of Interference Alignment on the Vienna MIMO Testbed. *The Tenth International Symposium on Wireless Communication Systems (ISWCS)*, 2013.
- [11] Emre Telatar. Capacity of Multi-antenna Gaussian Channels. *European transactions on telecommunications*, 10(6):585–595, 1999.
- [12] Abolfazl Sayed Motahari and Amir Keyvan Khandani. Capacity Bounds for the Gaussian Interference Channel. *Information Theory, IEEE Transactions on*, 55(2):620–643, 2009.

- [13] Anders Host-Madsen and Aria Nosratinia. The Multiplexing Gain of Wireless Networks. In *Information Theory, 2005. ISIT 2005. Proceedings. International Symposium on*, pages 2065–2069. IEEE, 2005.
- [14] Cenk M Yetis, Tiangao Gou, Syed A Jafar, and Ahmet H Kayran. Feasibility Conditions for Interference Alignment. In *Global Telecommunications Conference, 2009. GLOBECOM 2009. IEEE*, pages 1–6. IEEE, 2009.
- [15] Meisam Razaviyayn, Gennady Lyubeznik, and Zhi-Quan Luo. On the Degrees of Freedom Achievable Through Interference Alignment in a MIMO Interference Channel. *Signal Processing, IEEE Transactions on*, 60(2):812–821, 2012.
- [16] Gerard J Foschini and Michael J Gans. On Limits of Wireless Communications in a Fading Environment when using Multiple Antennas. *Wireless personal communications*, 6(3):311–335, 1998.
- [17] Guy Bresler, Dustin Cartwright, and David Tse. Feasibility of interference alignment for the MIMO interference channel: the symmetric square case. In *Information Theory Workshop (ITW), 2011 IEEE*, pages 447–451. IEEE, 2011.
- [18] Leonhard Edlinger. Vienna Wireless Testbed. Master’s thesis, Vienna University of Technology, November 2011.
- [19] Edin Huremović. Wireless Testbed Transmitter. Master’s thesis, Vienna University of Technology, August 2011.
- [20] Armin Disslbacher-Fink. Hardware-based Timing Synchronization. Master’s thesis, Vienna University of Technology, December 2010.
- [21] Heinz Haderer. Wireless Testbed Receiver. Master’s thesis, Vienna University of Technology, December 2011.
- [22] Jaiganesh Balakrishnan, Markus Rupp, and Harish Viswanathan. Optimal Channel Training for Multiple Antenna Systems. *Multiaccess, mobility and teletraffic for wireless communications*, 5:25, 2000.
- [23] Gerald Artner. Receiver Location Sensitivity of Interference Alignment. Master’s thesis, Vienna University of Technology, October 2013.